Index Modulation for Next Generation Wireless Communications

Babatunde Segun Adejumobi

Supervisor: Dr. Narushan Pillay

A thesis submitted in fulfilment of the requirement for the degree of

DOCTOR OF PHILOSOPHY IN ENGINEERING (ELECTRONIC)

School of Engineering
University of KwaZulu-Natal
South Africa

May, 2018

As the candidate's supervisor, I have approved this thesis for submission.

Signed.....Date.....

Name: Dr. Narushan Pillay

Declaration 1 - Plagiarism

I, **Babatunde Segun Adejumobi**, declare that;

1. The research reported in this thesis, except where otherwise indicated, is my original research.
2. This thesis has not been submitted for any degree or examination at any other university.
3. This thesis does not contain other persons' data, pictures, graphs or other information, unless specifically acknowledged as being sourced from other persons.
4. This thesis does not contain other persons' writing, unless specifically acknowledged as being sourced from other researchers. Where other written sources have been quoted, then:
   (a) Their words have been re-written but the general information attributed to them has been referenced,
   (b) Where their exact words have been used, then their writing has been placed in italics and inside quotation marks, and referenced.
5. This thesis does not contain text, graphics or tables copied and pasted from the Internet, unless specifically acknowledged, and the source being detailed in the thesis and in the References sections.

Signed.....Date.....

Declaration 2 - Publication

The following journal papers emanating from this work have been either published or are under review:

1. **Babatunde S. Adejumobi, Narushan Pillay, Stanley H. Mneney, and Olutayo O. Oyerinde** "Quadrature spatial modulation orthogonal frequency division multiplexing", *Journal of Telecommunication, Electronic and Computer Engineering*, vol. 10, no. 4, Oct.-Dec., 2018. *In Press)*

2. **Babatunde S. Adejumobi and Narushan Pillay** "Low-complexity detection for space-time block coded spatial modulation with cyclic structure," Journal of Communications, vol. 13, no. 7, Jul. 2018. *(Published)*

3. **Babatunde S. Adejumobi and Narushan Pillay** "RF mirror media-based space-time block coded spatial modulation techniques for two time-slots," *IET Communications*, 2018. *(Under Review)*

The following conference paper has been published during this doctoral research:

1. **Babatunde S. Adejumobi, Narushan Pillay, and Stanley H. Mneney** "A study of spatial media-based modulation using RF mirrors," in *Proceedings of IEEE AFRICON*, Sep. 2017, pp. 336–341. *(Published)*

Dedication

This thesis is dedicated to my late Dad, Sgt. Solomon Adejumobi (Rtd.)

Acknowledgements

My profound gratitude goes to the **Almighty God** for the strength, wisdom, knowledge and understanding He accorded me during this program and making it a success "...for without me ye can do nothing", **John 15:5**.

My supervisors Dr. Narushan Pillay and Prof. S. H. Mneney, have painstakingly groomed and nurtured me to become a competent researcher. You did not hold back your knowledge, expertise, and experiences but had to guide and train me throughout this program. This I do not take lightly. I am very grateful to you.

To my darling wife, Mrs. Rebecca O. Adejumobi, you stood by me during this period of my work, going through thick and thin. Thank you my **inestimable Treasure**.

I am indeed very grateful to my spiritual father, I will never forget when you told me to forget about all other things and return to school. I praise God because its a success. Thanks Dad.

To my Dad, Sgt. Solomon Adejumobi (Rtd.). The pain of your departure is great, I had always thought of coming home to show you I got a PhD. Your words "If you can't make my name better, then you must leave it the way it is" has been a great driving force. Despite your meager income, you had always done the best for us. I love you a lot, but God loves you more. Thanks Dad. To my loving mother, Mrs F. Adejumobi, your love, affection and prayers has always helped in no small measure. Thanks Mom.

To my siblings Mrs. A. Ogbonnaya, Mrs. M. Effiong, Mrs. I. Oseitutu, Miss O. Adejumobi, Miss I. Adejumobi and Mr. G. Adejumobi. Your love and affection no money can buy. Thanks for making my world a pleasant one.

To my In-laws, Mr Effiong, Pastor Ogbonnaya, Pastor Oseitutu, Mr and Deaconness Ibikunle, Thank you for your support and contribution. You are the best.

To the Pastors of God's Mercy Revival Ministries and my friends at D. S. Adegbenro ICT Polytechnic,

I say a big thank you.

I sincerely appreciate the staff of this great department, Dr. Walingo, Dr. Carpanen, Prof. Agee, Prof. Xu, Prof. Afullo, Dr. Jarvis, Advocate Bhero, it was great working with you. My friends Dr. Esenegho, Dr. Gourdazi, Dr. Mafimidiwo, Dr. Modisa, Segun, Diovu, Williams, Dele, Henry, Okiki, Kenny, Oluwole, Ayanda, Afolayan, Ayandeji, Armeline, Buky, Florence, Matthew, Juma, Peter, Yuwa, Uche. Thank you all.

I will like to acknowledge the contributions of Dr. O. O. Oyerinde, Pastor and Mrs Idowu and the Oyelekan's family to my PhD work, I appreciate your assistance.

Abstract

A multicarrier index modulation technique in the form of quadrature spatial modulation (QSM) orthogonal frequency division multiplexing (QSM-OFDM) is proposed, in which transmit antenna indices are employed to transmit additional bits. Monte Carlo simulation results demonstrates a 5 dB gain in signal-to-noise ratio (SNR) over other OFDM schemes. Furthermore, an analysis of the receiver computational complexity is presented.

A low-complexity near-ML detector for space-time block coded (STBC) spatial modulation (STBC-SM) with cyclic structure (STBC-CSM), which demonstrate near-ML error performance and yields significant reduction in computational complexity is proposed. In addition, the union-bound theoretical framework to quantify the average bit-error probability (ABEP) of STBC-CSM is formulated and validates the Monte Carlo simulation results.

The application of media-based modulation (MBM), to STBC-SM and STBC-CSM employing radio frequency (RF) mirrors, in the form of MBSTBC-SM and MBSTBC-CSM is proposed to improve the error performance. Numerical results of the proposed schemes demonstrate significant improvement in error performance when compared with STBC-CSM and STBC-SM. In addition, the analytical framework of the union-bound on the ABEP of MBSTBC-SM and MBSTBC-CSM for the ML detector is formulated and agrees well with Monte Carlo simulations. Furthermore, a low-complexity near-ML detector for MBSTBC-SM and MBSTBC-CSM is proposed, and achieves a near-ML error performance. Monte Carlo simulation results demonstrate a trade-off between the error performance and the resolution of the detector that is employed.

Finally, the application of MBM, an index modulated system to spatial modulation, in the form of spatial MBM (SMBM) is investigated. SMBM employs RF mirrors located around the transmit antenna units to create distinct channel paths to the receiver. This thesis presents an easy to evaluate theoretical bound for the error performance of SMBM, which is validated by Monte Carlo simulation results. Lastly, two low-complexity suboptimal mirror activation pattern (MAP) optimization techniques are proposed, which improve the error performance of SMBM significantly.

Contents

List of Figures

List of Figures

List of Tables

List of Tables

List of Acronyms

ABEP	Average Bit Error Probability
APM	Amplitude/Phase Modulation
AWGN	Additive White Gaussian Noise
BER	Bit Error Rate
BLAST	Bell Laboratories Layered Space-Time Architecture
CC	Computational Complexity
CGD	Coding Gain Distance
CP	Cyclic Prefix
CSI	Channel State Information
ED	Euclidean Distance
FFT	Fast Fourier Transform
FMT	Filtered Multi-Tone
GSM	Generalized Spatial Modulation
HSPA	High Speed Packet Access
H-STBC-SM	High Rate Space-Time Block Coded Spatial Modulation
i.i.d.	Independent and Identically Distributed
IAS	Inter-Antenna Synchronization
ICI	Inter-Channel Interference
IEEE	Institute of Electrical and Electronic Engineers

IFFT	Inverse Fast Fourier Transform
ISI	Inter-Symbol Interference
LC	Low-Complexity
LLR	Log-Likelihood Ratio
LTE	Long Term Evolution
MAP	Mirror Activation Pattern
MBM	Media-Based Modulation
MBSTBC-CSM	Media-Based Cyclic Structured Space-Time Block Coded Spatial Modulation
MBSTBC-SM	Media-Based Space-Time Block Coded Spatial Modulation
MGF	Moment Generating Function
MIMO	Multiple-Input Multiple-Output
ML	Maximum-Likelihood
MMSE	Minimum Mean-Square Error
MRC	Maximal-Ratio Combining
OFDM	Orthogonal Frequency Division Multiplexing
OP	Orthogonal Projection
OSIC	Ordered Successive Interference ancellation
PAPR	Peak-to-Average Power Ratio
PDF	Probability Density Function
PEP	Pairwise Error Probability
QAM	Quadrature Amplitude Modulation
QoS	Quality of Service
QPSK	Quadrature Phase Shift Keying
QSM	Quadrature Spatial Modulation
QSMBM	Quadrature Spatial Media-Based Modulation
RF	Radio Frequency

SE	Spectral Efficiency
SIMO	Single-Input Multiple-Output
SISO	Single-Input Single-Output
SM	Spatial Modulation
SMBM	Spatial Modulated Media-Based Modulation
SNR	Signal-to-Noise Ratio
SQRD	Sorted QR Decomposition
SSK	Space Shift Keying
STBC	Space-Time Block Code
STBC-CSM	Cyclic Structured Space-Time Block Coded Spatial Modulation
STBC-SM	Space-Time Block Coded Spatial Modulation
STBC-TSM	Space-Time Block Coded Spatial Modulation with Temporal Modulation
STCM	Space-Time Channel Modulation
USTLD	Uncoded Space-Time Labeling Diversity
V-BLAST	Vertical Bell Laboratories Layered Space-Time Architecture
WiMAX	Worldwide Interoperability for Microwave Access
ZF	Zero-Forcing

Part I

Introduction

Introduction

1 Multiple-Input Multiple-Output (MIMO)

The ever-increasing demand for multimedia services, which require substantial improvements in throughput and link reliability of wireless communication systems, has increased the research for the 5G wireless systems anticipated for the year 2020. The 5G network is anticipated to have improved quality of service (QoS), improved energy efficiency, full mobility of connected wireless networks, improved spectral efficiency, which is ten times larger than the current 4G wireless systems [1, 2]. To meet the proposed target for 5G communication, multiple-input multiple-output (MIMO) systems have shown increased attractiveness [3]. In conventional (traditional) MIMO systems, a single input data is encoded and transmitted by all the transmit antennas simultaneously, through different channel paths, while at the receiver, multiple copies of the transmitted symbol are received with different phases and at different times by all receive antennas. Hence, MIMO is able to achieve improved error performance over single-input single-output (SISO) systems because spatial diversity gain. However, in modern (conventional) MIMO systems, not all antennas are employed to transmit the encoded data [4–6].

Some of the benefits of MIMO, which achieved through multiplexing gain, diversity gain and the use of smart antennas includes the following [4, 7]:

a. Higher data rates/improved capacity is achieved, because multiple transmit antennas are employed.

b. Increase in transmission range.

c. MIMO is robust in dealing with multiple data streams.

d. Significant improvement in error performance as multiple copies of the same signal are received.

e. Improved QoS due to the diversity gain from multipath signals.

f. A diversity order of $N_t N_r$ may be achieved through MIMO, where N_t and N_r denote the

number of transmit and receive antennas, respectively.

Although MIMO has the aforementioned benefits, some significant challenges exist [4, 7]:

a. Multipath propagation of MIMO signals makes it susceptible to interchannel interference (ICI).

b. The need for inter-antenna synchronization (IAS) as a result of multiple transmit antennas employed.

c. MIMO systems employ multiple RF units, which increase the hardware and computational complexity.

d. The cost, power consumption, form factor and hardware components is increased.

The advantages offered by MIMO are achieved through the following [6]:

1.1 Spatial multiplexing

In spatial multiplexing techniques, multiple transmit antennas are employed to transmit independent information sequences, with each layer being superimposed [6, 8]. Employing N_t transmit antennas, the bit rate can be improved by a factor N_t without additional bandwidth, when compared with single-input multiple-output (SIMO)/single-input single-output (SISO) systems. At the receiver, an algorithm to separate the different layers is implemented to detect the transmitted information. A good example of the spatially multiplexed MIMO system, is the well known Bell-labs layered space-time architecture (BLAST) [9], the basic objective of spatial multiplexing is to provide higher bit rates [6].

1.2 Spatial diversity

Spatial diversity [10], exploits the advantage of multiple independent copies of transmitted symbols, arriving at the receiver from different pathways, hence, making it possible to improve the error performance of wireless communication. Unlike spatial multiplexing, which aims to increase data rate, the basic objective of spatial diversity is to improve the error performance of the system by counteracting the effects of multipath induced fading. However, when spatial diversity is combined with channel coding or adaptive modulation, it can achieve higher data rates [6]. The level of improvement achieved through spatial diversity depends on the fading characteristics of the channel, which is caused by the time and frequency variation of the channel [4]. Alamouti space-time block coded (STBC) systems are perfect examples of spatial diversity schemes [11, 12].

1.3 Smart antenna and beamforming

The basic objectives of smart antennas and beamformers, are to improve the signal-to-noise ratio (SNR) and to suppress co-channel interference. Beamforming antennas are arrays of antennas, having individual elements that can receive signals from a particular direction. The received signals, from the different antenna elements, arrive at different time instants and phase shifts because, of the antenna geometry. Employing phase shifters or delay elements, these phase shifts or delay times can be compensated for [6].

2 System Model of MIMO

Fig. 1 depicts the system model of an $N_t \times N_r$ MIMO system.

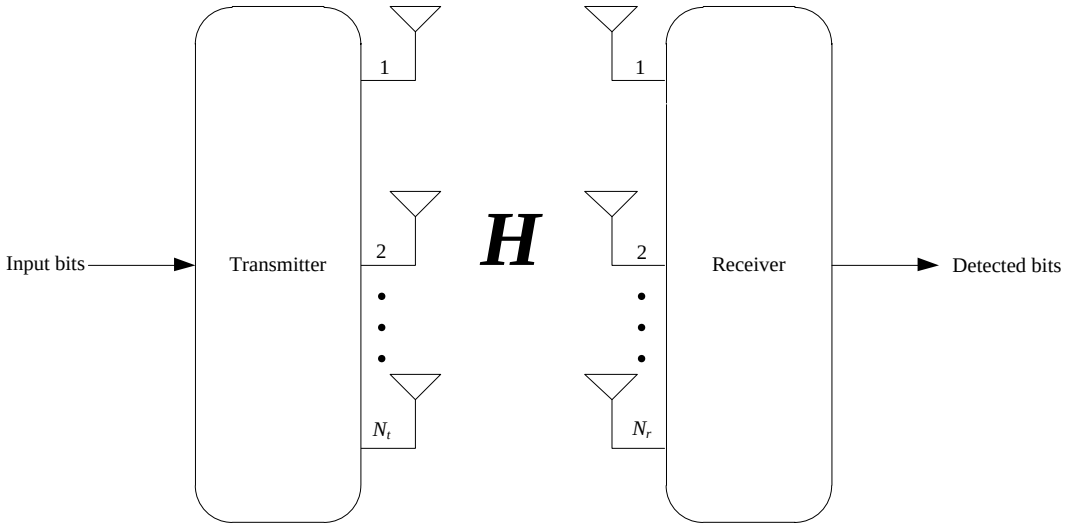

Fig. 1: System model of MIMO

An input bit stream is modulated into an M-ary amplitude and/or phase modulation (APM) $N_t \times 1$ transmission vector $\boldsymbol{x} = [x_1\ x_2\ \cdots\ x_{N_t}]^T$ and transmitted through an $N_r \times N_t$ channel $\boldsymbol{H} = [\boldsymbol{h}_1\ \boldsymbol{h}_2\ \cdots\ \boldsymbol{h}_{N_t}]$ having its elements represented as:

$$\boldsymbol{H} = \begin{bmatrix} h_{1,1} & h_{1,2} & \cdots & h_{1,N_t} \\ h_{2,1} & h_{2,2} & \cdots & h_{2,N_t} \\ \vdots & \vdots & \ddots & \vdots \\ h_{N_r,1} & h_{N_r,2} & \cdots & h_{N_r,N_t} \end{bmatrix} \tag{1}$$

where $h_{a,b}$, $a \in [1 : N_r]$ and $b \in [1 : N_t]$ is the channel fading coefficient from the b-th transmit antenna to the a-th receive antenna. The columns represent the channel vectors for the transmit antennas, while the rows represent the channel vectors for the receive antennas. Considering a frequency-flat Rayleigh fading channel, the $N_r \times 1$ receive signal vector $\boldsymbol{y}$ at the receiver may be represented as:

$$\boldsymbol{y} = \sqrt{\rho}\boldsymbol{H}\boldsymbol{x} + \boldsymbol{n} \tag{2}$$

where ρ is the average SNR at the receiver, $\boldsymbol{n} = [n_1 \ n_2 \ \cdots \ n_{N_r}]^T$ is an $N_r \times 1$ additive white Gaussian noise (AWGN) vector, whose entries are independently and identically distributed (i.i.d.) with a distribution according to $CN(0, 1)$. $\boldsymbol{H}$ denotes the $N_r \times N_t$ channel matrix which is an i.i.d. Rayleigh fading channel with a distribution according to $CN(0, 1)$.

The receiver receives the faded signal by the receiving antenna, demodulates it, while appropriate detection algorithms are implemented to estimate the transmitted symbol(s). The ML detector for MIMO is represented as [13]:

$$\hat{m} = \underset{m \in \boldsymbol{\Omega}}{\operatorname{argmin}} \, p_{\boldsymbol{y}} \left(\boldsymbol{y} \mid x_m, \boldsymbol{H} \right) \tag{3}$$

where $\hat{m}$ is the estimate of the m-th, $m \in [1 : M]$ transmitted symbol x_m of the APM constellation $\boldsymbol{\Omega}$, $p_{\boldsymbol{y}}$ is the probability density function (PDF) of the random variable $\boldsymbol{y}$. A reduced form for (3) is given as [13]:

$$\hat{m} = \underset{m \in \boldsymbol{\Omega}}{\operatorname{argmin}} \, \|\boldsymbol{g}\|_F^2 - 2\Re\left(\boldsymbol{y}^H \boldsymbol{H}\right) \tag{4}$$

where $\boldsymbol{g} = \boldsymbol{H}\boldsymbol{x}$, $\|\cdot\|_F$ denotes the Frobenius norm operator and $\Re(\cdot)$ denotes the real part of a complex variable.

In [3], a low-complexity near-ML detector based on orthogonal projection has been presented. A projection matrix $\boldsymbol{P}_{mat}$, which projects a signal orthogonal unto a subspace $\boldsymbol{h}_1, \boldsymbol{h}_2, \cdots, \boldsymbol{h}_{N_t}$ such that $\boldsymbol{P}_{mat}\boldsymbol{h}_1 = \boldsymbol{P}_{mat}\boldsymbol{h}_2 = \cdots = \boldsymbol{P}_{mat}\boldsymbol{h}_{N_t} = 0$ is given as [3]:

$$\boldsymbol{P}_{mat} = \boldsymbol{I}_{N_t} - \boldsymbol{H}_{2:N_t}(\boldsymbol{H}_{2:N_t}^H \boldsymbol{H}_{2:N_t})^{-1} \boldsymbol{H}_{2:N_t}^H \tag{5}$$

where $\boldsymbol{I}_{N_t}$ denotes an $N_t \times N_t$ identity matrix, $\boldsymbol{H}_{2:N_t} \triangleq [\boldsymbol{h}_2 \ \boldsymbol{h}_3 \ \cdots \ \boldsymbol{h}_{N_t}]$ and $(\cdot)^{-1}$ represents the inverse.

Considering (2), If $s = x_1$, it can be deduced that:

$$\boldsymbol{P}_{mat}(\boldsymbol{y} - \boldsymbol{h}_1 s) = \boldsymbol{P}_{mat}(\boldsymbol{h}_2 x_2 + \boldsymbol{h}_3 x_3 + \cdots + \boldsymbol{h}_{N_t} x_{N_t} + \boldsymbol{n}) = \boldsymbol{P}_{mat}(\boldsymbol{n}) \tag{6}$$

however, If $s \neq x_1$, (6) may be represented as:

$$\boldsymbol{P}_{mat}(\boldsymbol{y} - \boldsymbol{h}_1 s) = \boldsymbol{P}_{mat}(\boldsymbol{h}_1 x_1 - \boldsymbol{h}_1 s) + \boldsymbol{P}_{mat}(\boldsymbol{n}) \tag{7}$$

Comparing (6) and (7), it can be deduced that the norm of (6) is less than the norm of (7). Hence, the most likely candidate set of the transmitted APM symbol, which offer the minimum Frobenius norms and a subset of $\boldsymbol{\Omega}$ can be chosen. The ML detection can be performed on this subset, hence, reducing the computational complexity of the ML detector.

3 Innovative Implementations of MIMO

The demand for improved data services for next-generation multimedia applications require improvement in capacity, spectral efficiency and link reliability [14]. MIMO is able to achieve these by increasing the modulation order or employing an increased number of transmit/receive antennas. However, MIMO is limited by ICI, IAS, computational complexity of its detector, complexity of the hardware design, etc. [15]. Hence, different innovative implementations of MIMO, which offer multiplexing and/or diversity gains and mitigate the limitations of MIMO are presented in the subsections [8–11].

3.1 V-BLAST

In order to increase the capacity of MIMO, V-BLAST employs the spatial multiplexing of N_t transmit antennas to transmit N_t symbols. A major disparity between the traditional MIMO is that, whereas the N_t transmit antennas are employed to transmit the same symbol for traditionalMIMO, the symbols of BLAST are transmitted as parallel streams [16, 17]. Therefore, the spectral efficiency of traditional MIMO, which employs transmits all antennas to transmit a single symbol, is improved significantly by a factor of N_t. However, similar to MIMO, V-BLAST is plagued by ICI and IAS. Furthermore , the computational complexity of the joint detector for V-BLAST increases exponentially with the number of data streams [17].

In order to reduce the computational complexity, several detectors have been proposed. For example, optimal ordering of each sublayer was investigated in [18], where each sublayer is detected

separately. The substreams are detected in turns employing linear detecting weights, while the other substreams are assumed to be interferences. Furthermore, sorted QR decomposition has been employed to improve the computational complexity of the optimal ordered MMSE detector for V-BLAST, while retaining the error performance [19].

3.2 MIMO orthogonal frequency division multiplexing (MIMO-OFDM)

In order to achieve high data rates in single carrier systems, wider bandwidths are employed, however, intersymbol interference (ISI) in single-carrier systems occurs, when the signal bandwidth becomes greater than the coherence bandwidth. Traditionally, adaptive equalizers are employed to eliminate the ISI, however, with increased data rate, the complexity of the equalizers are significantly increased, hence, making a high data rate for single-carrier communication is not feasible [20]. To solve the problem of frequency selectivity in single-carrier transmission, multi-carrier schemes such as filtered multi-tone (FMT) transmission and OFDM have been introduced.

3.2.1 OFDM

OFDM is one of the most widely used modulation techniques, and can be found in standards like WiMAX, long term evolution (LTE) and LTE-advanced. It mitigates the effect of ISI, reduces computational complexity by employing a one-tap equalizer and improves power and spectral efficiency because it implements power and bit-loading algorithms [21].

OFDM splits a wideband signal into several independent narrowband orthogonal signals called subcarriers. An incoming stream of information bits, are mapped into APM symbols from an APM constellation set. These symbols are employed to form an $N \times 1$ vector of an OFDM symbol $\boldsymbol{x}[k]$ represented as:

$$\boldsymbol{x}[k] = \begin{bmatrix} x_0[k] & x_1[k] & \cdots & x_{N-1}[k] \end{bmatrix}^T \tag{8}$$

where $x_l[k]$, $l \in [0 : N-1]$ is the APM symbol transmitted through the l-th subcarrier of the k-th OFDM symbol, N is the size of the OFDM symbol and $[\cdot]^T$ denotes the transpose of a vector. In practice, the OFDM subcarriers $\boldsymbol{z}^\dagger(k) = \begin{bmatrix} z_0^\dagger(k) & z_1^\dagger(k) & \cdots & z_{N-1}^\dagger(k) \end{bmatrix}^T$ are produced by the implementation of the inverse fast Fourier transform (IFFT) on each element of $\boldsymbol{x}[k]$, where $(\cdot)^\dagger$ denotes a time domain signal. The N samples of the OFDM symbol generated by performing the IFFT may be expressed as [22]:

$$\boldsymbol{z}_l^{\dagger}(k) = \frac{1}{\sqrt{N}} \sum_{l=0}^{N-1} x_l[k] \text{exp}\left(\frac{i2\pi kl}{N}\right) \tag{9}$$

A cyclic prefix/suffix (CP) $\boldsymbol{c}^{\dagger}(k)$, having $V \times 1$ vector, taken from the beginning/end $\boldsymbol{z}_l^{\dagger}(k)$ is efficiently chosen, such that the sampling duration for $\boldsymbol{c}^{\dagger}(k)$ is greater than the delay spread of the received symbol. The CP is appended/prepended to the end/beginning of the OFDM symbol to reduce the effect of ISI [21, 22]. Hence, the new time domain vector formed $\boldsymbol{z}_{OFDM}^{\dagger}(k)$, is of the form represented as:

$$\boldsymbol{z}_{OFDM}^{\dagger}(k) = \Bigg[\underbrace{z_0^{\dagger}(k) \quad z_1^{\dagger}(k) \quad \cdots \quad z_{N-1}^{\dagger}(k)}_{\text{OFDM symbol}} \quad \underbrace{c_N^{\dagger}(k) \quad c_{N+1}^{\dagger}(k) \quad \cdots \quad c_{N+V-1}^{\dagger}(k)}_{\text{CP}}\Bigg] \tag{10}$$

The received time domain signal vector $\boldsymbol{y}_{OFDM}^{\dagger}(k)$ is given by:

$$\boldsymbol{y}_{OFDM}^{\dagger}(k) = \boldsymbol{h}^{\dagger}(k) \otimes \boldsymbol{z}_{OFDM}^{\dagger}(k) + \boldsymbol{n}^{\dagger}(k) \tag{11}$$

where $\otimes$ denotes a time convolution. $\boldsymbol{h}^{\dagger}(k)$ is the channel impulse response, $\boldsymbol{n}^{\dagger}(k)$ is an AWGN vector encountered at the receiver, whose entries are i.i.d. random variables with distribution $CN(0, \sigma^2)$. The received signal after the CP is removed is given by:

$$\boldsymbol{y}^{\dagger}(k) = \begin{bmatrix} y_1^{\dagger}(k) & y_2^{\dagger}(k) & \cdots & y_{N-1}^{\dagger}(k) \end{bmatrix} \tag{12}$$

The N-point FFT is performed on the time domain signal at the receiver after the removal of the CP. The FFT for an individual subcarrier is represented by [22]:

$$\boldsymbol{y}_l[k] = \frac{1}{\sqrt{N}} \sum_{l=0}^{N-1} y_l^{\dagger}(k) \text{exp}\left(\frac{-i2\pi kl}{N}\right), \qquad l \in [0 : N-1] \tag{13}$$

The frequency response of the received signal $\boldsymbol{y}_{OFDM}[k] = \begin{bmatrix} y_1[k] & y_2[k] & \cdots & y_{N-1}[k] \end{bmatrix}^T$ is given by [20]:

$$\boldsymbol{y}_{OFDM}[k] = \boldsymbol{h}[k] x_l[k] + \boldsymbol{n}[k] \tag{14}$$

where $\boldsymbol{n}[k]$ is an AWGN vector at the receiver, whose entries are i.i.d. random variables with distribution $CN(0, \sigma^2)$, $\boldsymbol{h}[k]$ is the frequency response of the channel.

The bit error of single carrier OFDM systems can further be improved by the MIMO implementation of OFDM (MIMO-OFDM). Hence, the next paragraph introduces MIMO-OFDM.

3.2.2 MIMO-OFDM

MIMO-OFDM [23, 24], combines the advantages of MIMO and OFDM to improve the error performance, capacity and reliability of MIMO, SISO and SIMO [21, 23]. MIMO-OFDM employs OFDM modulators, which perform IFFT of the incoming signal, and appends/prepends the CP to the time domain signal. This signal is transmitted using N_t transmit antennas via an $N_r \times N_t$ MIMO channel $\boldsymbol{H}$. The individual channel impulse response between the m-th transmit antenna and the n-th receive antenna, having L independent delayed path (taps), for an individual OFDM symbol is expressed as [20]:

$$\boldsymbol{h}^{\dagger}_{m,n}(k) = \sum_{\phi=0}^{L-1} \beta_{m,n}(\phi)\delta(t-\tau_{\phi}), \qquad \phi \in [1:L] \tag{15}$$

where $m \in [1:N_t]$, $n \in [1:N_r]$, $\beta_{m,n}$ and τ_{ϕ} are the fading coefficient and delay spread for the ϕ-th path between the m-th transmit antenna and the n-th receive antenna, respectively, and $\delta(\cdot)$ is the unit sample response given by the Dirac delta function.

The advantages of OFDM, apart from the elimination of ISI, includes efficient use of the spectrum due to overlapping of subcarriers. Furthermore, it is resistant to frequency selectivity because the wideband is divided into several narrowband frequencies [20]. The use of FFT and IFFT makes it computationally efficient, while different detection algorithms can be implemented with reasonable complexity. However, OFDM systems suffer from reduced error performance caused by high peak-to-average power ratio (PAPR) [25]. Some techniques employed in reducing high PAPR are: clipping and filtering of signals outside the required region [26], the application of specialized coding schemes such as simple odd parity code [27], use of partial transmit sequence or selective mapping [28], etc.

3.3 Alamouti space-time block codes (STBC)

The Alamouti STBC [11], exploits spatial diversity to improve the reliability of the traditional MIMO system by employing two time-slots. In the first time-slot, two APM symbols x_1 and x_2 are transmitted by the transmit antennas t_1 and t_2, respectively, while the symbols $-x_2^*$ and x_1^* are transmitted by t_1 and t_2 during the second time-slot, respectively. The Alamouti STBC codeword $\boldsymbol{X}$ may be represented as [20].

$$\boldsymbol{X} = \begin{bmatrix} x_1 & -x_2^* \\ x_2 & x_1^* \end{bmatrix} \tag{16}$$

where the rows and columns represent the transmit antennas and the time-slots, respectively.

Although the spectral efficiency of classical MIMO is not improved, the redundant copies of the transmitted symbols yield an improved error performance [29]. Furthermore, STBC is able to achieve maximum diversity without feedback from receivers and the receivers employ linear processing. However, the improvement in error performance is achieved with increased computational complexity, especially when the ML detector is employed [30]. A variation of STBC is the orthogonal STBC [31, 32].

3.4 Index modulation

Index modulation employs alternative ways than amplitude/frequency/phase to transmit information via the carrier of the transmitted signal. It employs the indices of distinct channel pathways to convey information by exploiting the ON/OFF status of subcarrier, antenna, light emitting diodes, time-slots, modulation types etc. [1]. Interestingly, this area of research has evolved significantly within a very short time frame.

Some advantages of index modulation are as follows [33]:

a. In contrast to traditional modulation schemes, that uses up its total transmission energy, index modulation can transfer saved transmission energy from inactive transmit components to the active components, hence, improving the error performance.

b. Index modulation performs energy-efficient information transmission by activating/deactivating components of its system and exploiting the same for transmitting information.

c. Systems, which employ index modulation are capable of improving its spectral efficiency without increasing its hardware complexity.

Several index modulated systems have been considered in the literature [33], however, an overview of some index modulated systems, which are employed during this research are discussed on the next page.

3.4.1 Spatial modulation (SM)

In SM, a single antenna from a group of N_t transmit antennas is employed to transmit a symbol at any given instance, hence, the need for IAS is eliminated, and ICI is canceled. The index of the transmit antenna, like all index modulated systems, conveys additional information. Furthermore, the spatial domain is employed to improve the spectral efficiency/error performance of classical MIMO only to a degree.

Some advantages of SM, are as follows [4]:

a. SM is energy efficient, because it employs a single RF chain at any given time.

b. As mentioned earlier, IAS and ICI is eliminated, since only one antenna is active and only one symbol is transmitted at any time instance.

c. The capacity of SM is improved in contrast to classical MIMO because of the additional bits employed.

d. Reduction in the cost of hardware cost and hardware complexity.

Although these advantages exist for SM, it has some limitations. Some of the disadvantages of SM are as follows:

a. It yields a logarithmic relationship between the number of transmit antennas and the spectral efficiency.

b. The number of transmit antennas that can be employed must be in the power of two.

c. Unlike generalized SM (GSM) [34, 35], SM can only transmit one symbol at any time. Hence, the spectral efficiency is reduced, when compared to GSM [34, 35].

d. SM does not exploit the potential for transmit diversity.

3.4.2 Space shift keying modulation (SSK)

SSK [36], employs the principle of SM to transmit information. In SSK, only the spatial domain is employed as constellation to transmit information. Unlike MIMO, which transmits information through the APM symbol, SSK employs a single transmit antenna at a time, with the transmitted tone as its constellation, while other antennas transmit at zero power. The symbol transmitted is not considered, however, the index of the transmitted symbol contains the information. Given the input

bits $[b_1\ b_2]$ for a 2×2 SSK system, the transmitted symbol, activated antenna index and the transmit antenna vector $\boldsymbol{x}$ are presented in Table 1.

Table 1: Example of SSK modulation [36]

bits	symbol	antenna index	$\boldsymbol{x}$
$[0\ \ 0]$	0	1	$[1\ \ 0\ \ 0\ \ 0]^T$
$[0\ \ 1]$	1	2	$[0\ \ 1\ \ 0\ \ 0]^T$
$[1\ \ 0]$	2	3	$[0\ \ 0\ \ 1\ \ 0]^T$
$[1\ \ 1]$	3	4	$[0\ \ 0\ \ 0\ \ 1]^T$

The SSK scheme demonstrates significant improvement over the phase shift keying maximal ratio combining (PSK-MRC) scheme and vertical-BLAST, however, the number of antennas needed to achieve higher data rates is large and could be unimplementable especially for smaller devices.

An improvement on the SSK scheme is the Bi-SSK scheme [35]. Bi-SSK employ a pair of transmit antennas to improve the data rate of SSK. However, this improvement is achieved with a trade-off in error performance as there is a marginal reduction in error performance of Bi-SSK over the SSK. Furthermore, although the data rate of Bi-SSK is improved, an increase in the RF chains ultimately increase the computational complexity of the system.

3.4.3 Quadrature spatial modulation (QSM)

In a bid to improve the advantages offered by SM, several studies aimed at improving the error performance and throughput of SM has been conducted. In this regard, QSM has been found to be a promising candidate [37, 38]. In QSM, the throughput of SM is improved by simultaneously transmitting the in-phase and the quadrature component of an APM symbol, employing one or two transmit antennas, whose indices are used to convey additional information. A diagram to illustrate the QSM system is depicted in Fig. 2. An incoming bit stream $\boldsymbol{d}$ of $\log_2(MN_t^2)$ bits, at the input of the QSM system is split into three parts at every instance.

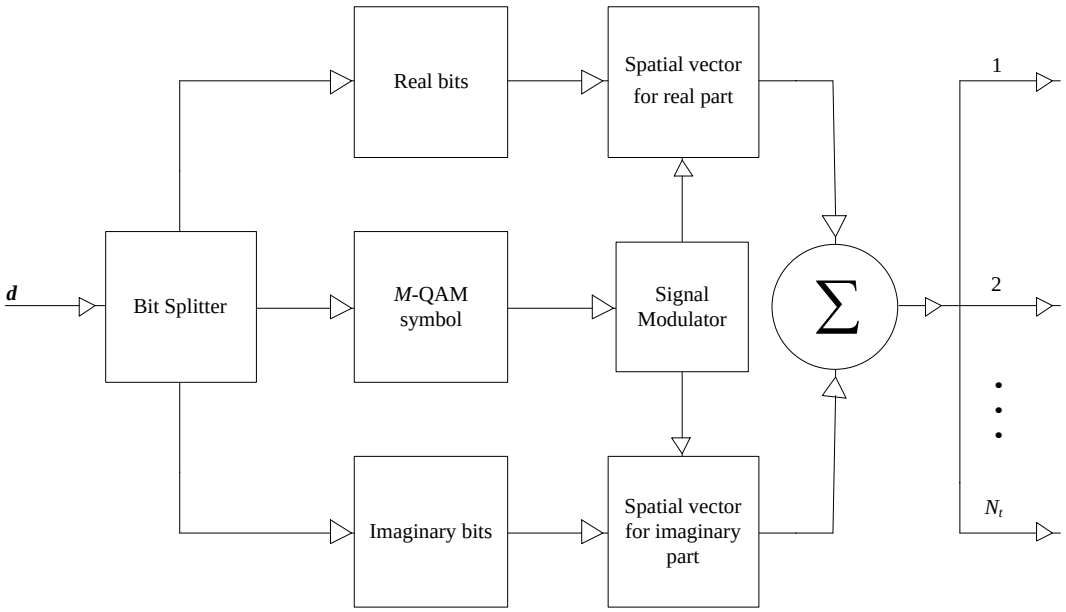

Fig. 2: System model of QSM modulator

The first $n = \log_2 M$ bits $[d_1\ d_2 \cdots d_n]$ are employed to select an APM symbol m^k_{QSM}, $k \in [1 : M]$. The second subgroup of $\log_2 N_t$ bits is used to activate the antenna with antenna index $\ell_{\Re}$ for transmitting the real part of the generated M-QAM symbol, while the third subgroup of $\log_2 N_t$ bits is used to activate the antenna with antenna index for transmitting the imaginary part of the M-QAM symbol, where $\ell_{\Re}, \ell_{\Im} \in [1 : N_t]$.

The complex symbol m^k_{QSM} being selected from the M-QAM symbol constellation is further broken down into its real and imaginary components being $m^{k,\Re}_{QSM}$ and $m^{k,\Im}_{QSM}$, respectively, such that:

$$m^k_{QSM} = m^{k,\Re}_{QSM} + im^{k,\Im}_{QSM} \tag{17}$$

where $i = \sqrt{-1}$ is the imaginary part of a complex number.

$m^{k,\Re}_{QSM}$ and $im^{k,\Im}_{QSM}$ are then transmitted by the $\ell_{\Re}$-th and $\ell_{\Im}$-th antennas, respectively, such that the signal vector $\boldsymbol{m}_{QSM}$ for the transmission is given in (18) as:

$$\boldsymbol{m}_{QSM} = \boldsymbol{m}^{k,\Re}_{\ell_{\Re}} + i\boldsymbol{m}^{k,\Im}_{\ell_{\Im}} \tag{18}$$

where $\boldsymbol{m}^{k,\Re}_{\ell_{\Re}}$ and $i\boldsymbol{m}^{k,\Im}_{\ell_{\Im}}$ are $N_t \times 1$ vectors having $m^{k,\Re}_{QSM}$ and $im^{k,\Im}_{QSM}$ as the non-zero entries in the

Table 2: Grouping of input bit stream for 4×4 antenna configuration 4-QAM modulation

Grouping $[d_1\ d_2 \cdots d_6]$	Symbol bits	Real bits	Imaginary bits
1 0 1 1 0 0	10	11	00
1 1 1 1 1 1	11	11	11
0 0 0 0 0 1	00	00	01
1 0 0 1 1 1	10	01	11
0 1 1 0 0 1	01	10	01

$\ell_{\Re}$-th and $\ell_{\Im}$-th positions, respectively. Hence, when $\ell_{\Re} \neq \ell_{\Im}$, $\boldsymbol{m}_{QSM}$ takes the form shown below:

$$\boldsymbol{m}_{QSM} = \begin{bmatrix} 0 & \cdots & 0 & \underbrace{m_{QSM}^{k,\Re}}_{\ell_{\Re}\text{-th position}} & 0 & \cdots & 0 & \underbrace{im_{QSM}^{k,\Im}}_{\ell_{\Im}\text{-th position}} & 0 & \cdots & 0 \end{bmatrix}^T \tag{19}$$

and when $\ell_{\Re} = \ell_{\Im}$, $\boldsymbol{m}_{QSM}$ takes the form:

$$\boldsymbol{m}_{QSM} = \begin{bmatrix} 0 & \cdots & 0 & \underbrace{m_{QSM}^{k,\Re} + im_{QSM}^{k,\Im}}_{\ell_{\Re}=\ell_{\Im}\text{-th position}} & 0 & \cdots & 0 \end{bmatrix}^T \tag{20}$$

The real and imaginary parts are transmitted orthogonally, hence, ICI is eliminated, unlike SM, which employs a single antenna for its transmission, such as to eliminate ICI. A numerical illustration of the QSM mapping technique is given in Table 2 and Table 3. Assume the grouped bits entering the input of the QSM modulator at every instant, is given as $[d_1\ d_2\ \cdots\ d_6]$, such that, a 4-QAM modulation scheme and four transmitting antennas are employed to transmit $[d_1\ d_2\ \cdots\ d_6]$.

The grouping is first carried out by taking a set of $\log_2(MN_t^2)$ bits, in this case, the first group of $\log_2(MN_t^2)$ bits in Table 2 are $[1\ 0\ 1\ 1\ 0\ 0]$. These bits are then split into three subgroups such as shown in Table 2. The $\log_2 M$ symbol bits for generating the 4-QAM symbol is $[1\ 0]$, $\log_2 N_t$ antenna bits used for transmitting the real part of the 4-QAM symbol is $[1\ 1]$ and $\log_2 N_t$ antenna bits used for transmitting the imaginary part of the 4-QAM symbol is $[0\ 0]$. After the grouping of the bits, further processing of the bits for spatial multiplexing is performed as shown in Table 3.

The symbol m_{QSM}^{k} is split into the real part $m_{QSM}^{k,\Re}$ and imaginary part $m_{QSM}^{k,\Im}$, which are transmitted by the $\ell_{\Re}$-th and $\ell_{\Im}$-th transmit antennas obtained from the real and imaginary bits in Table 2. For example, taking the first row of Table 3, it means the symbol "$+1$" will be transmitted by the fourth antenna and "$-i$" by the first antenna. Other antennas remain inactive, resulting in the vectors $\boldsymbol{m}_{\ell_{\Re}}^{k,\Re}$ for the real part and $\boldsymbol{m}_{\ell_{\Im}}^{k,\Im}$ for the imaginary part. The transmitted vector is then obtained by summing

Table 3: Outputs from the QSM modulator

4-QAM symbol	Spatial symbol		Activated antenna		$\boldsymbol{m}_{QSM}$
m_{QSM}^{k}	$m_{QSM}^{k,\Re}$	$im_{QSM}^{k,\Im}$	$\ell_{\Re}$	$\ell_{\Im}$	
$+1-i$	$+1$	$-i$	4	1	$\begin{bmatrix}-i & 0 & 0 & 1\end{bmatrix}$
$+1+i$	$+1$	$+i$	4	4	$\begin{bmatrix}0 & 0 & 0 & 1+i\end{bmatrix}$
$-1-i$	-1	$-i$	1	2	$\begin{bmatrix}-1 & -i & 0 & 0\end{bmatrix}$
$+1-i$	$+1$	$-i$	2	4	$\begin{bmatrix}0 & +1 & 0 & -i\end{bmatrix}$
$-1+i$	-1	$+i$	3	2	$\begin{bmatrix}0 & +i & -1 & 0\end{bmatrix}$

the vectors for the real and imaginary parts, which gives $\boldsymbol{m}_{QSM}$. This means that the transmission of m_{QSM}^{k} at this instant will be carried out by the first and the fourth antennas simultaneously, which are transmitted orthogonally to each other, hence canceling ICI. The signal at the receiver is given by:

$$\boldsymbol{y}_{QSM} = \sqrt{\rho}\left(\boldsymbol{h}_{\ell_{\Re}} x_{\Re} + i\boldsymbol{h}_{\ell_{\Im}} x_{\Im}\right) + \boldsymbol{n} \tag{21}$$

where ρ is the energy of the transmitted symbol$\boldsymbol{h}_{\ell_{\Re}}$ and $\boldsymbol{h}_{\ell_{\Im}}$ are the $\ell_{\Re}$-th and $\ell_{\Im}$-th column vectors for the frequency response of the $N_r \times N_t$ channel $\boldsymbol{H}$, $x_{\Re}$ and $x_{\Im}$ are the real and imaginary components of m_{QSM}^{k} being transmitted. $\boldsymbol{n}$ is an AWGN signal vector, whose entries are i.i.d. random variables with distribution $CN(0,\,1)$. The detector implements the ML rule given by:

$$\left[\hat{\ell}_{\Re}, \hat{\ell}_{\Im}, \hat{u}_{\Re}, \hat{u}_{\Im}\right] = \underset{\substack{\ell_{\Re},\ell_{\Im}\in[1:N_t],\\ u_{\Re},u_{\Im}\in[1:M]}}{\operatorname{argmin}} \left(\left\|\boldsymbol{y}_{QSM} - \sqrt{\rho}\left(\boldsymbol{h}_{\ell_{\Re}} x_{\Re} + i\boldsymbol{h}_{\ell_{\Im}} x_{\Im}\right)\right\|_F^2\right) \tag{22}$$

where $\hat{\ell}_{\Re}$ and $\hat{\ell}_{\Im}$, $\hat{\ell}_{\Re}, \hat{\ell}_{\Im} \in [1 : N_t]$ are the estimated antenna indices employed in transmitting the real and imaginary parts, respectively. $\hat{u}_{\Re}$ and $\hat{u}_{\Im}$, $\hat{u}_{\Re}, i\hat{u}_{\Im} \in \boldsymbol{\Omega}$ are the estimates of the real and imaginary parts of the transmitted M-QAM symbol, respectively.

For conventional MIMO, the received bits after detection will be just two bits, whereas for QSM, the spectral efficiency is improved, since the antenna detected also carries additional information. Apart from the verified improvement in spectral efficiency of QSM systems over SM noted in [37, 38], QSM is seen to be more energy efficient than SM, as SM requires approximately 3 dB more power to attain the same error performance of QSM [37, 39].

3.4.4 STBC-SM

STBC-SM [40], combines the spatial diversity offered by STBC [11], and the spectral efficiency improvement offered by index modulation systems, such as SM [41], to improve the error performance and spectral efficiency of STBC, while the error performance of SM is improved. In STBC-SM, two transmit antennas selected from a group of $N_t > 2$ transmit antennas, which are employed to transmit an Alamouti codeword. The spectral efficiency offered by the spatial domain of STBC-SM is $0.5 \log_2 c$ bits/s/Hz, where $c = \lfloor \frac{N_t(N_t-1)}{2} \rfloor_{2p}$, and $\lfloor w \rfloor_{2p}$ denotes the nearest power of two, less than or equal to w. ICI is eliminated in STBC-SM, however, it employs more than one RF chain, which increases the computational complexity, when the ML detector is employed for quasi-static frequency-flat Rayleigh fading channel. Several schemes, with the objective of improving the spectral efficiency/error performance/computational complexity, have been reported in the literature. For example, labeling diversity has been employed in [42], to improve the error performance or spectral efficiency of STBC-SM. Furthermore, a reduced computational complexity scheme for STBC-SM has been presented in [43]. Although, the error performance of SM is improved by STBC-SM, IAS and the need for the number of antennas employed to be equal to the power of two still exists.

3.4.5 STBC-SM with cyclic structure (STBC-CSM)

In order to improve the spectral efficiency of STBC-SM and SM, a new scheme, in the form of STBC-CSM, which employ cyclically rotated transmit antenna pairs, to transmit Alamouti codewords, has been proposed in [44]. Furthermore, unlike the STBC-SM, which takes its transmitted symbols $x_1$and x_2 from a single constellation set Ω_1 [40], STBC-CSM takes its transmitted symbols from two different constellations Ω_1 and Ω_2. The second constellation $\Omega_2 = \Omega_1 e^{j\theta_k}$, is a rotated version of Ω_1, where θ_k is the rotation angle θ of the k-th, $k \in [1 : N_t - 1]$ codebook. The spectral efficiency of STBC-CSM offered by the spatial domain is $0.5 \log_2 c$ bits/s/Hz, where $c = \lfloor N_t(N_t - 1) \rfloor_{2p}$, whereas $c = \lfloor \frac{N_t(N_t-1)}{2} \rfloor_{2p}$ for STBC-SM. Although this improvement exists, there is a decrease in the error performance of STBC-CSM. Furthermore, similar to STBC-SM, STBC-CSM also suffer from IAS and an increased computational complexity, because it employ more than one RF chain. Some advancement on STBC-CSM reported in the literature includes a constellation transformation-based STBC-CSM [45] , which improves the error performance of STBC-SM, and a reduced computational complexity detector, which can be employed, for quasi-static and fast frequency-flat Rayleigh fading channel [46].

3.4.6 STBC with temporal spatial modulation (STBC-TSM)

In [47], a new STBC scheme, which employs cyclic spatially modulated codebook with temporal permutation over four time-slots has been proposed. The spectral efficiency offered by the spatial domain is given as [47]:

$$\eta_{TSM} = \frac{1}{4}\log_2\left(\left\lfloor \frac{4!}{2}\frac{N_t!}{(N_t-4)!}\right\rfloor_{2p}\right) \text{ bits/s/Hz} \tag{23}$$

where $(\cdot)!$ denotes the factorial. Given a specified number of transmit antennas, it can be deduced from [47] that the spectral efficiency/error performance of STBC-SM and STBC-CSM has been improved by STBC-TSM. However, there exists a a trade-off, as the computational complexity for the ML detector of STBC-TSM is significantly increased, such as shown in Fig. 2(a) of [47]. A differential modulation scheme for STBC-TSM scheme is presented in [48].

3.4.7 Media-based modulation (MBM)

MBM employs the indices of parasitic elements located around a transmit antenna, such as RF mirrors, reconfigurable antennas and RF switches to convey information by altering the channel properties of the transmit antennas depending on the input bits. The ON/OFF status of these parasitic elements are employed to create distinct channel paths, which forms the spatial constellations of the media-based system. As would be seen in the later parts of this thesis, the application of MBM has advantages, which are not limited to the following [49–51]:

a. A single antenna is capable of forming several channel pathways.

b. Since the constellation size of an MBM system is not dependent on the transmit power, therefore, large constellation sizes are achievable.

c. With MBM, multipath fading is converted into AWGN, hence, improving the error performance of the system.

d. Smaller form factors of an MBM system can be achieved, since there are no restrictions on the physical size of MBM unit.

e. MBM allows selection of a subset of good channels by employing suitable algorithms. Hence, channel paths, which offer superior error performance can be selected.

Several applications of MBM have been reported in the literature. For example, the basic form of MBM is the SSK scheme, where the transmitted alphabet is its channel realizations [36, 49, 52].

Furthermore, RF switches as a form of MBM was considered in [53], a major limitation of RF switches is that high-speed switching, low insertion loss, and good isolation are critical for efficient implementation. In [54, 55], MBM, which employs m_{rf} RF mirrors around a single antenna were considered for SIMO in the form of SIMO-MBM. A spectral efficiency of $\eta_{SIMO-MBM} = \log_2 M + m_{rf}$ bits/s/Hz can be achieved through this scheme. Furthermore, in [50], the spectral efficiency of SM η_{SM} has been improved by the application of m_{rf} RF mirrors in the form of spatial MBM (SMBM) from $\eta_{SM} = \log_2 M + \log_2 N_t$ bits/s/Hz to $\eta_{SM-MBM} = \log_2 M + \log_2 N_t + m_{rf}$ bits/s/Hz. In [54], MBM was investigated for generalized SM (GSM) in the form of GSM-MBM.

Fig. 3 represents a simplified model of an $N_r \times 1$ SIMO-MBM system having m_{rf} mirrors.

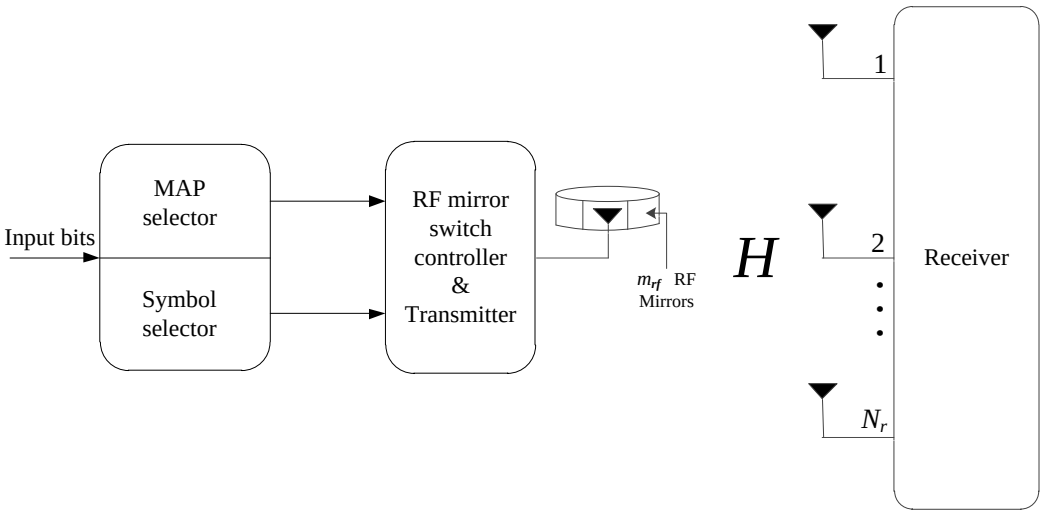

Fig. 3: System model of SIMO-MBM

The input bits of a SIMO-MBM system is split into two, such that $\log_2 M$ bits are employed to select a symbol x from a given APM constellation set. Another m_{rf} bits are employed to select a MAP from the available M_{rf} MAPs, which is activated during the transmission of x.

The received signal vector $\boldsymbol{y}$ may be represented as:

$$\boldsymbol{y} = \sqrt{\rho}\boldsymbol{H}\boldsymbol{e}_i x + \boldsymbol{n} \tag{24}$$

where $\boldsymbol{H}$ is an $N_r \times M_{rf}$ channel matrix, $\boldsymbol{e}_i$, $i \in [1 : M_{rf}]$ is an $M_{rf} \times 1$ vector, having the i-th element as unity, while other elements are zeros. Similar detector employed by the MIMO system can be applied for SIMO-MBM such as the MIMO detector in (3).

3.5 Closed-loop (adaptive) index modulation

In order to further improve the error performance of index modulated system, a closed-loop system is implemented. The closed-loop system implements certain algorithms based on perfect channel knowledge to improve error performance. For example, a closed-loop system to improve the error performance of SM based on optimal symbol modulation order was considered in [56], furthermore, an adaptive system based on constellation transformation algorithm has been presented in [45]. These systems have demonstrated superior error performance over their respective open-loop counterparts, viz; SM and STBC-SM. Based on this background, the motivation of this thesis is presented in the next section.

4 Research Motivation and Objectives

Traditional MIMO systems exploit spatial multiplexing to improve SIMO and SISO systems, however, IAS and ICI are major drawbacks of MIMO, because it employs more than one transmit antenna, hence, increasing the complexity of MIMO. SM [41], which was introduced to eliminate these drawbacks employs a single active antenna to transmit an APM symbol, with the transmit antenna conveying additional information through its index. Since a single active antenna is employed, the need for IAS is eliminated, while ICI is canceled. However, the logarithmic relationship between the number of transmit antennas of SM and its spectral efficiency $\delta_{SM} = \log_2 N_t + \log_2 M$ bits/s/Hz, limits the attractiveness of SM.

To improve the spectral efficiency of SM, GSM [35] and QSM [37, 38], have been proposed. In both cases, at least one transmit antenna is employed to transmit signals simultaneously. For example, in GSM [35], two transmit antennas independently transmit two separate symbols simultaneously, whereas, the indices of the transmit antenna pair are employed to convey additional information. Also, OFDM offers additional advantages, such as efficient usage of the available spectrum by allowing overlapping carrier frequencies, conversion of wideband into narrowband flat fading channels, elimination of ISI. Hence, the motivation to propose a MIMO multicarrier quadrature spatially modulated OFDM system in the form of QSM-OFDM. QSM-OFDM eliminates ISI and ICI by transmitting the in-phase and quadrature component separately through orthogonal carriers by different antennas simultaneously. The improvement offered by QSM-OFDM in terms of error performance/computational complexity is investigated and compared with SM-OFDM and other competing schemes. Several schemes which employ the OFDM technique have been considered in

the literature. For example, in [57], SM-OFDM has been investigated and found to outperform V-BLAST‘by 5 dB in the presence of Rician channel and 7 dB in the presence of spatial correlation. Furthermore, SM-OFDM for long term evoluation has been considered in [58], and is found to outperform V-BLAST-OFDM .

To improve the error performance of SIMO/classical MIMO, which employ a single time-slot for its transmission through diversity, a scheme, which employs two time-slots was introduced by Alamouti [11], in the form of STBC. Although it achieved the objective of improving the error performance, it has similar disadvantages as MIMO, viz; IAS and ICI. In [40], the advantages of SM and Alamouti STBC was integrated in the form of STBC-SM, to improve the error performance/spectral efficiency of SM and Alamouti STBC. Furthermore, the computational complexity of STBC-SM is significantly improved by employing the orthogonality of the Alamouti STBC codeword [40]. However, employing the orthogonality of the Alamouti STBC codewords is only applicable to quasi-static fading channels, where the fading coefficient for each of the two time-slots employed are assumed to be the same. To further improve the spectral efficiency of STBC-SM by exploiting the spatial domain, a cyclically rotated Alamouti STBC codeword has been proposed in [44], in the form of STBC-CSM. For STBC-CSM, the pair of symbols employed by the Alamouti codeword x_1 and x_2 are taken from two sets of APM constellations Ω_1, and a rotated version of Ω_1 given as $\Omega_2 = \Omega_1 e^{j\theta_k}$, where θ_k is the optimized rotation angle for the k-th codeword. The spectral efficiency offered by the spatial domain of STBC-CSM is $0.5 \log_2 c$ bits/s/Hz, where $c = \lfloor N_t(N_t - 1) \rfloor_{2p}$, whereas, $c = \lfloor \frac{N_t(N_t-1)}{2} \rfloor_{2p}$ for STBC-SM.

Although the spectral efficiency of STBC-SM is improved by STBC-CSM, there is reduction in error performance, as an increase in the number codewords for a given antenna increases the probability of error, which limits the advantage of this system. Furthermore, the computational complexity of the optimal STBC-CSM system, imposed by the ML detector, is significantly increased because of the exhaustive search over its entire codeword matrix. This makes it unattractive for modern wireless systems. Based on this motivation, this thesis investigates a low-complexity detector for STBC-CSM, which can be implemented for both quasi-static and fast fading channels. Furthermore, the expression for the union bound on the average bit error probability for the optimal ML detector is derived, of which, to the best of the author's knowledge, has not been presented in existing literature. Numerical results to validate the expression for the ABEP are presented, while the computational complexities for the optimal ML and the proposed low-complexity near-ML detectors are compared.

Several index modulated systems have been reported, which employ MBM to improve the capacity/link reliability of wireless systems, because of the various advantages it offers [49–55, 59]. For example, in [36], SSK as a form of index modulation, employs only one active transmit antenna

to convey information, with the transmitted tones as its constellations. Thus, eliminating ICI and the need for IAS, which are the well known limitations of MIMO. However, a large number of transmit antennas, which are needed to achieve higher data rates becomes a disadvantage for SSK. Furthermore, RF switches as a form of media-based index modulation, considered in [53], is criticized because of the switching speed, insertion loss, and isolation requirement, which are crucial parameters needed for its implementation.

More recently, RF mirrors as a form of MBM has become more attractive because of the ON/OFF status of the RF mirror, which create $M_{rf} = 2^{m_{rf}}$ distinct channel paths referred to as mirror activation patterns (MAPs), where m_{rf} is the number of RF mirrors associated with a given transmit antenna unit. The application of MBM to SIMO systems, in the form of SIMO-MBM has been considered in [54]. In SIMO-MBM, m_{rf} RF mirrors located around a single transmit antenna is able to achieve a spectral efficiency of $\eta_{SIMO-MBM} = \log_2 M + m_{rf}$ bits/s/Hz. Hence, improving the spectral efficiency of $\eta_{SIMO} = \log_2 M$ by m_{rf} bits/s/Hz. However, the limit to the number of RF mirrors that can be employed by a single transmit antenna unit becomes a disadvantage, as large number of RF mirrors becomes resource intensive, while training, which requires sending pilot signals is endangered due to channel-time variations [55]. Furthermore, GSM-MBM was proposed in [60], to improve the error performance/spectral efficiency of GSM, however, since it employs more than one RF chain, it faces similar challenges as MIMO, viz; ICI and IAS [49].

The attractiveness in employing RF mirrors has been demonstrated further, by improving the error performance/spectral efficiency of Alamouti STBC in space-time channel modulation (STCM) [59]. Furthermore, the application of MBM to uncoded space-time labeling diversity (USTLD) in the form of USTLD-STCM [42], to QSM in the form of quadrature channel modulation [61] and quadrature spatial MBM (QSMBM) [49] has demonstrated the effectiveness of RF mirrors to improve the error performance/spectral efficiency of wireless systems [51]. To this end, the author is motivated to investigate the application of MBM to improve the error performance and computational complexity of SM, in the form of SMBM. The expression for the union bound on ABEP of SMBM is formulated, which has not been presented in existing literature. Furthermore, this thesis proposes the application of MBM, which employs RF mirrors to improve the error performance of STBC-SM and STBC-CSM, employing an optimal ML detector in the form of media-based STBC-SM (MBSTBC-SM), and MBSTBC-SM with cyclic structure (MBSTBC-CSM). Furthermore, the effect of the different MAP configurations, similar to the MAP configurations in [59], are investigated for MBSTBC-SM/MBSTBC-CSM. The theoretical framework to characterize the union bound on the ABEP for the ML detector of MBSTBC-SM/MBSTBC-CSM is formulated, while numerical results

to validate the derived expression are presented. In order to reduce the computational complexity for the optimal ML detector of MBSTBC-SM/MBSTBC-CSM, a low-complexity near-ML detector, which employs orthogonal projection of signals is investigated for the proposed system.

One of the advantages of media-based index modulation is that, the MAPs comprise of good and bad channels, which are a subset of the M_{rf} MAPs. Hence, a subset of the available MAPSs can be selected to improve error performance [54]. Several antenna selection techniques have been presented in the literature. For example, in order to improve the performance of SM by exploiting transmit diversity, transmit antenna selection based on maximizing the minimum Euclidean distance of SM was considered in [62–64]. Furthermore, in [65], low computational complexity antenna selection scheme was investigated. For MAP optimization, Euclidean distance (ED) and mutual information-based selection techniques have been considered in [55, 60]. The drawback of employing the ED-MAP selection technique is that, the number of iterations employed by its search algorithm over all possible MAP enumerations are large. Hence, this thesis proposes two MAP optimized selection algorithms for SMBM.

5 Organization of Thesis

The thesis is grouped into three parts, which are organized as follows:

Part I Gives an introduction and layout of the thesis.

Part II The included papers, which have either been published, accepted for publication or under review with reputable peer reviewed journals/conference, which are approved by the department of higher education and training (DHET) South Africa are presented. Three journals and a conference paper are included in this part.

Part III The conclusion and possible future work is presented for this thesis.

6 Contributions of the Included Papers

6.1 Paper A: Quadrature Spatial Modulation Orthogonal Frequency Division Multiplexing (QSM-OFDM)

This paper has been accepted for publication with the following details:

B. S. Adejumobi and N. Pillay, "Quadrature Spatial Modulation Orthogonal Frequency", *Journal of Telecommunication, Electronic and Computer Engineering*, vol. 10, no. 4, Oct.-Dec. 2018.

This paper discusses the application of OFDM to QSM. The contributions of this paper are as follows:

a. An enhanced multi-carrier index modulation system in the form of QSM-OFDM is proposed, which yields an improved spectral efficiency/error performance.

b. The computational complexity of the proposed scheme is formulated and compared with competing schemes.

c. Numerical results to demonstrate the effectiveness of this scheme are presented and compared with competing schemes.

6.2 Paper B: Low-Complexity Detection for Space-Time Block Coded Spatial Modulation with Cyclic Structure

This paper has been published with the following details:

B. S. Adejumobi and N. Pillay, "Low-complexity detection for space-time block coded spatial modulation with cyclic structure" *Journal of Communications*, vol. 13, no. 7, Jul. 2018.

The contributions in this paper are as follows:

a. A low-complexity near-ML detector based on orthogonal projections of signals, that can be employed for quasi-static and fast frequency-flat Rayleigh fading channels, which yields a near-ML error performance is proposed.

b. A closed-form expression to evaluate the ABEP for the optimal ML detector of STBC-CSM is formulated.

c. An analytical framework to determine the computational complexity of ML and the proposed low-complexity near-ML detectors are presented.

d. Numerical results of Monte Carlo simulations to validate the ABEP expression for the ML detector and the effectiveness in terms of error performance of the low-complexity near-ML detector is presented.

6.3 Paper C: RF Mirror Media-Based Space-Time Block Coded Spatial Modulation Techniques for Two Time-slots

This paper is under review with "IET Communications". The contributions of this paper are as follows:

a. Index modulated media-based STBC-CSM/STBC-SM based on RF mirrors in the form of media-based STBC-SM (MBSTBC-SM) and media-based cyclically structured space-time block coded spatial modulation (MBSTBC-CSM) employing RF mirrors are proposed to improve the error performance of STBC-CSM and STBC-SM.

b. A closed-form expression to evaluate the union bound on ABEP of MBSTBC-CSM/MBSTBC-SM employing an optimal ML detector is presented.

c. A low-complexity near-ML detector for MBSTBC-CSM and MBSTBC-SM, which can be applied to quasi-static and fast frequency-flat Rayleigh fading channel is proposed.

d. Analysis of the computational complexities for the optimal ML and low-complexity near-ML detectors of MBSTBC-CSM and MBSTBC-SM are presented.

e. Numerical results to validate the expression of the ABEP for the optimal ML detector of MBSTBC-CSM and MBSTBC-SM employing different MAP configurations are presented, furthermore, results demonstrating the effects of the resolutions employed by the low-complexity near-ML detector are presented.

6.4 Paper D: A Study of Spatial Media-Based Modulation Using RF Mirrors

This conference paper has been published and the details are as follows:

B. S. Adejumobi, N. Pillay, and S. H. Mneney "A study of spatial media-based modulation using RF mirrors," in *Proceedings of IEEE AFRICON*, Sep. 2017, pp. 336-341.

This paper investigates the application of MBM to SM in the form of spatial MBM (SMBM) and presents the following contributions:

a. A theoretical ABEP bound for the ML detector of SMBM is formulated.

b. Numerical results from Monte Carlo simulations, are employed to validate the theoretical framework for the ABEP of SMBM, which were not in previous literature are presented SMBM.

c. Two low-complexity suboptimal MAP optimization techniques are proposed for a closed-loop SMBM system. Furthermore, the numerical results to demonstrate the effects of the proposed MAP optimization schemes are presented and discussed.

References

[1] E. Basar, "Index modulation techniques for 5G wireless networks," *IEEE Communications Magazine*, vol. 54, no. 7, pp. 168–175, Jul. 2016.

[2] X. Cheng, M. Zhang, M. Wen, and L. Yang, "Index modulation for 5G: Striving to do more with less," *IEEE Wireless Communications*, vol. 25, no. 2, pp. 126–132, Apr. 2018.

[3] S. Bahng, S. Shin, and Y. O. Park, "ML approaching MIMO detection based on orthogonal projection," *IEEE Communications Letters*, vol. 11, no. 6, pp. 474–476, Jun. 2007.

[4] S. E. Oladoyinbo, "Link adaptation for spatial modulation," Master's thesis, Unversity of KwaZulu-Natal, Durban, South Africa, 2016.

[5] F. Jameel, Faisal, M. A. A. Haider, and A. A. Butt, "Massive MIMO: A survey of recent advances, research issues and future directions," in *Proceedings of International Symposium on Recent Advances in Electrical Engineering (RAEE)*, Oct. 2017, pp. 1–6.

[6] J. Mietzner, R. Schober, L. Lampe, W. H. Gerstacker, and P. A. Hoeher, "Multiple-antenna techniques for wireless communications - a comprehensive literature survey," *IEEE Communications Surveys Tutorials*, vol. 11, no. 2, pp. 87–105, Apr.-Jun. 2009.

[7] RF Wireless World. (2012) Advantages of MIMO | disadvantages of MIMO. [Online]. Available: http://www.rfwireless-world.com/Terminology/Advantages-and-Disadvantages-of-MIMO.html

[8] L. Zheng and D. N. C. Tse, "Diversity and multiplexing: a fundamental tradeoff in multiple-antenna channels," *IEEE Transactions on Information Theory*, vol. 49, no. 5, pp. 1073–1096, May 2003.

[9] G. J. Foschini, "Layered space-time architecture for wireless communication in a fading environment when using multi-element antennas," *Bell Labs Technical Journal*, vol. 1, no. 2, pp. 41–59, Autumn 1996.

[10] S. N. Diggavi, N. Al-Dhahir, A. Stamoulis, and A. R. Calderbank, "Great expectations: the value of spatial diversity in wireless networks," *Proceedings of the IEEE*, vol. 92, no. 2, pp. 219–270, Feb. 2004.

[11] S. M. Alamouti, "A simple transmit diversity technique for wireless communications," *IEEE Journal on Selected Areas in Communications*, vol. 16, no. 8, pp. 1451–1458, Oct. 1998.

[12] V. Tarokh, H. Jafarkhani, and A. R. Calderbank, "Space-time block coding for wireless communications: performance results," *IEEE Journal on Selected Areas in Communications*, vol. 17, no. 3, pp. 451–460, Mar. 1999.

[13] J. Jeganathan, A. Ghrayeb, and L. Szczecinski, "Spatial modulation: optimal detection and performance analysis," *IEEE Communications Letters*, vol. 12, no. 8, pp. 545–547, Aug. 2008.

[14] E.Telatar, "Capacity of multi-antenna Gaussian channels," *European Transactions on Telecommunications*, vol. 10, no. 6, pp. 585–595, 1999.

[15] S. U. Hwang, S. Jeony, J. Choi, and J. Seo, "A layered spatial modulation technique for MIMO-OFDM systems," in *Proceedings of IEEE International Symposium on Broadband Multimedia Systems and Broadcasting (BMSB)*, Mar. 2010, pp. 1–5.

[16] A. Sibille, C. Oestges, and A. Zanella, *MIMO: from theory to implementation*. Academic Press, 2010.

[17] F. Li, "Performance analysis of V-BLAST detectors for the MIMO channel," *KTH Electrical Engineering*, 2007.

[18] P. W. Wolniansky, G. J. Foschini, G. D. Golden, and R. A. Valenzuela, "V-BLAST: an architecture for realizing very high data rates over the rich-scattering wireless channel," in *Proceedings of International Symposium on Signals, Systems, and Electronics*, Sep. 1998, pp. 295–300.

[19] D. Wubben, R. Bohnke, V. Kuhn, and K. D. Kammeyer, "MMSE extension of V-BLAST based on sorted QR decomposition," in *Proceedings of IEEE 58th Vehicular Technology Conference. VTC 2003-Fall (IEEE Cat. No.03CH37484)*, vol. 1, Oct. 2003, pp. 508–512.

[20] Y. S. Cho, J. Kim, W. Y. Yang, and C. G. Kang, *MIMO-OFDM wireless communications with MATLAB*. John Wiley & Sons, 2010.

[21] C. Y. Ma, C. Y. Wu, and C. C. Huang, "A simple ICI suppression method utilizing cyclic prefix for OFDM systems in the presence of phase noise," *IEEE Transactions on Communications*, vol. 61, no. 11, pp. 4539–4550, Nov. 2013.

[22] X.-G. Xia, "Precoded and vector OFDM robust to channel spectral nulls and with reduced cyclic prefix length in single transmit antenna systems," *IEEE Transactions on Communications*, vol. 49, no. 8, pp. 1363–1374, Aug. 2001.

[23] C. Ni, Y. Ma, and T. Jiang, "A novel adaptive tone reservation scheme for PAPR reduction in large-scale multi-user MIMO-OFDM systems," *IEEE Wireless Communications Letters*, vol. 5, no. 5, pp. 480–483, Oct. 2016.

[24] D. Lee, "MIMO OFDM channel estimation via block stagewise orthogonal matching pursuit," *IEEE Communications Letters*, vol. 20, no. 10, pp. 2115–2118, Oct. 2016.

[25] C. Studer and E. G. Larsson, "PAR-aware large-scale multi-user MIMO-OFDM downlink," *IEEE Journal on Selected Areas in Communications*, vol. 31, no. 2, pp. 303–313, Feb. 2013.

[26] R. O'Neill and L. B. Lopes, "Envelope variations and spectral splatter in clipped multicarrier signals," in *Proceedings of 6th International Symposium on Personal, Indoor and Mobile Radio Communications*, vol. 1, Sep. 1995, pp. 71–75.

[27] A. E. Jones, T. A. Wilkinson, and S. K. Barton, "Block coding scheme for reduction of peak to mean envelope power ratio of multicarrier transmission schemes," *Electronics Letters*, vol. 30, no. 25, pp. 2098–2099, Dec. 1994.

[28] S. H. Muller and J. B. Huber, "OFDM with reduced peak-to-average power ratio by optimum combination of partial transmit sequences," *Electronics Letters*, vol. 33, no. 5, pp. 368–369, Feb. 1997.

[29] T. H. Liu, "Analysis of the Alamouti STBC MIMO system with spatial division multiplexing over the Rayleigh fading channel," *IEEE Transactions on Wireless Communications*, vol. 14, no. 9, pp. 5156–5170, Sep. 2015.

[30] H. Jafarkhani, *Space-time coding: theory and practice*. Cambridge university press, 2005.

[31] M. K. Arti, "OSTBC transmission in large MIMO systems," *IEEE Communications Letters*, vol. 20, no. 11, pp. 2308–2311, Nov. 2016.

[32] M. H. Halmi, M. Abdellatif, and N. Nooridin, "Orthogonal space-time block codes for large MIMO systems," in *Proceedings of International Conference on Communications, Management and Telecommunications (ComManTel)*, Dec. 2015, pp. 78–82.

[33] E. Basar, M. Wen, R. Mesleh, M. D. Renzo, Y. Xiao, and H. Haas, "Index modulation techniques for next-generation wireless networks," *IEEE Access*, vol. 5, pp. 16 693–16 746, 2017.

[34] A. Younis, N. Serafimovski, R. Mesleh, and H. Haas, "Generalised spatial modulation," in *Proceedings of the Forty Fourth Asilomar Conference on Signals, Systems and Computers*, Nov. 2010, pp. 1498–1502.

[35] J. Wang, S. Jia, and J. Song, "Generalised spatial modulation system with multiple active transmit antennas and low complexity detection scheme," *IEEE Transactions on Wireless Communications*, vol. 11, no. 4, pp. 1605–1615, Apr. 2012.

[36] J. Jeganathan, A. Ghrayeb, L. Szczecinski, and A. Ceron, "Space shift keying modulation for MIMO channels," *IEEE Transactions on Wireless Communications*, vol. 8, no. 7, pp. 3692–3703, Jul. 2009.

[37] R. Mesleh, S. S. Ikki, and H. M. Aggoune, "Quadrature spatial modulation," *IEEE Transactions on Vehicular Technology*, vol. 64, no. 6, pp. 2738–2742, Jun. 2015.

[38] A. Afana, R. Mesleh, S. Ikki, and I. E. Atawi, "Performance of quadrature spatial modulation in amplify-and-forward cooperative relaying," *IEEE Communications Letters*, vol. 20, no. 2, pp. 240–243, Feb. 2016.

[39] R. Mesleh, S. S. Ikki, and O. S. Badarneh, "Impact of cochannel interference on the performance of quadrature spatial modulation MIMO systems," *IEEE Communications Letters*, vol. 20, no. 10, pp. 1927–1930, Oct. 2016.

[40] E. Basar, U. Aygolu, E. Panayirci, and H. V. Poor, "Space-time block coded spatial modulation," *IEEE Transactions on Communications*, vol. 59, no. 3, pp. 823–832, Mar. 2011.

[41] R. Y. Mesleh, H. Haas, S. Sinanovic, C. W. Ahn, and S. Yun, "Spatial modulation," *IEEE Transactions on Vehicular Technology*, vol. 57, no. 4, pp. 2228–2241, Jul. 2008.

[42] K. Govindasamy, H. Xu, and N. Pillay, "Space-time block coded spatial modulation with labeling diversity," *International Journal of Communication Systems*, vol. 31, no. 1, 2017.

[43] H. Xu and N. Pillay, "Simple near-maximum-likelihood low-complexity detection scheme for Alamouti space-time block coded spatial modulation," *IET Communications*, vol. 8, no. 15, pp. 2611–2618, Oct. 2014.

[44] X. Li and L. Wang, "High rate space-time block coded spatial modulation with cyclic structure," *IEEE Communications Letters*, vol. 18, no. 4, pp. 532–535, Apr. 2014.

[45] F. Chen, F. Zha, and H. Zhang, "Adaptive space-time block coded spatial modulation algorithm based on constellation transformation," *Journal of Communications*, vol. 11, no. 11, pp. 1020–1027, Nov. 2016.

[46] B. S. Adejumobi and N. Pillay, "Low-complexity detection for space-time block coded spatial modulation with cyclic structure," *Journal of Communications*, vol. 13, no. 7, p. early access, Jul. 2018.

[47] A. G. Helmy, M. D. Renzo, and N. Al-Dhahir, "Enhanced-reliability cyclic generalized spatial-and-temporal modulation," *IEEE Communications Letters*, vol. 20, no. 12, pp. 2374–2377, Dec. 2016.

[48] ——, "Differential spatially modulated space-time block codes with temporal permutations," *IEEE Transactions on Vehicular Technology*, vol. 66, no. 8, pp. 7548–7552, Aug. 2017.

[49] N. Pillay and H. Xu, "Quadrature spatial media-based modulation with RF mirrors," *IET Communications*, vol. 11, no. 16, pp. 2440–2448, 2017.

[50] B. S. Adejumobi, N. Pillay, and S. H. Mneney, "A study of spatial media-based modulation using RF mirrors," in *Proceedings of IEEE AFRICON*, Sep. 2017, pp. 336–341.

[51] N. Pillay and H. Xu, "Uncoded space-time labeling diversity -Application of media-based modulation with RF mirrors," *IEEE Communications Letters*, vol. 22, no. 2, pp. 272–275, Feb. 2018.

[52] A. K. Khandani, "Media-based modulation: A new approach to wireless transmission," in *Proceedings of IEEE International Symposium on Information Theory*, Jul. 2013, pp. 3050–3054.

[53] Z. Bouida, H. El-Sallabi, A. Ghrayeb, and K. A. Qaraqe, "Reconfigurable antenna-based space-shift keying (SSK) for MIMO Rician channels," *IEEE Transactions on Wireless Communications*, vol. 15, no. 1, pp. 446–457, Jan. 2016.

[54] Y. Naresh and A. Chockalingam, "On media-based modulation using RF mirrors," *IEEE Transactions on Vehicular Technology*, vol. 66, no. 6, pp. 4967–4983, Jun. 2017.

[55] E. Seifi, M. Atamanesh, and A. K. Khandani, "Media-based modulation: A new frontier in wireless communications," 2015.

[56] P. Yang, Y. Xiao, Y. Yu, and S. Li, "Adaptive spatial modulation for wireless mimo transmission systems," *IEEE Communications Letters*, vol. 15, no. 6, pp. 602–604, Jun. 2011.

[57] S. Ganesan, R. Mesleh, H. Ho, C. W. Ahn, and S. Yun, "On the performance of spatial modulation ofdm," in *Fortieth Asilomar Conference on Signals, Systems and Computers*, Oct 2006, pp. 1825–1829.

[58] P. Yang, Y. Xiao, B. Zhou, and S. Li, "Initial performance evaluation of spatial modulation ofdm in lte-based systems," in *6th International ICST Conference on Communications and Networking in China (CHINACOM)*, Aug 2011, pp. 102–107.

[59] E. Basar and I. Altunbas, "Space-time channel modulation," *IEEE Transactions on Vehicular Technology*, vol. 66, no. 8, pp. 7609–7614, Aug. 2017.

[60] Y. Naresh and A. Chockalingam, "On media-based modulation using RF mirrors," in *Proceedings of Information Theory and Applications Workshop (ITA)*, Jan. 2016, pp. 1–10.

[61] I. Yildirim, E. Basar, and I. Altunbas, "Quadrature channel modulation," *IEEE Wireless Communications Letters*, vol. 6, no. 6, pp. 790–793, Dec. 2017.

[62] R. Rajashekar, K. V. S. Hari, and L. Hanzo, "Quantifying the transmit diversity order of euclidean distance based antenna selection in spatial modulation," *IEEE Signal Processing Letters*, vol. 22, no. 9, pp. 1434–1437, Sep. 2015.

[63] P. Yang, Y. Xiao, L. Li, Q. Tang, Y. Yu, and S. Li, "Link adaptation for spatial modulation with limited feedback," *IEEE Transactions on Vehicular Technology*, vol. 61, no. 8, pp. 3808–3813, Oct. 2012.

[64] N. Pillay and H. Xu, "Comments on "antenna selection in spatial modulation systems"," *IEEE Communications Letters*, vol. 17, no. 9, pp. 1681–1683, Sep. 2013.

[65] ——, "Low-complexity transmit antenna selection schemes for spatial modulation," *IET Communications*, vol. 9, no. 2, pp. 239–248, 2015.

Part II

Included Papers

Paper A

Quadrature Spatial Modulation Orthogonal Frequency Division Multiplexing

Babatunde S. Adejumobi and Narushan Pillay

Published

Journal of Telecommunication, Electronic and Computer Engineering Journal

Abstract

This paper investigates the application of quadrature spatial modulation (QSM) to orthogonal frequency division multiplexing (OFDM). In comparison to spatial modulation OFDM (SM-OFDM), the proposed QSM-OFDM achieves an enhanced spectral efficiency by decomposing the amplitude and/or phase modulated signal into its real and imaginary components as the transmitted symbols. The index/indices of the activated transmit antenna(s) are employed to convey additional information. These symbols are transmitted orthogonally to eliminate inter-channel interference with little trade-off in synchronization. The average bit error probability for QSM-OFDM and other schemes, including the SM-OFDM, conventional multiple-input multiple-output (MIMO-OFDM), maximal-ratio combining single-input multiple-output (MRC-OFDM), vertical Bell Laboratories layered space-time architecture (VBLAST-OFDM) and Alamouti-OFDM systems are demonstrated using Monte Carlo simulation. The expressions for the receiver computational complexities in terms of the number of real operations are further derived. QSM-OFDM yields a significant signal-to-noise ratio gain of $\approx$ 5 *dB with little trade-off in computational complexity over SM-OFDM, while substantial gains greater than* 5 *dB are evident, when compared to MIMO-OFDM, MRC-OFDM, and ALAMOUTI-OFDM.*

1 Introduction

Recent applications have placed a great demand for high data rates and spectrally efficient systems with extremely low error rates; hence, the rapid growth in research areas that can improve future wireless systems in terms of capacity and link reliability. In traditional wireless communication systems, designers have resorted to employing high-order modulation schemes, such as $(M \geq 64)$ M-ary quadrature amplitude modulation (MQAM) to increase spectral efficiency. However, it becomes disadvantageous when high-order MQAM $(M \geq 16)$ is used, because of channel fading and the additive noise from the wireless equipment [1]. The use of multiple-input multiple-output (MIMO) antenna arrangements, such as in WiMAX, HSPA, IEEE 802.11ac, etc., when combined with spatial multiplexing has become a very promising technique in achieving reliable and spectrally efficient communications [2]. An example is the Bell Laboratories layered space-time architecture (BLAST), where the transceiver architecture is designed, such that independent data is simultaneously transmitted employing different antennas, thereby leading to an increase in multiplexing gain [3].

MIMO can also be used to reduce error rates by simultaneously transmitting identical data from multiple antennas as in space-time coding/space-frequency coding [4]. This is performed in order to exploit the advantage of having multiple received signals, which arrive at the receiver along different pathways. MIMO increases the transmit diversity and ensures reliability as well as a sufficient quality of service. As noted in [5], MIMO systems such as BLAST, suffer from high inter-channel interference (ICI) as a result of the simultaneous transmissions from multiple antennas. Furthermore, due to high ICI, computational complexity in MIMO systems increases because of the need for complex receiver algorithms. The complexity cannot be reduced without a trade-off in the error performance of the system. In order to deal with the limitations offered by conventional MIMO systems mentioned earlier, spatial modulation (SM) [5, 6], generalized SM (GSM) [7], space shift keying (SSK) [8], generalized SSK (GSSK) [9] and generalized differential scheme for SM systems [10], were introduced as promising techniques to alleviate these limitations.

In SM, since only a single transmit antenna is activated at a given instant of time [5, 10], this helps in eliminating ICI. The need for synchronization amongst the transmit antennas, as well as the complexity of detection at the receiver is reduced as SM utilizes a single radio frequency (RF) chain [11]. Comparing SM to other conventional MIMO techniques, it has been observed that SM techniques improve error rates even with limited transmit antennas, and are robust in dealing with channel imperfections [5]. SM systems [5, 6, 10], improve spectral efficiency by exploiting the index of the activated transmit antenna, to convey additional information. Employing a single antenna eliminates ICI as well as the need for synchronization at the transmitter. However, a major limitation of SM is that, the spectral efficiency does not increase linearly with the total number of transmitting antennas as in the case of vertical-BLAST (VBLAST). In GSM and GSSK [7, 9], more than one antenna is allowed to transmit different symbols, using the antenna indices as a spatial constellation in the spatial domain but is found to be inferior to SM and SSK in terms of error performance. This is further improved in bi-space shift keying (Bi-SSK) modulation [12], such as to improve the throughput of the low-complexity receiver of the SSK system, with little trade-off in the error performance. In [13], SM technique, which employ two time-slots, to transmit two symbols in each time-slot, has been considered. however, the complexity of the detection is significantly increased, when the ML detector is applied.

In 2006, Ganesan et al. [14] proposed a scheme, where SM is combined with OFDM. This is done, such as to produce a spectrally enhanced, efficient multicarrier system, which is robust to channel imperfections [5, 14] and yields an improved error performance [1]. The advantage of OFDM arises because the wireless channel is divided into several narrowband, low-rate, frequency non-selective

subcarriers, which allows for the parallel simultaneous transmission of multiple symbols [15]. SM-OFDM utilizes the SM mapping style, where a group of information bits is mapped into an amplitude and/phase modulation (APM) symbol and a particular transmit antenna, which is then transmitted using the MIMO-OFDM system [1]; such that, both the activated transmit antenna and the APM symbols, are used to convey information [1, 5, 14]. The SM-OFDM scheme was tested for two different channel conditions; viz. Rician fading channel, and a combined effect of spatially correlated (SC) and mutually coupled (MC) channels. Furthermore, Mesleh et al. established the combined effect of all the three channels in [14]. Hwang et al. demonstrated the error performance of SM-OFDM using a soft-output maximum-likelihood (ML) detector [1]. In [16], precoders were utilized to improve error performance in SM-OFDM. Although SM-OFDM yields a significant improvement in error performance over existing schemes, there is still room for improvement.

A new technique of quadrature spatial modulation (QSM), proposed in [17] to improve the throughput of SM, was achieved by extending the spatial constellations of SM to the in-phase and quadrature components by utilizing methods as in [5, 7, 12]. One of the antennas is made to transmit the real part of the modulated symbol, while a second antenna transmits the imaginary part of the modulated symbol [17]. ICI is eliminated, since the data being transmitted is orthogonal and the modulation of the data is performed both on the real and imaginary parts of the carrier [17, 18]. For example, in [19], antenna selection of QSM has been considered, however, the authors did not considered the application of a multicarrier QSM.

Motivated by the above, the contributions in this paper are as follows:

a. The design of an enhanced multi-carrier modulation system, which improves the spectral efficiency/error performance of SM-OFDM in the form of QSM-OFDM is proposed. This is achieved by integrating the OFDM technology [20, 21], with QSM. QSM-OFDM eliminates ICI and ISI, which are well-known limitations of MIMO.

b. The expressions for the computational complexities in terms of the number of real operations performed, are formulated for the proposed scheme and competing schemes.

c. Employing Monte Carlo simulations, numerical results to demonstrate the effectiveness of the proposed scheme are presented.

The remaining parts of this paper are organized as follows: Section 2 addresses the design of the QSM-OFDM system model. Section 3 analyzes the computational complexities associated with the different schemes under comparison, while the simulation results as well as related discussions are presented in Section 4 . Finally, Section 5 provides necessary conclusions and recommendations.

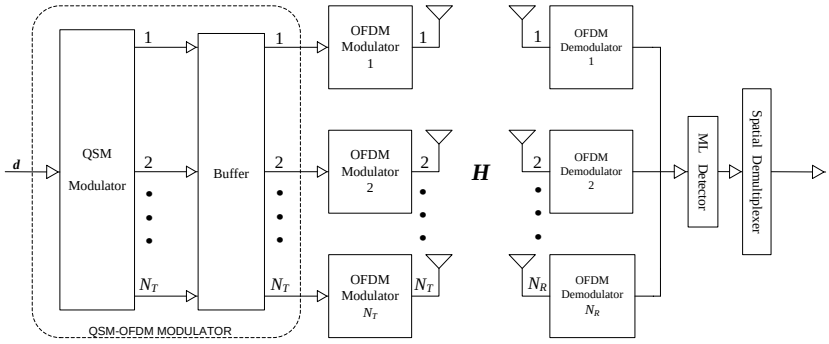

Fig. A.1: System model of the proposed QSM-OFDM

Notation: The following notations are employed throughout this paper; bold and capital letters represent matrices, while bold small letters denote column vectors of matrices. Letters with subscript or superscript, such as $(\cdot)_{\Re}$ and $(\cdot)_{\Im}$ represents vectors or variables for real and imaginary parts, respectively. Other notations include $(\cdot)^T$, $(\cdot)^H$, $(\cdot)^{-1}$, $(\cdot)^{\dagger}$, $\| \cdot \|_F$, $\Re(\cdot)$ and $\otimes$, which represent transpose, Hermitian, inverse, time domain signal, Frobenius norm, real part of a complex variable and time convolution, respectively. Throughout this paper, N_t, N_r and M shall represent the number of transmit antennas, the number of receive antennas and the MQAM modulation order, respectively. $i = \sqrt{-1}$ represents a complex number.

2 QSM-OFDM

2.1 The QSM-OFDM Transmitter

A generalized block diagram for the system model of the proposed QSM-OFDM is shown in Fig. A.1. The QSM modulator in Fig. A.1, is similar to the QSM modulator in [17].

In QSM-OFDM, the input bit stream $\boldsymbol{d}$ having $N_{FFT}\log_2(MN_t^2)$ bits, entering the QSM-OFDM modulator is rearranged into a $q \times N_{FFT}$ binary matrix $\boldsymbol{C}(k)$, which is represented as:

$$\boldsymbol{C}(k) = \begin{bmatrix} C_{1,1} & C_{1,2} & \cdots & C_{1,q} \\ C_{2,1} & C_{2,2} & \cdots & C_{2,q} \\ \vdots & \vdots & \ddots & \vdots \\ C_{N_{FFT},1} & C_{N_{FFT},2} & \cdots & C_{N_{FFT},q} \end{bmatrix} \tag{A.1}$$

where N_{FFT} is the total number of OFDM subcarriers, which is determined by the size of the fast Fourier transform (FFT) employed, q is the total number of bits per subcarrier for a given OFDM symbol of the size $\log_2(MN_t^2)$. The bit splitter of the QSM modulator splits each row (subcarrier)

Table A.1: Grouping of input bits for the proposed QSM-OFDM

Subcarrier	Grouping	Symbol	Real	Imaginary
p	$c_1\ c_2 \ldots\ c_q$	bits	bits	bits
1	1 1 1 1 1 1	11	11	11
2	0 0 0 0 0 1	00	00	01
3	1 0 1 1 0 0	10	11	00
$\vdots$	$\vdots$	$\vdots$	$\vdots$	$\vdots$
N_{FFT}	1 0 0 1 1 1	10	01	11

of the q bits into three different subgroups as shown in Table A.1, using a 4×4 transceiver system with 4QAM for illustration. Firstly, $\log_2(M)$ bits are used to select an MQAM symbol for the p-th subcarrier, x_p^m, $m \in [1 : M]$ and $p \in [1 : N_{FFT}]$.

Another $\log_2(N_t)$ bits are employed to select the $\ell_{\Re p}$-th antenna for transmitting the real part of the complex variable x_p^m of the p-th subcarrier, and the third subgroup of $\log_2(N_t)$ bits are employed to select the $\ell_{\Im p}$-th antenna for transmitting the imaginary part of the complex variable x_p^m of the p-th subcarrier, where $\ell_{\Re p}, \ell_{\Im p} \in [1 : N_t]$. The bit processing of Table A.1 is presented in Table A.2.

The symbol x_p^m is further decomposed into its real $x_p^{m,\Re}$ and imaginary $x_p^{m,\Im}$ components, such that:

$$x_p^m = x_p^{m,\Re} + i x_p^{m,\Im} \tag{A.2}$$

These components are then mapped to form the vectors for the N_t OFDM symbols of the p-th subcarrier, such that:

Table A.2: Outputs from the QSM modulator

p	4QAM symbol	Spatial symbol		Activated antenna		$\boldsymbol{x}^p_{QSM-OFDM}$
	x_p^m	$x_p^{m,\Re}$	$ix_p^{m,\Im}$	$\ell_{\Re_p}$	$\ell_{\Im_p}$	
1	$+1+i$	$+1$	$+i$	4	4	$\begin{bmatrix}0 & 0 & 0 & 1+i\end{bmatrix}$
2	$-1-i$	-1	$-i$	1	2	$\begin{bmatrix}-1 & -i & 0 & 0\end{bmatrix}$
3	$+1-i$	$+1$	$-i$	4	1	$\begin{bmatrix}-i & 0 & 0 & 1\end{bmatrix}$
$\vdots$	$\vdots$	$\vdots$	$\vdots$	$\vdots$	$\vdots$	$\vdots$
N_{FFT}	$+1-i$	$+1$	$-i$	2	4	$\begin{bmatrix}0 & 1 & 0 & -i\end{bmatrix}$

$$\boldsymbol{x}^{p}_{QSM-OFDM} = \boldsymbol{x}^{m,\Re}_{\ell_{\Re p}} + \boldsymbol{x}^{m,\Im}_{\ell_{\Im p}} \tag{A.3}$$

where $\boldsymbol{x}^{m,\Re}_{\ell_{\Re p}}$ and $\boldsymbol{x}^{m,\Im}_{\ell_{\Im p}}$ are $N_t \times 1$ vectors with $x^{m,\Re}_{p}$ and $ix^{m,\Im}_{p}$ as the non-zero entry placed at the $\ell_{\Re p}$-th and $\ell_{\Im p}$-th positions, respectively, for the p-th subcarrier, $p \in [1 : N_{FFT}]$. The outputs from the QSM modulator $\boldsymbol{x}^{p}_{QSM-OFDM}$, when $\ell_{\Re p} \neq \ell_{\Im p}$ is of the form represented as:

$$\boldsymbol{x}^{p}_{QSM-OFDM} = \begin{bmatrix} 0 \cdots 0 & \underbrace{x^{m,\Re}_{p}}_{\ell_{\Re}\text{-th position}} & 0 \cdots 0 & \underbrace{ix^{m,\Im}_{p}}_{\ell_{\Im}\text{-th position}} & 0 \cdots 0 \end{bmatrix}^{T} \tag{A.4}$$

and when $\ell_{\Re} = \ell_{\Im}$, $\boldsymbol{x}^{p}_{QSM-OFDM}$ takes the form:

$$\boldsymbol{x}^{p}_{QSM-OFDM} = \begin{bmatrix} 0 & \cdots & 0 & \underbrace{x^{m,\Re}_{p} + ix^{m,\Im}_{p}}_{\ell_{\Re}=\ell_{\Im}\text{-th position}} & 0 & \cdots & 0 \end{bmatrix}^{T} \tag{A.5}$$

The outputs of the QSM modulator $\boldsymbol{x}^{p}_{QSM-OFDM}$, for $p \in [1 : N_{FFT}]$, is buffered in order to stack N_{FFT} values of $\boldsymbol{x}^{p}_{QSM-OFDM}$ to form matrix $\boldsymbol{J}$, such that $\boldsymbol{J}$ is an $N_t \times N_{FFT}$ frequency domain matrix represented as:

$$\boldsymbol{J} = \begin{bmatrix} j_1[1] & j_1[2] & \cdots & j_1[N_{FFT}] \\ j_2[1] & j_2[2] & \cdots & j_2[N_{FFT}] \\ \vdots & \vdots & \ddots & \vdots \\ j_{N_t}[1] & j_{N_t}[2] & \cdots & j_{N_t}[N_{FFT}] \end{bmatrix} \tag{A.6}$$

where each column p, of matrix $\boldsymbol{J}$ represents the data to be transmitted on the p-th subcarrier, while each row ℓ of matrix $\boldsymbol{J}$ is the OFDM symbol to be transmitted by the ℓ-th antenna, $\ell \in [1 : N_t]$. For example, $j_\ell[p]$ is the data on the p-th subcarrier of the ℓ-th OFDM symbol and will be transmitted employing the ℓ-th antenna.

The OFDM modulator processes the signal in order to obtain the complex baseband time domain signals by performing an inverse FFT (IFFT), which may be expressed as:

$$\boldsymbol{x}^{\dagger}_{\ell}(t) = \frac{1}{\sqrt{N_{FFT}}} \sum_{p=0}^{N_{FFT}-1} \boldsymbol{J}_{\ell}(p)\, e^{i\frac{2\pi tp}{N_{FFT}}},\ 0 \leq t \leq N_{FFT} - 1 \tag{A.7}$$

where $\boldsymbol{x}^{\dagger}_{\ell}(t)$ is the time domain signal obtained at the t-th time interval of the ℓ-th antenna. This process is followed by the addition of a cyclic prefix (CP) in order to eliminate inter-symbol interference (ISI) before the onward simultaneous transmission by N_t transmit antennas via the MIMO channel $\boldsymbol{H}$.

2.2 The QSM-OFDM Receiver

At the receiver, the transmitted data encounters the additive white Gaussian noise (AWGN). The received time domain signal vector $\boldsymbol{y}_l^{\dagger}(t)$, $l \in [1 : N_r]$, at any time t, for a single subcarrier may be represented as:

$$\boldsymbol{y}_l^{\dagger}(t) = \boldsymbol{H}^{\dagger}(t,\tau) \otimes \boldsymbol{x}_{\ell}^{\dagger}(t) + \boldsymbol{w}_l^{\dagger}(t) \tag{A.8}$$

where $\boldsymbol{H}^{\dagger}(t,\tau)$ is the time domain multipath Rayleigh fading channel matrix with a delay spread τ arriving at time t. The frequency flat multipath Rayleigh fading distribution channel matrix representation of $\boldsymbol{H}^{\dagger}(t,\tau)$ at any time t, for the p-th subcarrier may be defined as:

$$\boldsymbol{H}_p = \begin{bmatrix} h_{1,1} & h_{1,2} & \cdots & h_{1,N_t} \\ h_{2,1} & h_{2,2} & \cdots & h_{2,N_t} \\ \vdots & \vdots & \ddots & \vdots \\ h_{N_r,1} & h_{N_r,2} & \cdots & h_{N_r,N_t} \end{bmatrix} \tag{A.9}$$

and $\boldsymbol{w}_l^{\dagger}(t)$ is the $N_r \times 1$ AWGN vector, whose entries are i.i.d. random variables with Gaussian distribution $CN(0,\ \sigma_W^2)$.

The received time domain signal $\boldsymbol{y}_l^{\dagger}(t)$ is demodulated by employing a bank of N_r OFDM demodulators, while the OFDM demodulator removes the CP and performs the FFT operation. The frequency domain output for a single subcarrier may be represented as:

$$\boldsymbol{y}_p = \sqrt{\rho}\left(\boldsymbol{h}_{\ell_{\Re}}^p x_{\Re}^p + i\boldsymbol{h}_{\ell_{\Im}}^p x_{\Im}^p\right) + \boldsymbol{w}_p \tag{A.10}$$

where $\boldsymbol{y}_p$, $p \in [1 : N_{FFT}]$ is the frequency domain vector of the received signal for the p-th subcarrier of the OFDM symbol, $\boldsymbol{h}_{\ell_{\Re}}^p = [h_{1,\ell_{\Re}}^p\ h_{2,\ell_{\Re}}^p\ \ldots\ h_{N_r,\ell_{\Re}}^p]^T$ represents the $N_r \times 1$ $\ell_{\Re}$-th column of the frequency response channel matrix $\boldsymbol{H}_p$ for the real variables of the p-th subcarrier of the OFDM symbol. $\boldsymbol{h}_{\ell_{\Im}}^p = [h_{1,\ell_{\Im}}^p\ h_{2,\ell_{\Im}}^p\ \ldots\ h_{N_r,\ell_{\Im}}^p]^T$ is the $N_r \times 1$ $\ell_{\Im}$-th column of the frequency response of the channel matrix $\boldsymbol{H}_p$, for the imaginary variables of the p-th subcarrier of the OFDM. $x_{\Re}^p$ and $x_{\Im}^p$ represent the real and imaginary complex variables, respectively, of the symbol-under-test by the ML detector, such as to determine the correct estimate of the received signal, and $\boldsymbol{w}_p$ is the AWGN for the p-th subcarrier of the OFDM symbol, whose entries are i.i.d. with a distribution of $CN(0,\sigma^2)$. $\rho = \frac{E_s}{N_t}$, and E_s is the energy of the transmitted symbol. The receiver implements a joint

ML detection scheme over all possible symbols with the assumption that perfect knowledge of the channel is known. The equation for the joint ML detector as it applies to QSM-OFDM adopted from [17] may be represented as:

$$\left[\hat{\ell}_{\Re}, \hat{\ell}_{\Im}, \hat{u}_{\Re}, \hat{u}_{\Im}\right] = \underset{\substack{\ell_{\Re},\ell_{\Im}\in[1:N_t],\\ u_{\Re},u_{\Im}\in[1:M]}}{\operatorname{argmin}} \left(\left\| \boldsymbol{y}_p - \sqrt{\rho}\left(\boldsymbol{h}^p_{\ell_{\Re}} x^p_{\Re} + i\boldsymbol{h}^p_{\ell_{\Im}} x^p_{\Im} \right) \right\|^2_F \right) \tag{A.11}$$

where $\hat{\ell}_{\Re}$ and $\hat{\ell}_{\Im}$, $\hat{\ell}_{\Re}, \hat{\ell}_{\Im} \in [1 : N_t]$ are the detected antenna indices for the antennas transmitting the real and imaginary symbols for the p-th subcarrier, respectively, and $\hat{u}_{\Re}$ and $\hat{u}_{\Im}$, $\hat{u}_{\Re}, \hat{u}_{\Im} \in [1 : M]$ are the detected estimates for the real and the imaginary symbols $u_{\Re}$ and $u_{\Im}$ for the p-th subcarrier. A further simplification of (A.11) gives:

$$\left[\hat{\ell}_{\Re}, \hat{\ell}_{\Im}, \hat{u}_{\Re}, \hat{u}_{\Im}\right] = \underset{\substack{\ell_{\Re},\ell_{\Im}\in[1:N_t],\\ u_{\Re},u_{\Im}\in[1:M]}}{\operatorname{argmin}} \left(\|\boldsymbol{g}\|^2_F - 2\Re(\boldsymbol{y}_p{}^H \boldsymbol{g}) \right) \tag{A.12}$$

where $\boldsymbol{g} = \sqrt{\rho}\left(\boldsymbol{h}^p_{\ell_{\Re}} x^p_{\Re} + i\boldsymbol{h}^p_{\ell_{\Im}} x^p_{\Im} \right)$.

The estimates for $\hat{\ell}_{\Re}, \hat{\ell}_{\Im}$, $\hat{u}_{\Re}$ and $\hat{u}_{\Im}$, are spatially demultiplexed in order to obtain the detected bits at the output.

3 Receiver Computational Complexity Analysis

This section presents a comparison of the receiver computational complexities for the different systems being compared with the proposed QSM-OFDM, viz; Alamouti-OFDM, VBLAST-OFDM, SM-OFDM and MRC-OFDM. In this paper, the computational complexities are resolved to the number of real multiplications and additions being carried out at the receiver [22]. It should be noted that where possible, the arithmetic path that gives the lower computational complexity in achieving a given detection at the receiver is assumed, and the total complexity is the sum of the real multiplications and real additions for each subcarrier. As a background for the calculation of computational complexities in terms of real operations performed during processing, a complex multiplication (CM) is achieved by performing four real multiplications $(4m)$ and two real additions $(2a)$, which makes a total of 6 real operations, while a complex addition (CA) is obtained by performing $2a$, as explained in [22].

3.1 QSM-OFDM

The total computational complexity for the proposed QSM-OFDM for a single subcarrier is given as:

$$\delta_{\mathrm{QSM-OFDM}} = 25MN_t^2N_r + 3MN_t^2 - 1 \tag{A.13}$$

The $\|\boldsymbol{g}\|_F^2$ in (A.12) is obtained by $10N_rm$ and $8N_ra$. $\boldsymbol{y}^H\boldsymbol{g}$ is obtained by $4N_rm + (3N_r - 1)a$, since $\boldsymbol{g}$ is stored and there is no need for recalculation. Additional $m+a$ is used to obtain $\|\boldsymbol{g}\|_F^2 - 2\Re(\boldsymbol{y}^H\boldsymbol{g})$. However, there are MN_t^2 iterations of $\|\boldsymbol{g}\|_F^2 - 2\Re(\boldsymbol{y}^H\boldsymbol{g})$, after which the MN_t^2 outputs are compared using $(MN_t^2 - 1)a$ to obtain a minimum value, thus, making the computational complexity in terms of real operations $MN_t^2(14N_r + 1)m + (11MN_t^2N_r + 2MN_t^2 - 1)a$.

3.2 MRC-OFDM [23]

The product $\boldsymbol{H}^H\boldsymbol{Y}$ gives an N_tN_r CM and $N_tN_r - N_t$ CA, which can be achieved by $4N_tN_rm + 2N_t(2N_r - 1)a$. The product $\boldsymbol{H}^H\boldsymbol{H}$ has $N_t^2N_r$ CM and $N_t^2N_r - N_t^2$ CA obtained by performing $4N_t^2N_rm + \left(4N_t^2N_r - 2N_t^2\right)a$. The division $\frac{\boldsymbol{H}^H\boldsymbol{Y}}{\boldsymbol{H}^H\boldsymbol{H}}$ is performed by using $2m$. The computational complexity needed to obtain an estimate of the transmitted symbol is ignored because a one-to-one mapping is performed [24]. Thus, MRC-OFDM has $(4N_t^2N_r + 4N_tN_r + 2)m + (4N_t^2N_r - 2N_t^2 + 4N_tN_r - 2N_t)a$, giving a total complexity for MRC-OFDM as:

$$\delta_{\mathrm{MRC-OFDM}} = 8N_t^2N_r - 2N_t^2 + 8N_tN_r - 2N_t + 2 \tag{A.14}$$

3.3 Alamouti-OFDM [15]

The computational complexity for $\|\boldsymbol{g}\|_F^2 - 2\Re(\boldsymbol{y}^H\boldsymbol{g})$ imposed by the Alamouti ML detector, is similar to subsection 3.1 and requires $25N_r$+1 operations. The number of iterations the detector performs is M^2, hence, to determine the minimum, the ML detector requires $(M^2 - 1)$a operations. Since the detection performed is for two MQAM symbols, thus, the total complexity for a single subcarrier is obtained by dividing the total number of real operations by 2, which gives:

$$\delta_{\mathrm{Alamouti-OFDM}} = \frac{1}{2}\left(25N_rM^2 - M^2 - 25N_r - 1\right) \tag{A.15}$$

3.4 VBLAST-OFDM [3]

Depending on the VBLAST detection algorithm being used, the computational complexities can vary in different ways. Using the MMSE-OSIC described in [3], the CM imposed is given as $N_t^3+2N_t^2N_r+N_r$. This value is obtained by the multiplications of the channel matrix and an inverse matrix, hence resulting in $(4N_t^3+8N_tN_r+4N_r)m+(2N_t^3+4N_tN_r+2N_r)a$. A minimum of $N_t^3+2N_t^2N_r-N_t^2-N_tN_r+N_r-1$ CA were made in actualizing this, resulting in $2\left(N_t^3+2N_t^2N_r-N_t^2-N_tN_r+N_r-1\right)a$. The total number of operations in terms of m and a employed to determine the layer having the minimum estimation error of G_{MMSE} in ([3],(11)) i.e., the layer having the minimum Euclidean norm is given as $2N_tN_rm+(N_tN_r+N_t-1)a$. The computational complexity of the quantization slicing function $\hat{\mathrm{e}}=\mathbf{Q}(\boldsymbol{G}_{\text{MMSE}}\times\boldsymbol{y})$, which is used to estimate the transmitted symbol is ignored because, a one-to-one mapping is performed [24]. The total number of real operations to be carried out by a receiver in detecting the transmitted symbol by a single transmit antenna is given as:

$$10N_t^3+4N_t^2N_r-2N_t^2+13N_tN_r+8N_r+N_t-3 \tag{A.16}$$

Since the technique used for the VBLAST-OFDM recursively decreases in the number of transmit antennas N_t due to the elimination of detected symbols, the overall number of real operations can be written as:

$$\delta_{\text{VBLAST-OFDM}}=\sum_{\ell=1}^{N_t}\left(10N_{t,\ell}^3+4N_{t,\ell}^2N_r-2N_{t,\ell}^2\ +13N_{t,\ell}N_r+8N_r+N_{t,\ell}-3\right) \tag{A.17}$$

where $N_{t,\ell}$ is the number of transmit antennas for the ℓ-th, $\ell\in[1:N_t]$ iteration.

3.5 SM-OFDM [1]

The SM-OFDM ML detection process requires $(4N_r+2N_tN_r)m+(5N_r+N_tN_r-1)a$, while a total of MN_t iterations and $(MN_t-1)a$ operations are employed to obtain the minimum from the Frobenius norms. The total number of real operations can then be given as:

$$\delta_{\text{SM}-\text{OFDM}}=MN_t\left(3N_tN_r+9N_r-1\right) \tag{A.18}$$

Table A.3, summarizes the computational complexities for the different OFDM schemes and are pictorially represented by the bar chart in Fig. A.2.

Table A.3: Comparison of computational complexity for different OFDM systems

SYSTEM	4 bits/s/Hz	6 bits/s/Hz	8 bits/s/Hz
VBLAST	550	550	4516
SM	944	5,312	21,248
QSM	1,647	6,591	26,367
Alamouti	10,496	167,936	2,686,976

The axis on the right (secondary axis) indicates values for the computational complexity of Alamouti-OFDM, because of the high computational complexity, while the axis on the left (primary axis) is for the other schemes, such as VBLAST-OFDM, SM-OFDM and QSM-OFDM being compared in this work. The ALAMOUTI-OFDM scheme has a very high computational complexity when compared with other schemes in this paper.

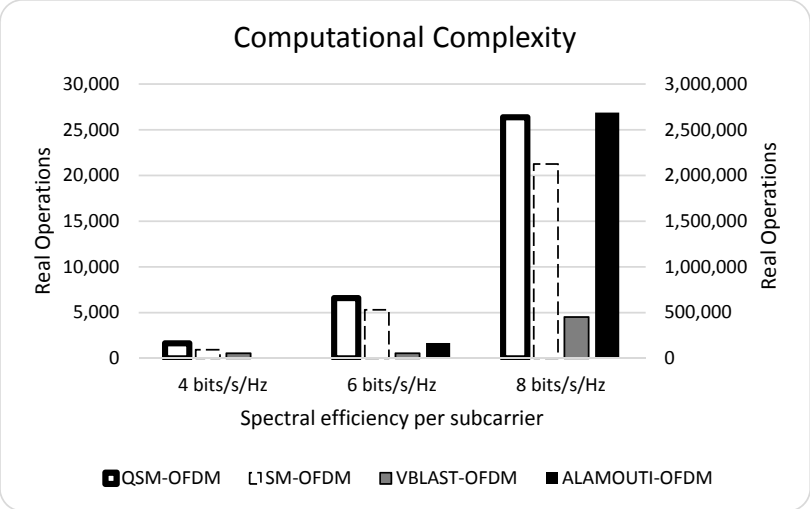

Fig. A.2: Bar chart showing the computational complexities of different system

There is a 24% increase in the computational complexity (in terms of real operations) of the proposed QSM-OFDM scheme over the SM-OFDM when the spectral length for each subcarrier of the OFDM symbol is high (6 bits/s/Hz and 8 bits/s/Hz), as can be seen in Table A.3 and Fig. A.2. However, there is a 74% increase in computational complexity when each OFDM subcarrier is 4 bits/s/Hz. The VBLAST-OFDM is seen to have the lowest computational complexity in all the schemes compared. However, because the RF chains of VBLAST increases with the number of transmit antenna, it is more prone to ICI, furthermore, the complexity involved in the design is higher due to inter-antenna synchronization (IAS). Nevertheless, it has been included for comparison purposes.

4 Simulation Results and Discussion

In this section, the bit error rate (BER) performance demonstrated by the proposed QSM-OFDM scheme employing Monte Carlo simulations is quantified. Simulations were performed for 4, 6 and 8 bits/s/Hz as shown in Fig. A.3, Fig. A.4 and Fig. A.5, respectively. Parameters used for the simulations are given in Table A.4 [1], while Table A.5 compares the BER performance of QSM-OFDM with other schemes.

Table A.4: Parameters for simulation [1]

Parameters	Value
Carrier frequency	2 GHz
Number of subcarriers	256
Antenna Configurations	2×4 and 2×4
CP	32
Channel Property	ITU EPA model
Modulation Scheme	MQAM
Maximum delay spread	6 Hz

The following assumptions were made for the simulations; multipath channels are statistically independent for the different pathways, time and frequency synchronization is perfect and the total signal power is the same for all transmissions, while AWGN is assumed in all cases. In all schemes used for comparison in this paper, the ML detector is employed. Employing the ML detector in the VBLAST-OFDM system is impracticable because of the extremely large computational complexity. The ML detector for V-BLAST involves M^{N_t} iterations per subcarrier, which is quite large. Hence, the optimal minimum mean square error (MMSE) detection, which is combined with the ordered successive interference cancellation (OSIC) as used in [3], is employed in VBLAST-OFDM simulation of this paper.

Considering Fig. A.3, the improvement of the proposed QSM-OFDM over SM-OFDM is greater than 3 dB at a BER of 10^{-5}, while a 7 dB gain in SNR is achieved over the Alamouti-OFDM scheme at a BER of 10^{-5}, while the QSM-OFDM outperforms the MIMO-OFDM and MRC-OFDM by approximately 2 dB in SNR at the same BER. VBLAST-OFDM shows a slightly better error performance of ≈ 1 dB in SNR over QSM-OFDM. Howbeit, VBLAST-OFDM suffers from high ICI as all antennas are made to transmit different symbols. Also, the need for IAS is a major disadvantage for VBLAST-OFDM as the number of RF chains increase with the number of transmit antennas.

In Fig. A.4, the proposed QSM-OFDM outperforms the SM-OFDM, MIMO-OFDM and MRC-OFDM by 4 dB, 6 dB and 5 dB gain in SNR, respectively, gain at a BER of 10^{-5}. This is achieved when a 4×4 antenna configuration is used with 4QAM for QSM-OFDM, in order to obtain a 6 bits/s/Hz transmission per subcarrier. However, these gains are reduced by ≈ 2 dB, when a 2×4 antenna configuration is used with 16QAM. Furthermore, QSM-OFDM achieves significant improvement of 10 dB in SNR over Alamouti-OFDM at BER of 10^{-3}.

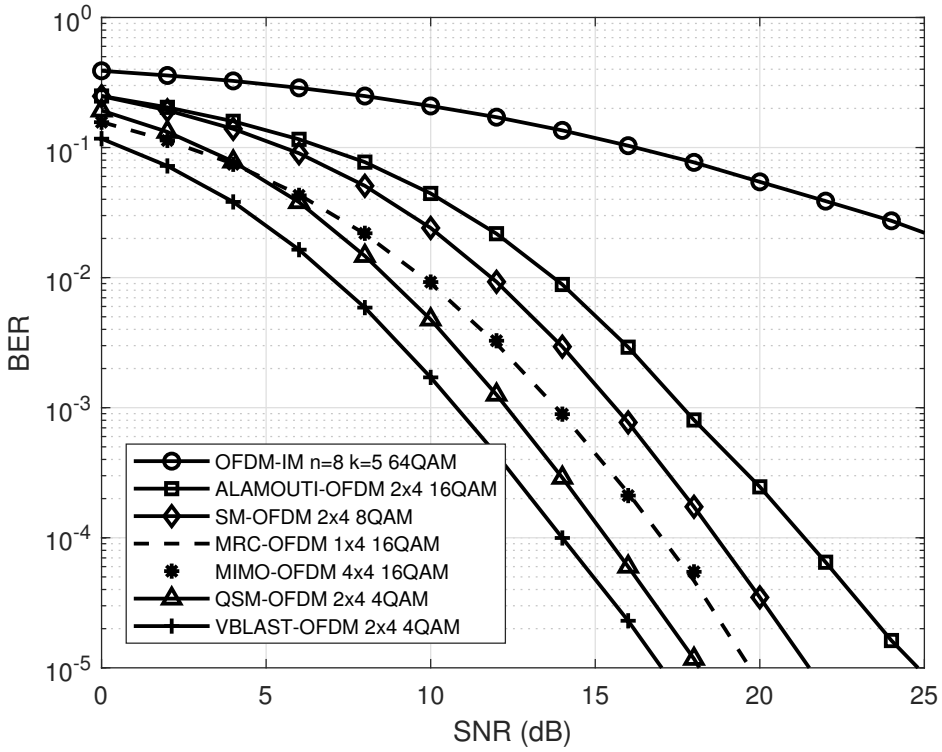

Fig. A.3: BER versus SNR for 4 bits/s/Hz for QSM-OFDM and other schemes.

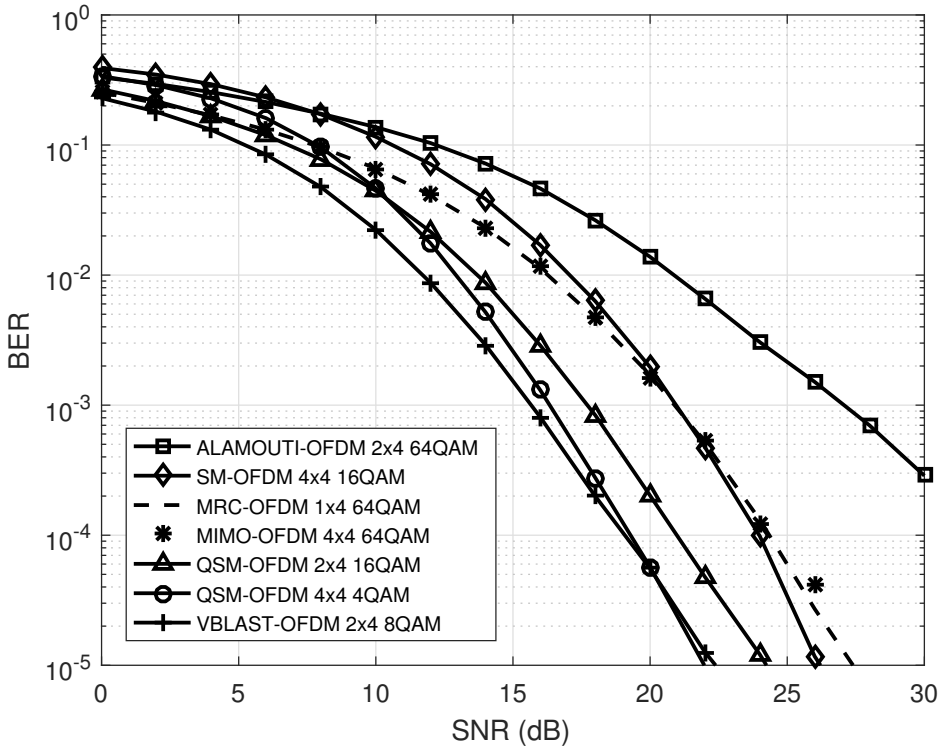

Fig. A.4: BER versus SNR for 6 bits/s/Hz for QSM-OFDM and other schemes.

The VBLAST-OFDM has a slightly better error performance of approximately 1.5 dB in SNR over QSM-OFDM at a BER of 10^{-5}, when the same number of transmit antennas is employed. However, when the number of transmit antennas for QSM-OFDM is increased for the same spectral length per subcarrier, the QSM-OFDM is seen to outperform VBLAST-OFDM at higher SNR. Furthermore, due to the limitations of VBLAST-OFDM mentioned earlier, the QSM-OFDM in this regard, remains a better candidate for modern communication systems.

Considering Fig. A.5, which is the 8 bits/s/Hz transmission for a given subcarrier, the proposed QSM-OFDM outperforms the SM-OFDM scheme by approximately 5 dB when the BER is 10^{-5}. Higher SNR gain is recorded when QSM-OFDM is compared with other schemes. Furthermore, QSM-OFDM demonstrates better performance over Alamouti-OFDM and MIMO-OFDM, by achieving a ≥ 10 dB gain in SNR at a BER of 10^{-5}. Also, the QSM-OFDM is seen to outperform VBLAST-OFDM at higher SNR. A summary of the BER performance of the proposed QSM-OFDM system being compared with other OFDM systems is presented in Table A.5.

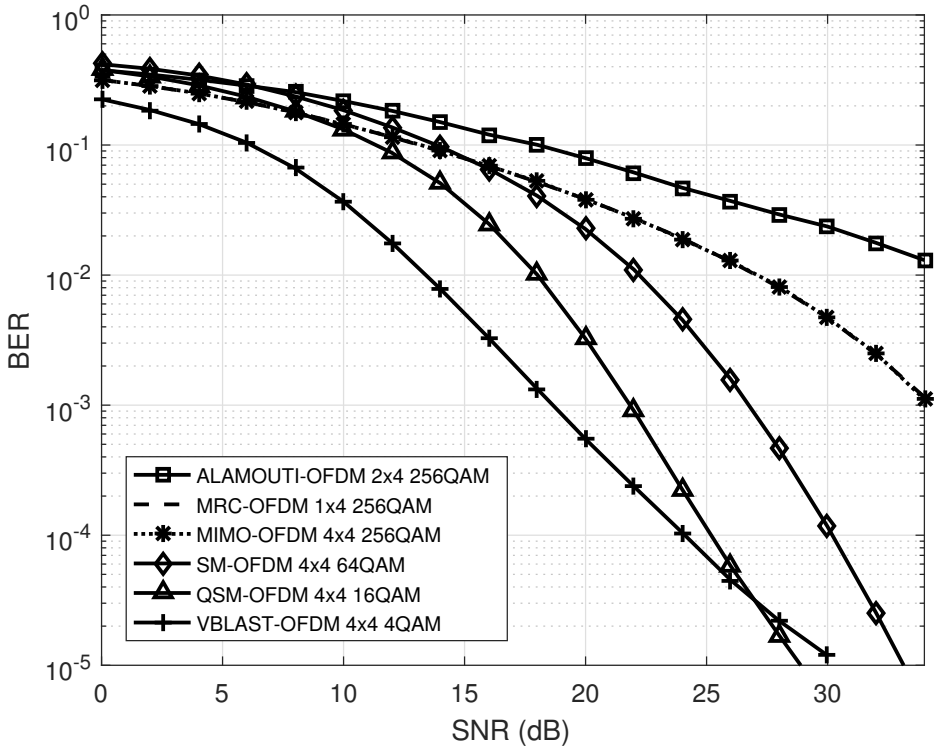

Fig. A.5: BER versus SNR for 8 bits/s/Hz for QSM-OFDM and other schemes.

The error performance of QSM-OFDM over SM-OFDM is about 4 dB gain in SNR when 4 bits/s/Hz is used for each subcarrier of the OFDM symbol. The gain in error performance is maintained with a narrow increase when the 6 bits/s/Hz and 8 bits/s/Hz are used, respectively. The error performance of QSM-OFDM over Alamouti-OFDM is highest. It is seen to increase when the spectral length per subcarrier being used for the QSM-OFDM system is increased. When QSM-OFDM is compared with MIMO-OFDM and MRC-OFDM, its error performance is minimal ($\approx$ 2 dB) when a 4 bits/s/Hz is used for each subcarrier of the OFDM symbol but increases to 5 dB and 15 dB when 6 bits/s/Hz and 8 bits/s/Hz are used, respectively.

5 Conclusion

This paper has analyzed the advantage of exploiting the spatial domain as a means of increasing the spectral efficiency of the system and also benefiting from the gains of OFDM in eliminating ISI and co-channel interference. The results showed that the proposed QSM-OFDM has a better error performance than the SM-OFDM system without additional cost of hardware. Also, SM-OFDM will need a minimum of 4 dB signal power to attain the same BER of QSM-OFDM if the spectral

Table A.5: Comparison of BER performances of QSM-ODFM over other schemes.

Scheme	4 bits/s/Hz		6 bits/s/Hz		8 bits/s/Hz	
	Configuration	Gain (dB)	Configuration	Gain (dB)	Configuration	Gain (dB)
MIMO-OFDM	2×4 16QAM	2	4×4 64QAM	5	4×4 256QAM	> 15
SM-OFDM	2×4 8QAM	4	4×4 16QAM	4	4×4 64QAM	≈ 5
Alamouti-OFDM	2×4 16QAM	7	2×4 64QAM	12	2×4 256QAM	> 20
MRC-OFDM	1×4 16QAM	2	1×4 64QAM	5	1×4 256QAM	> 15

efficiency is made equal. The proposed QSM-OFDM scheme displayed superior error performance over MRC-OFDM, MIMO-OFDM, and Alamouti-OFDM. From the results, QSM-OFDM also demonstrates a better error performance than VBLAST-OFDM at high SNR. Since the number of RF chains for VBLAST-OFDM increases with the number of transmit antennas it becomes more susceptible to ICI and IAS than the QSM-OFDM. Hence, the proposed QSM-OFDM scheme becomes the preferred candidate for modern day communication. Since recent research has focused on energy and spectral efficient devices, the QSM-OFDM becomes a more promising model for future wireless communication as its design is implementable for the OFDM system.

References

[1] S. U. Hwang, S. Jeon, S. Lee, and J. Seo, "Soft-output ML detector for spatial modulation OFDM systems," *IEICE Electronics Express*, vol. 6, no. 19, pp. 1426–1431, Oct. 2009.

[2] P. Yang, M. Di Renzo, Y. Xiao, S. Li, and L. Hanzo, "Design guidelines for spatial modulation," *IEEE Communications Surveys & Tutorials*, vol. 17, no. 1, pp. 6–26, Jan.-Mar. 2015.

[3] R. Bohnke, D. Wubben, V. Kuhn, and K.-D. Kammeyer, "Reduced complexity MMSE detection for BLAST architectures," in *Proceedings of IEEE Global Telecommunications Conference*, vol. 4, Dec. 2003, pp. 2258–2262.

[4] V. Tarokh, N. Seshadri, and A. R. Calderbank, "Space-time codes for high data rate wireless communication: performance criterion and code construction," *IEEE Transactions on Information Theory*, vol. 44, no. 2, pp. 744–765, Mar. 1998.

[5] R. Y. Mesleh, H. Haas, S. Sinanovic, C. W. Ahn, and S. Yun, "Spatial modulation," *IEEE Transactions on Vehicular Technology*, vol. 57, no. 4, pp. 2228–2241, Jul. 2008.

[6] N. Pillay and H. Xu, "Low-complexity transmit antenna selection schemes for spatial modulation," *IET Communications*, vol. 9, no. 2, pp. 239–248, 2015.

[7] J. Wang, S. Jia, and J. Song, "Generalised spatial modulation system with multiple active transmit antennas and low complexity detection scheme," *IEEE Transactions on Wireless Communications*, vol. 11, no. 4, pp. 1605–1615, Apr. 2012.

[8] J. Jeganathan, A. Ghrayeb, L. Szczecinski, and A. Ceron, "Space shift keying modulation for MIMO channels," *IEEE Transactions on Wireless Communications*, vol. 8, no. 7, pp. 3692–3703, Jul. 2009.

[9] J. Jeganathan, A. Ghrayeb, and L. Szczecinski, "Generalized space shift keying modulation for MIMO channels," in *Proceedings of IEEE 19th International Symposium on Personal, Indoor and Mobile Radio Communications*, Sep. 2008, pp. 1–5.

[10] K. Kadathlal, H. Xu, and N. Pillay, "Generalised differential scheme for spatial modulation systems," *IET Communications*, vol. 11, no. 13, pp. 2020–2026, 2017.

[11] M. D. Renzo, H. Haas, A. Ghrayeb, S. Sugiura, and L. Hanzo, "Spatial modulation for generalized MIMO: Challenges, opportunities, and implementation," *Proceedings of the IEEE*, vol. 102, no. 1, pp. 56–103, Jan. 2014.

[12] H. W. Liang, R. Y. Chang, W. H. Chung, H. Zhang, and S. Y. Kuo, "Bi-space shift keying modulation for MIMO systems," *IEEE Communications Letters*, vol. 16, no. 8, pp. 1161–1164, Aug. 2012.

[13] K. Govindasamy, H. Xu, and N. Pillay, "Space-time block coded spatial modulation with labeling diversity," *International Journal of Communication Systems*, vol. 31, no. 1, 2017.

[14] S. Ganesan, R. Mesleh, H. Ho, C. W. Ahn, and S. Yun, "On the performance of spatial modulation OFDM," in *Proceedings of Fortieth Asilomar Conference on Signals, Systems and Computers*, Oct. 2006, pp. 1825–1829.

[15] Y. S. Cho, J. Kim, W. Y. Yang, and C. G. Kang, *MIMO-OFDM wireless communications with MATLAB*. John Wiley & Sons, 2010.

[16] F. Yu, X. Lei, L. Peng, Y. Xiao, P. Wei, and X. Wen, "Performance analysis of spatial modulation OFDM system with N-continuous precoder," in *Proceedings of IEEE 83rd Vehicular Technology Conference (VTC Spring)*, May 2016, pp. 1–5.

[17] R. Mesleh, S. S. Ikki, and H. M. Aggoune, "Quadrature spatial modulation," *IEEE Transactions on Vehicular Technology*, vol. 64, no. 6, pp. 2738–2742, Jun. 2015.

[18] L. Xiao, P. Yang, S. Fan, S. Li, L. Song, and Y. Xiao, "Low-complexity signal detection for large-scale quadrature spatial modulation systems," *IEEE Communications Letters*, vol. 20, no. 11, pp. 2173–2176, Nov. 2016.

[19] S. Naidu, N. Pillay, and H. Xu, "Transmit antenna selection schemes for quadrature spatial modulation," *Wireless Personal Communications*, vol. 99, no. 1, pp. 299–317, 2018.

[20] R. W. Chang, "Synthesis of band-limited orthogonal signals for multichannel data transmission," *The Bell System Technical Journal*, vol. 45, no. 10, pp. 1775–1796, Dec. 1966.

[21] B. Saltzberg, "Performance of an efficient parallel data transmission system," *IEEE Transactions on Communication Technology*, vol. 15, no. 6, pp. 805–811, Dec. 1967.

[22] A. M. Elshokry, "Complexity and performance evaluation of detection schemes for spatial multiplexing MIMO systems," *Master's thesis, Faculty of Engineering, Islamic University Gaza*, 2010.

[23] M. J. H. Liu, Z Yin and X. Zhang, "Ser analysis of the mrc-ofdm receiver with pulse blanking over frequency selective fading channel," *EURASIP Journal on Wireless Communications and Networking*, vol. 2016, no. 1, p. 135, May 2016.

[24] H. Xu, "Simplified maximum likelihood-based detection schemes for M-ary quadrature amplitude modulation spatial modulation," *IET Communications*, vol. 6, no. 11, pp. 1356–1363, Jul. 2012.

Paper B

Low-Complexity Detection For Space-Time Block Coded Spatial Modulation With Cyclic Structure

Babatunde S. Adejumobi and Narushan Pillay

Published

Journal of Communications

Abstract

This paper proposes a low-complexity near-maximum-likelihood (ML) detector for space-time block coded spatial modulation with cyclic structure (STBC-CSM). The proposed detector yields a significant reduction in computational complexity, which is $\geq 59\%$ *compared to the traditional ML detector, while simulation results demonstrate near-ML error performance. The union bound theoretical framework to quantify the average bit-error probability of* M*-ary quadrature amplitude modulation STBC-CSM over a frequency-flat Rayleigh fading channel is formulated and validates the Monte Carlo simulation results.*

1 Introduction

The demand for improved data services has become a necessity in modern day wireless communication [1, 2]. Space-time block coded (STBC) spatial modulation (STBC-SM) [3], a novel multiple-input multiple-output (MIMO) based transmission system, which exploits the advantages of both the Alamouti STBC and SM [4], have the potential to meet this demand. STBC-SM employs a pair of transmit antennas selected from a spatial (antenna) constellation to transmit a pair of amplitude and/or phase modulation (APM) constellation symbols over two time-slots [2, 3]. Since the transmit antenna pair indices and the APM symbols of STBC-SM are employed in transmitting information, the spectral efficiency (SE)/error performance is improved compared to Alamouti STBC and SM.

Several schemes, which make use of the STBC-SM technique have been proposed. For example, labeling diversity was applied to STBC-SM in [5], similar to the method of [2, 6], to improve error performance. In [7], STBC-SM with cyclic structure (STBC-CSM), employs cyclic rotation of activated transmit antenna pairs within a codebook to transmit Alamouti codewords taken from two different constellation sets, thereby significantly increasing the SE of conventional STBC-SM. STBC-SM with temporal modulation (STBC-TSM) [8], was proposed to further improve the SE of STBC-SM, by employing a cyclic spatially rotated codebook with temporal permutations. However, although STBC-TSM is able to further improve the SE of STBC-SM, the computational complexity (CC) per time-slot, in terms of real multiplications, was 90% greater than STBC-CSM [8]. Hence, STBC-CSM is still of interest.

The advantages of STBC-CSM is reduced by the CC imposed by the maximum-likelihood (ML) detector employed. The optimal ML detector for STBC-CSM in [7] has a large CC as it performs an

exhaustive search over all possible matrices, thereby making it impracticable, especially when high-order M-ary APM constellations are employed. Although, linear detectors can be employed to reduce the CC due to the orthogonality of the STBC-CSM codeword [3, 7], this is only applicable in quasi-static fading channels. In [9], low-complexity near ML detection is performed by equalization, employing the Frobenious norm of the simplified channel. However, the application of this is method in a fast fading channel is not possible because it is based on the orthogonality of the Alamouti codeword. In [10], orthogonal projection (OP) of signals was employed as a tool to reduce the CC of a MIMO system. Furthermore, in [5], OP was employed to reduce the CC of STBC-SM with labeling diversity, the results in both cases demonstrated near-ML error performance and a significant reduction in CC when compared with their corresponding ML detectors.

Furthermore, although simulated error performances of STBC-CSM was reported in [7], there was no theoretical framework to validate the average bit-error probability (ABEP).

Based on the above motivations, a closed-form expression to evaluate the ABEP of STBC-CSM is proposed. Furthermore, an LC detector based on OP of signals, which yields a near-ML error performance is proposed. In addition, an analytical framework to determine the CC of the proposed detector is presented.

The remainder of this paper is organized as follows: Section 2 presents the background of STBC-CSM. The proposed theoretical framework of the union bound on the ABEP for STBC-CSM is then presented. The proposed near-ML LC detector of STBC-CSM is then formulated and the CC of the detectors are analyzed. In Section 3, the numerical results are presented and discussed, and finally, the paper is concluded in Section 4.

Notation: The following notations are employed throughout this paper; bold and capital letters represent matrices, while bold small letters denote column vectors of matrices. $(\cdot)^{-1}$, $(\cdot)^{T}$, $(\cdot)^{H}$ and $(\cdot)^{*}$ represents inverse, transpose, Hermitian and complex conjugate, respectively. $Q(\cdot)$ and $||\cdot||_F$ denotes Q-function and Frobenius norm, respectively. Also $\underset{w}{\operatorname{argmin}}(\cdot)$ represents the minimum of an argument with respect to w and $\lfloor w \rfloor_{2p}$ denotes the floor of the nearest power of two, less than or equal to w. $\boldsymbol{I}_w$ denotes a $w \times w$ identity matrix having all elements in its diagonal as unity.

2 STBC-CSM

2.1 Background/System model

Given N_t transmit antennas, the STBC-CSM code set, which employs several transmit antenna pairs denoted as (t_1, t_2), where $t_1, t_2 \in [1 : N_t]$ comprises of $N_t - 1$ codebooks, $\boldsymbol{\chi}_k$, $k \in [1 : N_t - 1]$. Each codebook contains N_t codewords. The l-th, $l \in [1 : N_t]$ codeword of the k-th codebook of STBC-CSM is given by $\boldsymbol{\chi}_{k,l} = \boldsymbol{G}^{l-1}\boldsymbol{D}_k e^{j\theta_k}$ [7], where θ_k is the optimized rotation angle of the k-th codebook given in (Table II, [7]), $\boldsymbol{G}$ is an $N_t \times N_t$ right-shift matrix [7] with $\boldsymbol{G}^0 = \boldsymbol{I}_{N_t}$ and $\boldsymbol{D}_k$ is an $N_t \times 2$ matrix defined as [7]:

$$\boldsymbol{D}_k = \begin{bmatrix} x_p & 0 & \dots & x_q & \dots & 0 \\ -x_q^* & 0 & \dots & x_p^* & \dots & 0 \\ & & & \underset{(1+k)\text{-th column}}{} & & \end{bmatrix}^T \tag{B.1}$$

where x_p, $p \in [1 : M]$ is a symbol from an M-ary quadrature amplitude modulation (M-QAM) constellation Ω_1, and x_q, $q \in [1 : M]$ is a symbol from a rotated M-QAM constellation $\Omega_2 = \Omega_1 e^{j\phi}$, where ϕ is the optimized rotation angle of Ω_2 given in (Table II, [7]). The number of usable codewords is $c = \lfloor N_t(N_t - 1) \rfloor_{2p}$ [7], yielding a SE of $0.5 \log_2 c + \log_2 M$ bits/s/Hz. In the case of STBC-SM, $c = \lfloor \binom{N_t}{2} \rfloor_{2p}$.

Given the transmission of the codeword $\boldsymbol{\chi}_\ell = \boldsymbol{\chi}_{k,l}$, for the ℓ-th, $\ell \in [1 : c]$ transmit antenna pair, where $\ell = N_t(k-1) + l$, the received STBC-CSM signal vectors for time-slots 1 and 2 may be formulated as [5]:

$$\boldsymbol{y}_1 = \sqrt{\frac{\rho}{2}} \left(\boldsymbol{h}^1_{\ell,t_1} s^1_p + \boldsymbol{h}^1_{\ell,t_2} s^1_q \right) + \boldsymbol{\eta}_1 \tag{B.2}$$

$$\boldsymbol{y}_2 = \sqrt{\frac{\rho}{2}} \left(\boldsymbol{h}^2_{\ell,t_1} s^2_q + \boldsymbol{h}^2_{\ell,t_2} s^2_p \right) + \boldsymbol{\eta}_2 \tag{B.3}$$

where $\boldsymbol{y}_i$,$i \in [1 : 2]$ is an $N_r \times 1$ received signal vector for the i-th time-slot. $\frac{\rho}{2}$ is the average signal-to-noise ratio (SNR) at each receive antenna. $s^1_p = x_p e^{j\theta_k}$ and $s^1_q = x_q e^{j\theta_k}$ are the transmitted symbols for time-slot 1, while $s^2_q = -\left(x_q e^{j\theta_k}\right)^*$ and $s^2_p = (x_p e^{j\theta_k})^*$ are transmitted in time-slot 2. $\boldsymbol{h}^i_{\ell,t_1}, \boldsymbol{h}^i_{\ell,t_2} \in \boldsymbol{H}_i$ are the channel vectors between the ℓ-th, $\ell \in [1 : c]$ pair of transmit antennas (t_1, t_2) and the N_r receive antennas. $\boldsymbol{H}_i = \begin{bmatrix} \boldsymbol{h}^i_{\ell,1} & \boldsymbol{h}^i_{\ell,2} & \cdots & \boldsymbol{h}^i_{\ell,N_t} \end{bmatrix}$, denotes the $N_r \times N_t$ frequency-flat Rayleigh fading channel, where the channel is assumed constant during each time-slot and takes on independent values in time-slot i [6]. $\boldsymbol{h}^i_{\ell,\varphi} = \begin{bmatrix} h^{i,\ell}_{1,\varphi} & h^{i,\ell}_{2,\varphi} & \cdots & h^{i,\ell}_{N_r,\varphi} \end{bmatrix}^T$, $\varphi \in [1 : N_t]$ are $N_r \times 1$ column vectors of the φ-th transmit antenna. $\boldsymbol{\eta}_i$ denotes the $N_r \times 1$ additive white Gaussian noise

(AWGN) vector. The entries of $\boldsymbol{H}_i$ and $\boldsymbol{\eta}_i$ are independent and identically distributed (i.i.d.) over time-slot i according to the $CN(0,1)$ distribution.

The optimal ML detector of STBC-CSM performs a joint detection to estimate the index of the transmit antenna pair and transmitted symbol, and is defined as:

$$\left[\hat{\ell},\hat{p},\hat{q}\right] = \underset{\substack{\hat{x}_p\in\Omega_1,\,\hat{x}_q\in\Omega_2\\ \hat{\ell}\in[1:c]}}{\operatorname{argmin}} \left(\left\| \boldsymbol{y}_1 - \sqrt{\frac{\rho}{2}}\left(\boldsymbol{h}^1_{\ell,t_1}s^1_p + \boldsymbol{h}^1_{\ell,t_2}s^1_q\right)\right\|^2_F + \left\| \boldsymbol{y}_2 - \sqrt{\frac{\rho}{2}}\left(\boldsymbol{h}^2_{\ell,t_1}s^2_q + \boldsymbol{h}^2_{\ell,t_2}s^2_p\right)\right\|^2_F \right) \quad \text{(B.4)}$$

where $\hat{\ell}$, $\hat{p}$ and $\hat{q}$ denote the estimates of ℓ, p and q, respectively.

The ML detector imposes a high CC as will be discussed in Section 2.3, hence the need for a LC detector.

2.2 Proposed ABEP analysis for STBC-CSM

Employing a union bound, the ABEP may be formulated as:

$$ABEP \leq \frac{1}{cM^2}\sum_{\boldsymbol{S}}\sum_{\hat{\boldsymbol{S}}}\frac{N_{\boldsymbol{S}\hat{\boldsymbol{S}}}P\left(\boldsymbol{S}\rightarrow\hat{\boldsymbol{S}}\right)}{\log_2 c + 2\log_2 M} \quad \text{(B.5)}$$

where $P(\boldsymbol{S}\rightarrow\hat{\boldsymbol{S}})$ is the pairwise error probability (PEP) given that the transmitted codeword $\boldsymbol{S}$ is received erroneously as $\hat{\boldsymbol{S}}$.

$N_{\boldsymbol{S}\hat{\boldsymbol{S}}}$ is the number of bits in error that is associated with the PEP event $P(\boldsymbol{S}\rightarrow\hat{\boldsymbol{S}})$. $\boldsymbol{S}$ is an $N_t\times 2$ transmit codeword having s^i_p, $i\in[1:2]$ and s^i_q as the only non-zero elements in the i-th column corresponding to the t_1-th and t_2-th positions, respectively.

Consider $\boldsymbol{H}_1 = \begin{bmatrix}\boldsymbol{h}^1_{\ell,t_1} & \boldsymbol{h}^1_{\ell,t_2}\end{bmatrix}$ and $\boldsymbol{H}_2 = \begin{bmatrix}\boldsymbol{h}^2_{\ell,t_1} & \boldsymbol{h}^2_{\ell,t_2}\end{bmatrix}$, $\boldsymbol{H}_1,\boldsymbol{H}_2\in\boldsymbol{H}$, the conditional PEP $P(\boldsymbol{S}\rightarrow\hat{\boldsymbol{S}}\mid\boldsymbol{H})$ may be formulated as [2]:

$$P\left(\boldsymbol{S}\rightarrow\hat{\boldsymbol{S}}\mid\boldsymbol{H}\right) = P\left(\left\| \boldsymbol{y}_1 - \sqrt{\frac{\rho}{2}}\left(\boldsymbol{h}^1_{\hat{\ell},t_1}s^1_{\hat{p}} + \boldsymbol{h}^1_{\hat{\ell},t_2}s^1_{\hat{q}}\right)\right\|^2_F + \left\| \boldsymbol{y}_2 - \sqrt{\frac{\rho}{2}}\left(\boldsymbol{h}^2_{\hat{\ell},t_1}s^2_{\hat{q}} + \boldsymbol{h}^2_{\hat{\ell},t_2}s^2_{\hat{p}}\right)\right\|^2_F < \|\boldsymbol{\eta}_1\|^2_F + \|\boldsymbol{\eta}_2\|^2_F \right) \quad \text{(B.6)}$$

Similar to the method of [2, 6], (B.6) can be simplified as:

$$P\left(\boldsymbol{S} \rightarrow \hat{\boldsymbol{S}} \mid \boldsymbol{H}\right) = Q\left(\sqrt{\frac{\rho}{8}\left(\|\boldsymbol{H}_1\|_F^2 \|\boldsymbol{S}_1\|_F^2 + \|\boldsymbol{H}_2\|_F^2 \|\boldsymbol{S}_2\|_F^2\right)}\right) \tag{B.7}$$

where $\boldsymbol{S}_1 = \hat{\boldsymbol{S}}_{c_1} - \boldsymbol{S}_{c_1}$ and $\boldsymbol{S}_2 = \hat{\boldsymbol{S}}_{c_2} - \boldsymbol{S}_{c_2}$, $\hat{\boldsymbol{S}}_{c_i}$ and $\boldsymbol{S}_{c_i}$, $i \in [1:2]$ denotes the i-th column of $\hat{\boldsymbol{S}}$ and $\boldsymbol{S}$, respectively. Similar to [6], based on the moment generating function (MGF), the unconditional PEP $P(\boldsymbol{S} \rightarrow \hat{\boldsymbol{S}})$ is defined as [2, 6]:

$$P\left(\boldsymbol{S} \rightarrow \hat{\boldsymbol{S}}\right) = \frac{1}{2g}\left[\frac{1}{2}M_1\left(\frac{1}{2}\right)M_2\left(\frac{1}{2}\right) + \sum_{\upsilon=1}^{g-1} M_1\left(\frac{1}{2\sin^2\theta_\upsilon}\right)M_2\left(\frac{1}{2\sin^2\theta_\upsilon}\right)\right] \tag{B.8}$$

where $M_i(w) = \left(\frac{1}{1+2w\sigma_{\alpha_i}^2}\right)^{N_r}$, $i \in [1:2]$, $\sigma_{\alpha_i}^2 = \frac{\rho}{8}\|\boldsymbol{S}_i\|_F^2$, and $\theta_\upsilon = \frac{\upsilon\pi}{2g}$, with g the number of iterations needed for convergence of the trapezoidal approximation of the Q-function.

2.3 Proposed LC detector for STBC-CSM

In this section, motivated to reduce the CC of STBC-CSM, a near-ML LC detector based on OP [5] to reduce the CC of the STBC-CSM ML detector is proposed.

A LC detector for STBC-CSM, which employs OP, firstly selects ζ_1 and ζ_2 likely candidates $\boldsymbol{z}_p^\ell = [\hat{z}_{p,1}^\ell\ \hat{z}_{p,2}^\ell\ \cdots\ \hat{z}_{p,\zeta_1}^\ell]$ and $\boldsymbol{z}_q^\ell = [\hat{z}_{q,1}^\ell\ \hat{z}_{q,2}^\ell\ \cdots\ \hat{z}_{q,\zeta_2}^\ell]$ of the transmitted symbols s_p^1 and s_q^1, respectively, for the ℓ-th transmit antenna pair, where $\ell \in [1:c]$, $\boldsymbol{z}_p^\ell \subseteq \Omega_1 e^{j\theta_k}$ and $\boldsymbol{z}_q^\ell \subseteq \Omega_2 e^{j\theta_k}$, with $\zeta_1\zeta_2 << M^2$.

Employing the method in [5, 10], the projection matrix $\boldsymbol{P}_{\ell,t_a}^i$, where $i, a \in [1:2]$, which corresponds to the projection space, $\boldsymbol{h}_{\ell,t_a}^i$ is computed, such that $\boldsymbol{P}_{\ell,t_a}^i \boldsymbol{h}_{\ell,t_a}^i = 0$. The projection matrix $\boldsymbol{P}_{\ell,t_a}^i$ may be defined as [5]:

$$\boldsymbol{P}_{\ell,t_a}^i = \boldsymbol{I}_{N_r} - \boldsymbol{h}_{\ell,t_a}^i \left(\left(\boldsymbol{h}_{\ell,t_a}^i\right)^H \boldsymbol{h}_{\ell,t_a}^i\right)^{-1} \left(\boldsymbol{h}_{\ell,t_a}^i\right)^H \tag{B.9}$$

where $\boldsymbol{P}_{\ell,t_a}^i$ projects a signal orthogonal to the subspace of the channel vector $\boldsymbol{h}_{\ell,t_a}^i$. $\boldsymbol{h}_{\ell,t_a}^i$ is the channel vector of the t_a-th transmit antenna during the i-th time-slot. If $\hat{z}_{p,m}^\ell = s_p^1$, $m \in [1:\zeta_1]$ and $\hat{z}_{q,n}^\ell = s_q^1$, $n \in [1:\zeta_2]$, then the sum of the projections can be formulated as [5]:

$$\boldsymbol{P}_{\ell,t_2}^1\left(\boldsymbol{y}_1 - \sqrt{\frac{\rho}{2}}\boldsymbol{h}_{\ell,t_1}^1 \hat{z}_{p,m}^\ell\right) + \boldsymbol{P}_{\ell,t_1}^2\left(\boldsymbol{y}_2 - \sqrt{\frac{\rho}{2}}\boldsymbol{h}_{\ell,t_2}^2 (\hat{z}_{p,m}^\ell)^*\right) = \boldsymbol{P}_{\ell,t_2}^1\boldsymbol{\eta}_1 + \boldsymbol{P}_{\ell,t_1}^2\boldsymbol{\eta}_2 = \boldsymbol{\psi}_1 \tag{B.10}$$

$$\boldsymbol{P}^1_{\ell,t_1}\left(\boldsymbol{y}_1-\sqrt{\frac{\rho}{2}}\boldsymbol{h}^1_{\ell,t_2}\hat{z}^{\ell}_{q,n}\right)+\boldsymbol{P}^2_{\ell,t_2}\left(\boldsymbol{y}_2+\sqrt{\frac{\rho}{2}}\boldsymbol{h}^2_{\ell,t_1}(\hat{z}^{\ell}_{q,n})^*\right)=\boldsymbol{P}^1_{\ell,t_1}\boldsymbol{\eta}_1+\boldsymbol{P}^2_{\ell,t_2}\boldsymbol{\eta}_2=\boldsymbol{\psi}_2 \quad \text{(B.11)}$$

however, if $\hat{z}^{\ell}_{p,m}\neq s^1_p$ and $\hat{z}^{\ell}_{q,n}\neq s^1_q$, the sum of the projections in (B.10) and (B.11) yields [5]:

$$\boldsymbol{P}^1_{\ell,t_2}\left(\sqrt{\frac{\rho}{2}}\boldsymbol{h}^1_{\ell,t_1}\left(s^1_p-\hat{z}^{\ell}_{p,m}\right)\right)+\boldsymbol{P}^2_{\ell,t_1}\left(\sqrt{\frac{\rho}{2}}\boldsymbol{h}^2_{\ell,t_2}\left(s^2_p-(\hat{z}^{\ell}_{p,m})^*\right)\right)+\boldsymbol{\psi}_1 \quad \text{(B.12)}$$

$$\boldsymbol{P}^1_{\ell,t_1}\left(\sqrt{\frac{\rho}{2}}\boldsymbol{h}^1_{\ell,t_2}\left(s^1_q-\hat{z}^{\ell}_{q,n}\right)\right)+\boldsymbol{P}^2_{\ell,t_2}\left(\sqrt{\frac{\rho}{2}}\boldsymbol{h}^2_{\ell,t_1}\left(s^2_q+(\hat{z}^{\ell}_{q,n})^*\right)\right)+\boldsymbol{\psi}_2 \quad \text{(B.13)}$$

From [5], it can be deduced that the Frobenius norms of (B.12) and (B.13) are greater than the Frobenius norms of (B.10) and (B.11), respectively. Hence, based on OP, the proposed LC near-ML detection algorithm for the STBC-CSM system follows:

Step 1: Compute the projection spaces $\boldsymbol{r}^i_{\ell,t_a,s_p}$ and $\boldsymbol{r}^i_{\ell,t_a,s_q}$, $i,a\in[1:2]$, $p,q=[1:M]$, $\ell=[1:c]$ given in (B.14)-(B.17), and the projection matrices $\boldsymbol{P}^i_{\ell,t_a}$ formed from (B.9) for the ℓ-th antenna pair [5].

$$\boldsymbol{r}^1_{\ell,t_1,s_p}=\boldsymbol{y}_1-\sqrt{\frac{\rho}{2}}\boldsymbol{h}^1_{\ell,t_1}s^1_p \quad \text{(B.14)}$$

$$\boldsymbol{r}^1_{\ell,t_2,s_q}=\boldsymbol{y}_1-\sqrt{\frac{\rho}{2}}\boldsymbol{h}^1_{\ell,t_2}s^1_q \quad \text{(B.15)}$$

$$\boldsymbol{r}^2_{\ell,t_1,s_q}=\boldsymbol{y}_2-\sqrt{\frac{\rho}{2}}\boldsymbol{h}^2_{\ell,t_1}s^2_q \quad \text{(B.16)}$$

$$\boldsymbol{r}^2_{\ell,t_2,s_p}=\boldsymbol{y}_2-\sqrt{\frac{\rho}{2}}\boldsymbol{h}^2_{\ell,t_2}s^2_p \quad \text{(B.17)}$$

Step 2: Determine ζ_1 and ζ_2 most likely candidate sets $\boldsymbol{z}^{\ell}_p=[\hat{z}^{\ell}_{p,1}\ \hat{z}^{\ell}_{p,2}\ \cdots\ \hat{z}^{\ell}_{p,\zeta_1}]$ and $\boldsymbol{z}^{\ell}_q=[\hat{z}^{\ell}_{q,1}\ \hat{z}^{\ell}_{q,2}\ \cdots\ \hat{z}^{\ell}_{q,\zeta_2}]$, respectively, for the ℓ-th transmit antenna pair by choosing ζ_1 and ζ_2 symbols, which give the smallest projection norms from the metrics given in (B.18) and (B.19), respectively.

$$\hat{z}^{\ell}_p=\underset{\boldsymbol{r}^i_{\ell,t_a,s_p}}{\operatorname{argmin}}\left\|\boldsymbol{P}^1_{\ell,t_2}\boldsymbol{r}^1_{\ell,t_1,s_p}+\boldsymbol{P}^2_{\ell,t_1}\boldsymbol{r}^2_{\ell,t_2,s_p}\right\|^2_F \quad \text{(B.18)}$$

$$\hat{z}^{\ell}_q=\underset{\boldsymbol{r}^i_{\ell,t_a,s_q}}{\operatorname{argmin}}\left\|\boldsymbol{P}^1_{\ell,t_1}\boldsymbol{r}^1_{\ell,t_2,s_q}+\boldsymbol{P}^2_{\ell,t_2}\boldsymbol{r}^2_{\ell,t_1,s_q}\right\|^2_F \quad \text{(B.19)}$$

Step 3: Determine $\hat{\ell}$, $\hat{p}$ and $\hat{q}$ by an exhaustive search across all elements in $\boldsymbol{z}_p^{\ell}$ and $\boldsymbol{z}_q^{\ell}$ for all antenna pairs by employing the ML rule according to [5]:

$$[\hat{\ell},\hat{p},\hat{q}] = \underset{\hat{\ell}\in[1:c],\boldsymbol{z}_p^{\ell},\boldsymbol{z}_q^{\ell}}{\operatorname{argmin}} \left\{ \left\| \boldsymbol{y}_1 - \sqrt{\frac{\rho}{2}} \left(\boldsymbol{h}_{\ell,t_1}^1 \hat{z}_{p,m}^{\ell} + \boldsymbol{h}_{\ell,t_2}^1 \hat{z}_{q,n}^{\ell} \right) \right\|_F^2 + \left\| \boldsymbol{y}_2 - \sqrt{\frac{\rho}{2}} \left(\boldsymbol{h}_{\ell,t_2}^2 (\hat{z}_{p,m}^{\ell})^* - \boldsymbol{h}_{\ell,t_1}^2 (\hat{z}_{q,n}^{\ell})^* \right) \right\|_F^2 \right\} \quad \text{(B.20)}$$

where $\hat{z}_{p,m}^{\ell} \in \boldsymbol{z}_p^{\ell}$, $\hat{z}_{q,n}^{\ell} \in \boldsymbol{z}_q^{\ell}$, $\ell \in [1:c]$, $m \in [1:\zeta_1]$ and $n \in [1:\zeta_2]$.

2.4 CC analysis

Similar to [1, 5], the CC in terms of complex operations are formulated. Furthermore, it is assumed that calculated values are stored in memory, hence, redundant operations are not considered.

Computing $\boldsymbol{h}_{\ell,t_1}^1 s_p^1$, $\boldsymbol{h}_{\ell,t_2}^1 s_q^1$, $\boldsymbol{h}_{\ell,t_1}^2 s_q^2$ and $\boldsymbol{h}_{\ell,t_2}^2 s_p^2$ in (B.4) requires $4N_r$ complex multiplications. Also, another $4N_r$ complex additions are required to sum elements within the Frobenius norm operators. Since there are two Frobenius norm operators having $N_r \times 1$ vector, an additional $2N_r$ complex multiplications and $2N_r - 2$ complex additions are added to the CC. Furthermore, because an exhaustive search, which involves c iterations of the complex operations mentioned are to be performed, the total CC in terms of complex operations of the ML detector becomes:

$$\delta_{ML} = cM^2 \left(12N_r - 2\right) \quad \text{(B.21)}$$

For the LC detection algorithm, the CC involved in computing the four projection matrices $\boldsymbol{P}_{\ell,t_1}^1$, $\boldsymbol{P}_{\ell,t_2}^{1,}$, $\boldsymbol{P}_{\ell,t_1}^2$ and $\boldsymbol{P}_{\ell,t_2}^2$ in (B.18) and (B.19) is given as [5]:

$$\delta_{pm} = c\left(8N_r^2 + 12N_r - 4\right) \quad \text{(B.22)}$$

To determine the ζ_1 and ζ_2 estimates of x_p and x_q most likely candidates given in (B.18) and (B.19), the CC is given as [5]:

$$\delta_{lc} = c\left(8MN_r^2 + 16MN_r - 4N_r + 4M\right) \quad \text{(B.23)}$$

The solution for the CC of the exhaustive ML search in (B.20), across the most likely candidates $\boldsymbol{z}_p^{\ell}$ and $\boldsymbol{z}_q^{\ell}$ is similar to the ML search in (B.4), however, the CC is reduced because the search is across $\zeta_1\zeta_2$ symbols, and $\zeta_1\zeta_2 << M^2$. Hence, the total CC for this stage is given as:

$$\delta_{ML_{lc}} = c\zeta_1\zeta_2(12N_r - 2) \quad \text{(B.24)}$$

The total CC in terms of complex operations of the proposed LC near-ML detector may be defined as:

$$\delta_{\textit{STBC-CSM LC}} = (\delta_{pm} + \delta_{lc} + \delta_{ML_{lc}}) = 2c\left[4N_r^2(M+1) + 2N_r(4M + 3\zeta_1\zeta_2 + 4) - (2M + \zeta_1\zeta_2 + 2)\right] \quad \text{(B.25)}$$

It is important to note that the expression for the CC is not the same as the CC in [5]. This is because $c = \lfloor N_t(N_t-1)\rfloor_{2p}$ for STBC-CSM, whereas $c = \lfloor \frac{N_t(N_t-1)}{2}\rfloor_{2p}$ in [5]. Furthermore, the values for ζ_1 and ζ_2 are not necessarily the same as those in [5], they are arbitrary values which offer near-ML error performance for the STBC-CSM scheme.

Table B.1 presents numerical values of the CCs in terms of complex operations for the ML and LC detectors, with SE $= 5$ and 6 bits/s/Hz. The values of ζ_1 and ζ_2 are arbitrary values chosen, which offer near-ML error performance. The LC detector yields a 59% and 66% reduction in CC over the ML detector for SE $= 5$ and 6 bits/s/Hz, respectively.

Table B.1: Comparison of CCs between ML and LC detectors

STBC-CSM CONFIGURATION	SE	ML	LC
$N_t = 3$, $N_r = 4$, $c = 4$, $M = 16$, $\zeta_1 = 6$, $\zeta_2 = 6$	5	47,104	19,408
$N_t = 5$, $N_r = 4$, $c = 16$, $M = 16$, $\zeta_1 = 6$, $\zeta_2 = 3$	6	188,416	64,384

3 Numerical results

In this section, the bit-error rate (BER) of STBC-CSM with 16-QAM and $N_r = 4$ is demonstrated for the ML detector and the proposed LC detector. The formulated theoretical ABEP of (B.5) is also evaluated and used to validate the ML detection simulation results.

In Fig. B.1 and Fig. B.2, the notation $(N_t, N_r, c, M, \text{SE})$ is employed to denote the configuration of STBC-CSM when the ML detector is employed, while $(N_t, N_r, c, M, \text{SE}, \zeta_1, \zeta_2)$ is employed to denote the configuration of STBC-CSM when the LC detector is employed.

In all simulations, the BER of the LC detector demonstrates a close match with the ML detector as depicted in Fig. B.1 and Fig. B.2. It is also evident that the evaluated theoretical ABEP of (B.5) agrees well with the ML detection simulation results at high SNR.

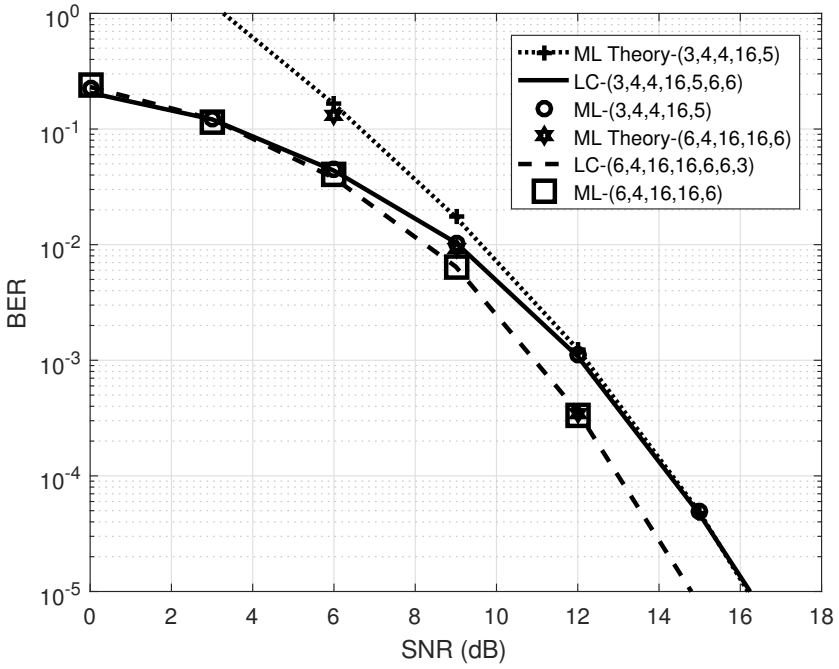

Fig. B.1: BER performances for ML, LC detectors including theoretical ABEP of the STBC-CSM ML detector employing; $N_t = 3,\ c = 4,$ SE $= 5$ bits/s/Hz and $N_t = 6,\ c = 16,$ SE $= 6$ bits/s/Hz

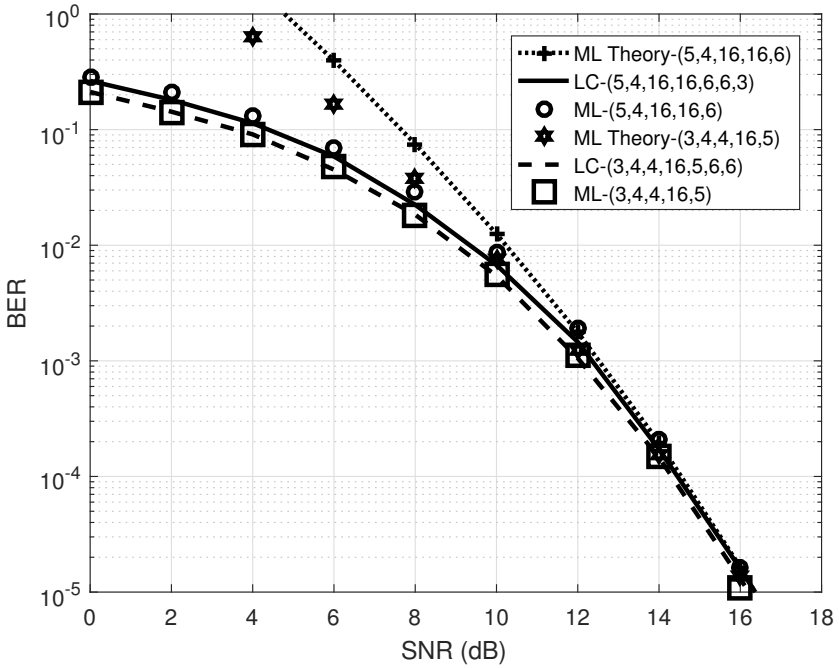

Fig. B.2: BER performances for ML, LC detectors including theoretical ABEP of the STBC-CSM ML detector employing; $N_t = 3,\ c = 4,$ SE $= 5$ bits/s/Hz and $N_t = 5,\ c = 16,$ SE $= 6$ bits/s/Hz

4 Conclusion

The theoretical ABEP of STBC-CSM with M-QAM was formulated and validates simulation results at high SNR. Furthermore, a LC near-ML detector based on OP was formulated and matches very closely with the ML detector, while significantly reducing the CC of STBC-CSM to 59% and 66% , when SE $= 5$ and 6 bits/s/Hz, respectively. Also, STBC-CSM offers improved spectral efficiency than STBC-SM, when the same number of transmit antennas are employed.

References

[1] B. S. Adejumobi, N. Pillay, and S. H. Mneney, "A study of spatial media-based modulation using RF mirrors," in *Proceedings of IEEE AFRICON*, Sep. 2017, pp. 336–341.

[2] N. Pillay and H. Xu, "Uncoded space-time labeling diversity-application of media-based modulation with RF mirrors," *IEEE Communications Letters*, vol. 22, no. 2, pp. 272–275, Feb. 2018.

[3] E. Basar, U. Aygolu, E. Panayirci, and H. V. Poor, "Space-time block coded spatial modulation," *IEEE Transactions on Communications*, vol. 59, no. 3, pp. 823–832, Mar. 2011.

[4] D. Lee, S. Nooshabadi, and K. Kim, "Dual-mode SM/STBC system with antenna subset selection employing ML detection," *AEU-International Journal of Electronics and Communications*, vol. 64, no. 12, pp. 1128–1136, Dec. 2010.

[5] K. Govindasamy, H. Xu, and N. Pillay, "Space-time block coded spatial modulation with labeling diversity," *International Journal of Communication Systems*, vol. 31, no. 1, p. e3395, 2017.

[6] H. Xu, K. Govindasamy, and N. Pillay, "Uncoded space-time labeling diversity," *IEEE Communications Letters*, vol. 20, no. 8, pp. 1511–1514, Aug. 2016.

[7] X. Li and L. Wang, "High rate space-time block coded spatial modulation with cyclic structure," *IEEE Communications Letters*, vol. 18, no. 4, pp. 532–535, Apr. 2014.

[8] A. G. Helmy, M. D. Renzo, and N. Al-Dhahir, "Enhanced-reliability cyclic generalized spatial-and-temporal modulation," *IEEE Communications Letters*, vol. 20, no. 12, pp. 2374–2377, Dec. 2016.

[9] H. Xu and N. Pillay, "Simple near-maximum-likelihood low-complexity detection scheme for alamouti space-time block coded spatial modulation,," *IET Commun.,*, vol. 8, no. 15, pp. 2611–2618, 2014.

[10] S. Bahng, S. Shin, and Y. O. Park, "ML approaching MIMO detection based on orthogonal projection," *IEEE Communications Letters*, vol. 11, no. 6, pp. 474–476, Jun. 2007.

Paper C

RF Mirror Media-Based Space-Time Block Coded Spatial Modulation Techniques For Two Time-Slots

Babatunde S. Adejumobi and Narushan Pillay

Under Review

IET Communications

Abstract

Space-time block coded spatial modulation (STBC-SM) with cyclic structure (STBC-CSM) employs cyclical rotation of activated transmit antenna pairs to transmit Alamouti codewords taken from two different constellation sets to improve the spectral efficiency of STBC-SM. Furthermore, existing literature has shown that media-based modulation (MBM), which employs radio frequency (RF) mirrors demonstrate significant improvement in spectral efficiency/error performance of wireless systems. Hence, this paper proposes the application of MBM to STBC-CSM and STBC-SM in the form of media-based STBC-CSM (MBSTBC-CSM) and MBSTBC-SM, respectively. The theoretical framework of the union-bound on average bit-error probability of M-QAM MBSTBC-CSM and MBSTBC-SM, for the maximum-likelihood (ML) detector is formulated and agrees well with Monte Carlo simulations. Furthermore, due to the large computational complexity of the ML detector, we propose a low-complexity near-ML detector for MBSTBC-CSM and MBSTBC-SM, which achieves a near-ML bit error rate performance with 41% reduction in computational complexity.

1 Introduction

Next-generation multimedia applications and services demand significant improvement in capacity and link reliability [1]. Consequently, recent research has focused on multiple-input multiple-output (MIMO) systems, which have the potential of meeting these demands, but not without limitations. For example: the need for inter-antenna synchronization (IAS) between transmit antennas, high system computational complexity/cost and inter-channel interference (ICI) are challenges in employing classical MIMO techniques [1, 2]. To address these challenges, while retaining the advantages of MIMO systems, several schemes have been recently proposed.

Spatial modulation (SM), a novel MIMO based transmission approach, which eliminates IAS, ICI and requires a single radio frequency (RF) chain has been proposed in [2, 3]. The key idea behind SM is to map a group of bits, which are employed to select a symbol from the amplitude and/or phase modulation (APM) constellation and an antenna index in the spatial constellation. The selected antenna is then employed to transmit the modulated symbol over a wireless channel. However, despite the advantages possessed by SM, it does not achieve transmit diversity [4]. Furthermore, the logarithmic relationship between the spectral efficiency and the number of transmit antennas is a major disadvantage, as a large number of transmit antennas are needed to attain high throughput.

To improve the spectral efficiency/error performance/computational complexity of SM, several

schemes based on SM have been proposed [5]. For example, in [6], several low-complexity transmit antenna selection schemes, which reduce the computational complexity of classical SM by 57%, and improve the error performance SM by $\approx$ 10 dB in SNR, was proposed. A transmit precoder based SM (TPSM) was introduced in [7] for large-scale MIMO. TPSM eliminates multi-user interference and enhances detection of spatial symbols for large scale MIMO.

In [4], space-time block coded (STBC) spatial modulation (STBC-SM), a scheme which introduces diversity to SM by combining the advantages of SM and STBC, was proposed. STBC-SM employs a pair of transmit antennas selected from a set, to transmit an Alamouti STBC codeword in two time-slots. The computational complexity of the STBC-SM ML detector is significantly reduced due to the orthogonality of the Alamouti codeword. However, employing more than 8 transmit antennas, a large number of rotation angles have to be optimized, which causes a reduction in the minimum coding gain distance (CGD) [4, 8, 9].

To further improve the spectral efficiency/transmit diversity of STBC-SM, several schemes have been proposed. For example, a high-rate STBC-SM (H-STBC-SM), which employs spatial constellation matrices for four and six transmit antennas was introduced in [10]. H-STBC-SM improves the spectral efficiency of STBC-SM by increasing the codewords to twice that of STBC-SM, however, this results in reduction of error performance when compared with STBC-SM. In [11], another high-rate STBC-SM, which employs the linear combination of Alamouti STBC parameters was discussed. It was found to perform better than the STBC-SM scheme in [9], which employs an (n, k) error correcting code to form the STBC-SM codewords. However, this system is only designed for an even number of transmit antennas, hence limiting its application.

STBC-SM with temporal modulation (STBC-TSM) [12], was proposed to further improve the spectral efficiency of STBC-SM, by employing a cyclic spatially rotated codebook with temporal permutations. Although STBC-TSM is able to further improve the spectral efficiency of STBC-SM, the computational complexity in terms of real multiplications for each time-slot is 90% more than STBC-SM [12].

In [13], STBC-SM with cyclic structure (STBC-CSM), employs cyclical rotation of transmit antenna pairs to transmit Alamouti codewords formed from two different APM constellation sets. Hence, the spectral efficiency offered by the spatial domain of STBC-CSM is an improvement over STBC-SM. Furthermore, STBC-CSM require fewer transmit antennas and lower cost, to achieve the same spectral efficiency as STBC-SM. However, this improvement is not without a trade-off, as there is a corresponding reduction in error performance, thereby, decreasing the benefits of this scheme [13].

In [14–16], a new technique in wireless communication called media-based modulation (MBM) was proposed. MBM embeds information into the variation of a finite number of channel states by changing the radio frequency (RF) properties, such as permeability, resistivity and permittivity around the antenna to create distinct channel realizations. The application of MBM to a system can offer the following:

1. Converts static multi-path fading channels into additive white Gaussian noise (AWGN) as noted in [14, 15], hence, the error performance is improved drastically,
2. Increases the number of channel realizations without requiring additional power,
3. Significantly improves error performance by selecting a subset of channel realizations, which yield superior error performance.

Several forms of MBM are reported in the literature, for example, in [17], the use of RF switches were employed as a form of MBM, however, the switching speed becomes a crucial parameter for RF switching designs. In [18, 19], the channel realizations of the transmitted tones were employed as the transmitted alphabets of a space shift keying modulation system.

Employing RF mirrors as a form of MBM is particularly attractive because the ON/OFF status of the RF mirrors creates distinct channel realizations (mirror activation patterns (MAPs)) and serve as spatial constellations [19]. Furthermore, it yields a linear increase in spectral efficiency, unlike the logarithmic increase obtained in some systems without MBM, like SM.

As discussed in [16, 17, 19], significant improvement in error performance/spectral efficiency can be achieved, when MBM is applied to conventional single-input multiple-output (SIMO) systems, in the form of SIMO-MBM. However, SIMO-MBM systems becomes resource intensive when a large number of mirrors are employed due to channel-time variations. Furthermore, MBM was applied to MIMO, in the form of MIMO-MBM [16, 19]. This combination results in a superior error performance over the conventional MIMO system. In [19], media-based generalized SM (GSM-MBM) was shown to have an improved error performance over conventional GSM. However, GSM-MBM faces similar challenges as MIMO.

More recently, MBM has been applied to quadrature spatial modulation (QSM) in the form of quadrature spatial media-based modulation (QSMBM) [20] and quadrature channel modulation (QCM) [21]. The presented schemes exhibit significant improvement in spectral efficiency, while retaining a relatively good error performance. Furthermore, MBM has been applied to the Alamouti space-time block code (ASTBC) and uncoded space-time labeling diversity (USTLD) in the form of space-time channel modulation (STCM) [22] and USTLD-STCM [23], respectively, to improve their

spectral efficiency/error performance.

Based on this background, the motivations for this work are as follows:

a. Although STBC-CSM requires fewer transmit antennas to achieve the spectral efficiency of STBC-SM, the STBC-SM system demonstrates a slightly superior error performance than STBC-CSM. Furthermore, the application of MBM to traditional/recent MIMO systems results in significant improvement in error performance/spectral efficiency [19, 20, 22, 23], hence, the motivation to apply the concept of MBM to STBC-CSM and STBC-SM to improve the error performance/spectral efficiency of these systems.

b. The high computational complexity imposed by the optimal maximum-likelihood (ML) detector for STBC systems exists because an exhaustive search over all possible matrices is performed, however, this becomes impracticable in real-life especially when high-order M-ary APM constellations are employed. The application of linear detectors, such as zero forcing (ZF) and minimum mean square error (MMSE) detectors have been employed to reduce computational complexity of wireless systems, However, its error performance is seriously degraded, when compared to the ML detector [24]. To further improve MMSE and ZF, nonlinear detectors like ordered successive interference cancellation (OSIC), have been employed [24, 25]. However, it does not achieve near-ML error performance due to insufficient receive diversity and imperfect interference cancellation [24]. Furthermore, the orthogonality of the STBC-SM codeword is employed as a criterion to achieve a low-complexity ML detector [4]. However, this detector cannot be applied to a fast fading channel, which have values that change at every time slot. Hence, the motivation is to investigate a near-ML low-complexity detector for STBC-CSM having a reduced computational complexity that can be employed for both quasi-static and fast fading Rayleigh channels. The method of orthogonal projection is a better choice over other low-complexity schemes, since it is capable of near-ML error performance with very reduced computational complexity and can be employed for both the quasi-static and fast fading channels [24, 26].

Based on these motivations, the contributions in this paper are as follows:

a. The application of MBM to improve the error performance/spectral efficiency of STBC-CSM and STBC-SM, in the form of media-based STBC-SM (MBSTBC-SM) and media-based cyclically structured space-time block coded spatial modulation (MBSTBC-CSM) is proposed. It employs m_{rf} RF mirrors to transmit the Alamouti codeword, where m_{rf} is the number of RF mirrors associated with each transmit antenna unit. Furthermore, it employs the different MAP schemes

illustrated in [22], the MBSTBC-CSM symbols taken from two different constellation sets are transmitted by a pair of transmit antennas, which are cyclically rotated within a codebook [13].

b. A closed-form expression to evaluate the union bound on average bit-error probability (ABEP) of an $N_t \times N_r$ M-ary QAM (M-QAM) MBSTBC-CSM and MBSTBC-SM over an independent and identically distributed (i.i.d) fast frequency-flat Rayleigh fading channel is formulated, and validates numerical results of the Monte Carlo simulations.

c. Although several low-complexity schemes have been proposed for STBC systems, most of these schemes are dependent on the orthogonality of the Alamouti codeword. For example, equalization of symbols was proposed in [8]. Furthermore, the principle of orthogonality was applied in STBC-SM [4]. However, these methods can only be applied in quasi-static fading channels. Hence, a low-complexity near-ML detector for MBSTBC-CSM and MBSTBC-SM, which may be employed for quasi-static or fast fading channels and is capable of approaching near-ML detection, by applying the principle of orthogonal projection of signals, is proposed.

The remainder of this paper is structured as follows: Section 2 presents a brief background and system model of the proposed MBSTBC-CSM and MBSTBC-SM systems. In Section 3, a closed-form expression for calculating the union bound on ABEP of the proposed M-QAM $N_t \times N_r$ MBSTBC-CSM and MBSTBC-SM systems is formulated. Furthermore, a low-complexity near-ML detection scheme for MBSTBC-CSM and MBSTBC-SM, which employs orthogonal projection is proposed in Section 4, while the computational complexity analysis of the ML and the low-complexity detectors are presented in Section 5. Simulation results and discussions on MBSTBC-CSM and MBSTBC-SM are presented in Section 6. Finally, the paper is concluded in Section 7.

Notation: The following notations are employed throughout this paper; bold and capital letters represent matrices, while bold small letters denote column vectors. Other notations include $(\cdot)^T$, $(\cdot)^H$, $(\cdot)^*$ and $(\cdot)^{-1}$, which represent transpose, Hermitian, complex conjugate and inverse, respectively. $\underset{w}{\operatorname{argmin}}\,(\cdot)$ represents the minimum of an argument with respect to w, $\lfloor w \rfloor_{2p}$, $Q(\cdot)$ and $||\cdot||_F$ denote the nearest power of two, less than or equal to the w, Q-function and Frobenius norm, respectively. $\boldsymbol{I}_{N_t}$ is an $N_t \times N_t$ identity matrix having all elements in its diagonal as unity. $j = \sqrt{-1}$ and $\Re(\cdot)$ denote a complex number and the real part of a complex number, respectively.

2 MBSTBC-CSM/MBSTBC-SM

2.1 Background of STBC-CSM/STBC-SM

Similar to the STBC-SM system, STBC-CSM [13] employs the concept of Alamouti STBC and SM. However, a difference between STBC-CSM and STBC-SM, is that the activated transmit antenna pair (t_1, t_2) for STBC-CSM, is cyclically rotated along the total antenna array within a given codebook. The total STBC-CSM code set comprises of $N_t - 1$ codebooks, $\boldsymbol{\chi}_k$, $k \in [1 : N_t - 1]$, with each codebook containing N_t codewords. The l-th, $l \in [1 : N_t]$ codeword of the k-th codebook for STBC-CSM $\boldsymbol{\chi}_{k,l}$, is defined by [13]:

$$\boldsymbol{\chi}_{k,l} = \boldsymbol{G}^{l-1}\boldsymbol{D}_k e^{j\theta_k} \tag{C.1}$$

where θ_k is the optimized rotation angle for the k-th codebook and $\boldsymbol{G}$ is an $N_t \times N_t$ right-shift matrix having $\boldsymbol{G}^0 = \boldsymbol{I}_{N_t}$ [13]. $\boldsymbol{D}_k$ is an $N_t \times 2$ matrix defined as [13]:

$$\boldsymbol{D}_k = \begin{bmatrix} x_1 & 0 & \dots & x_2 & \dots & 0 \\ -x_2^* & 0 & \dots & x_1^* & \dots & 0 \end{bmatrix} \begin{matrix} \\ \\ \downarrow \\ \text{the } (1+k)\text{-th column} \end{matrix} \tag{C.2}$$

For example, given $N_t = 3$, the $N_t - 1$ codebooks, $\boldsymbol{\chi}_k$ formed from the antenna pairs are given as [13]:

$$\begin{aligned} \boldsymbol{\chi}_1 &= \left\{ \begin{bmatrix} x_p & -x_q^* \\ x_q & x_p^* \\ 0 & 0 \end{bmatrix}, \begin{bmatrix} 0 & 0 \\ x_p & -x_q^* \\ x_q & x_p^* \end{bmatrix}, \begin{bmatrix} x_q & x_p^* \\ 0 & 0 \\ x_p & -x_q^* \end{bmatrix} \right\} e^{j\theta_1} \\ \boldsymbol{\chi}_2 &= \left\{ \begin{bmatrix} x_p & -x_q^* \\ 0 & 0 \\ x_q & x_p^* \end{bmatrix}, \begin{bmatrix} x_q & x_p^* \\ x_p & -x_q^* \\ 0 & 0 \end{bmatrix}, \begin{bmatrix} 0 & 0 \\ x_q & x_p^* \\ x_p & -x_q^* \end{bmatrix} \right\} e^{j\theta_2} \end{aligned} \tag{C.3}$$

where x_p, $p \in [1 : M]$ is a symbol from an M-QAM constellation Ω_1, and x_q, $q \in [1 : M]$ is a symbol from a rotated M-QAM constellation $\Omega_2 = \Omega_1 e^{j\phi}$, M is the modulation order of the APM constellation, ϕ is the optimized rotation angle for Ω_2. The optimized values for θ and ϕ are given in (Table II, [13]). Each row and column of the STBC-CSM codeword matrix represents the transmit antenna index and the time-slot, respectively. However, the number of usable codewords is $c = \lfloor N_t(N_t - 1) \rfloor_{2p}$ [13], whereas, it is $c = \lfloor \frac{N_t(N_t-1)}{2} \rfloor_{2p}$ for STBC-SM. The individual codeword for STBC-SM is similar to the codewords for STBC-CSM except that, the transmit antenna indices of the

codewords in a given codebook are non-overlapping. The spectral efficiency of STBC-CSM/STBC-SM is $\delta = 0.5 \log_2 c + \log_2 M$ bits per channel use (bpcu).

2.2 System model of the proposed MBSTBC-CSM/MBSTBC-SM

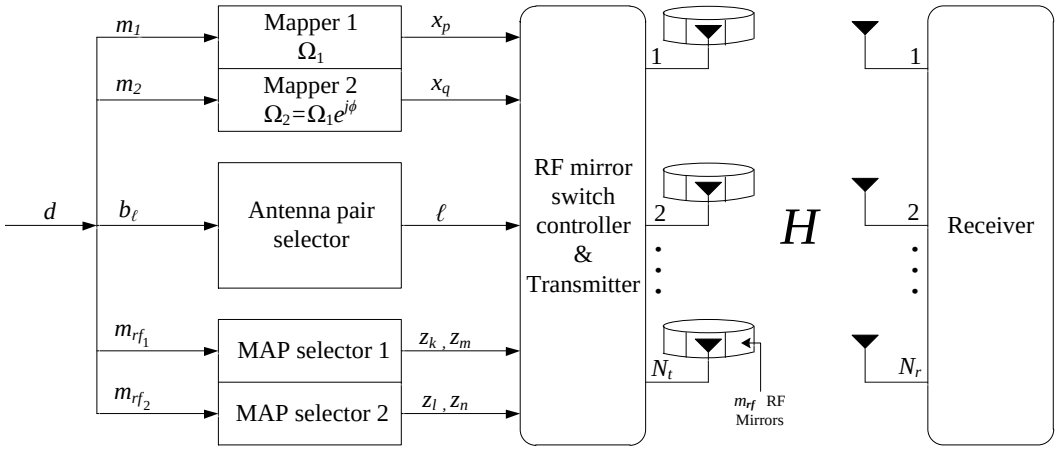

Fig. C.1: System model of MBSTBC-CSM or MBSTBC-SM

Consider the system model of an $N_t \times N_r$ M-QAM MBSTBC-CSM/MBSTBC-SM system, with each antenna equipped with m_{rf} RF mirrors as illustrated in Fig. C.1. A set of input bits of length $d = 2\log_2 M + \log_2 c + \gamma m_{rf}$ are split into three groups of $2\log_2 M$, $b_\ell = \log_2 c$ and γm_{rf} bits, where M denotes the constellation size of the Gray-coded M-QAM being employed for the proposed system, c is the number of usable codewords employed by MBSTBC-CSM and MBSTBC-SM. m_{rf} is the number of RF mirror units associated with each transmit antenna and γ, $\gamma \in [1:2]$ is a scaler multiplier determined by the scheme employed, as reported in [22]. The first group of d input bits, $2\log_2 M$ bits are further subdivided into two groups m_1 and m_2 each having $\log_2 M$ bits. These bits are employed to select the symbols x_p and x_q, $p, q \in [1:M]$, which denote the p-th and q-th symbols of the M-QAM constellations Ω_1 and Ω_2, respectively, where $\Omega_2 = \Omega_1 e^{j\phi}$ and ϕ is the optimized rotation angle given in [13]. Note, for MBSTBC-SM $\phi = 0$, while for MBSTBC-CSM $0 < \phi \leq \pi$. The second group of d input bits, b_ℓ bits are employed to select the ℓ-th, $\ell \in [1:c]$ transmit antenna pair (t_1, t_2), $t_1, t_2 \in [1:N_t]$ that is employed to transmit the Alamouti codeword. Lastly, γm_{rf} bits, are employed to select the MAP indices z_k, z_l, z_m and z_n of the available $M_{rf} = 2^{m_{rf}}$ MAPs associated with each transmit antenna, where z_k, z_l, z_m, $z_n \in [1:M_{rf}]$. z_k and z_l are the MAP indices employed by the transmit antennas t_1 and t_2, respectively, during time-slot 1, while z_m and z_n are the MAP indices for the transmit antennas t_1 and t_2, respectively, during time-slot 2.

Three schemes are reported in [22]. In Scheme 2, $\gamma = 1$ [22]; the MAP index $z_k = z_l = z_m = z_n$,

i.e., the MAP indices activated for time-slots 1 and 2 and for all activated transmit antennas are the same. A tabular illustration presenting the bit assignments and the outputs from the RF mirror switch controller of MBSTBC-CSM/MBSTBC-SM with $c = 4$, 4-QAM employing Scheme 2 is presented in Table C.1.

Table C.1: Bit assignments and outputs from RF switch controller for Scheme 2

Bits	m_1	p	m_2	q	b_ℓ	ℓ	t_1, t_2	m_{rf}	z_k
11000110	11	4	00	1	01	2	3,4	10	3
01011101	01	2	01	2	11	4	1,4	01	2

In Scheme 1 and 3, $\gamma = 2$, however, the difference between Scheme 1 and Scheme 3 is that, in Scheme 1, $z_m = z_k$ and $z_n = z_l$, while in Scheme 3, $z_m = z_l$ and $z_n = z_k$ [22]. Given that N_t is the same for MBSTBC-CSM and MBSTBC-SM the spectral efficiency of MBSTBC-CSM $R_c \geq R_s$, where R_s is the spectral efficiency of MBSTBC-SM. This is because $c = \lfloor N_t\,(N_t - 1) \rfloor_{2p}$ for MBSTBC-CSM, whereas $c = \lfloor \frac{N_t(N_t-1)}{2} \rfloor_{2p}$ for MBSTBC-SM. Furthermore, the spectral efficiency of Scheme 2 $R_{S_2} < R_{S_1} = R_{S_3}$, where R_{S_1} and R_{S_3} are the spectral efficiencies of Scheme 1 and Scheme 3, respectively. This is because 2 groups of m_{rf} bits are assigned to select z_k and z_l as illustrated in Table C.2.

Table C.2: Bit assignments for Scheme 1 and Scheme 3

Bits	m_1	m_2	b_ℓ	m_{rf_1}	m_{rf_2}
1100011001	11	00	01	10	01
0101110110	01	01	11	01	10

The outputs of the mapped bit assignments of Table C.2 are presented in Table C.3.

Table C.3: Outputs from RF switch controller for Scheme 1 and Scheme 3

Bits	p	q	ℓ	t_1, t_2	z_k	z_l
1100011001	4	1	2	3,4	3	2
0101110110	2	2	4	1,4	2	3

During the first time-slot, the ℓ-th transmit antenna pair (t_1, t_2) transmits the symbols $s_{p_1} = x_p e^{j\theta_k}$ and $s_{q_1} = x_q e^{j\theta_k}$ with the z_k-th and z_l-th MAP activated, respectively, while in the second time-slot, $s_{q_2} = -(x_q e^{j\theta_k})^*$ and $s_{p_2} = (x_p e^{j\theta_k})^*$ are transmitted by the same transmit antenna pair, with

the z_m-th and z_n-th MAP indices activated, respectively, where θ_k is the rotation angle of the k-th codebook in which the ℓ-th selected codeword is located. The received signal vectors $\boldsymbol{y}_1$ and $\boldsymbol{y}_2$ of MBSTBC-CSM/MBSTBC-SM over a fast frequency-flat Rayleigh fading channel during time-slots 1 and 2 may be defined as:

$$\boldsymbol{y}_1 = \sqrt{\frac{\rho}{2}} \left(\boldsymbol{H}^1_{\ell,t_1} s_{p_1} \boldsymbol{e}_{z_k} + \boldsymbol{H}^1_{\ell,t_2} s_{q_1} \boldsymbol{e}_{z_l} \right) + \boldsymbol{\eta}_1 \tag{C.4.1}$$

$$\boldsymbol{y}_2 = \sqrt{\frac{\rho}{2}} \left(\boldsymbol{H}^2_{\ell,t_1} s_{q_2} \boldsymbol{e}_{z_m} + \boldsymbol{H}^2_{\ell,t_2} s_{p_2} \boldsymbol{e}_{z_n} \right) + \boldsymbol{\eta}_2 \tag{C.4.2}$$

respectively, where $\frac{\rho}{2}$ is the average signal-to-noise ratio (SNR) at the receive antennas, $\boldsymbol{H}^i_{\ell,t_1}$ and $\boldsymbol{H}^i_{\ell,t_2}$, $\ell \in [1:c]$, $i \in [1:2]$, $t_1, t_2 \in [1:N_t]$, are the $N_r \times M_{rf}$ channel matrix for the transmit antennas t_1 and t_2, respectively, employed during time-slot i. $\boldsymbol{H}^i_{\ell,t_1}, \boldsymbol{H}^i_{\ell,t_2} \in \boldsymbol{H}_i = [\boldsymbol{H}^i_{\ell,1}\ \boldsymbol{H}^i_{\ell,2}\ \cdots \boldsymbol{H}^i_{\ell,N_t}]$ and $\boldsymbol{H} = [\boldsymbol{H}_1\ \boldsymbol{H}_2]$. $\boldsymbol{\eta}_1$ and $\boldsymbol{\eta}_2$ are $N_r \times 1$ AWGN vectors for time-slot 1 and 2, respectively. $\boldsymbol{H}^i_{\ell,t_\alpha} = [\boldsymbol{h}^{i,\ell}_{t_\alpha,1} \quad \boldsymbol{h}^{i,\ell}_{t_\alpha,2} \quad \cdots \quad \boldsymbol{h}^{i,\ell}_{t_\alpha,M_{rf}}]$, the entries of the vectors $\boldsymbol{h}^{i,\ell}_{t_\alpha,\psi} = [h^{i,\ell,t_\alpha}_{1,\psi} \quad h^{i,\ell,t_\alpha}_{2,\psi} \quad \cdots \quad h^{i,\ell,t_\alpha}_{N_r,\psi}]^T$, $\psi \in [1:M_{rf}]$ and $\boldsymbol{\eta}_i = [\eta_{1,i} \quad \eta_{2,i} \quad \cdots \quad \eta_{N_r,i}]^T$, $i \in [1:2]$ are i.i.d. according to $CN(0,1)$ distribution. $\boldsymbol{e}_{z_k}$ and $\boldsymbol{e}_{z_l}$ are $M_{rf} \times 1$ vectors for time-slot 1 having the z_k-th and z_l-th element as unity, respectively, while other elements are zeros. $\boldsymbol{e}_{z_m}$ and $\boldsymbol{e}_{z_n}$ are $M_{rf} \times 1$ vectors for time-slot 2 having the z_m-th and z_n-th element as unity, respectively, while other elements are zeros. Note, the expectation of the transmitted symbol is unity.

The expression in (C.4.1) and (C.4.2) for the received signal vectors during time-slots 1 and 2 may be rewritten as:

$$\boldsymbol{y}_1 = \sqrt{\frac{\rho}{2}} \left(\boldsymbol{h}^{1,\ell}_{t_1,z_k} s_{p_1} + \boldsymbol{h}^{1,\ell}_{t_2,z_l} s_{q_1} \right) + \boldsymbol{\eta}_1 \tag{C.5.1}$$

$$\boldsymbol{y}_2 = \sqrt{\frac{\rho}{2}} \left(\boldsymbol{h}^{2,\ell}_{t_1,z_m} s_{q_2} + \boldsymbol{h}^{2,\ell}_{t_2,z_n} s_{p_2} \right) + \boldsymbol{\eta}_2 \tag{C.5.2}$$

where $\boldsymbol{h}^{1,\ell}_{t_1,z_k}$ and $\boldsymbol{h}^{1,\ell}_{t_2,z_l}$ are the z_k-th and z_l-th column vectors of the channel matrix $\boldsymbol{H}^1_{\ell,t_1}$ and $\boldsymbol{H}^1_{\ell,t_2}$, given that the z_k-th and z_l-th MAPs are activated at the t_1-th and t_2-th transmit antennas, respectively, during time-slot 1. Also, $\boldsymbol{h}^{2,\ell}_{t_1,z_m}$ and $\boldsymbol{h}^{2,\ell}_{t_2,z_n}$ are the z_m-th and z_n-th column vectors of $\boldsymbol{H}^2_{\ell,t_1}$ and $\boldsymbol{H}^2_{\ell,t_2}$, given that the z_m-th and z_n-th MAPs are activated at the t_1-th and t_2-th transmit antennas, respectively, during time-slot 2. Considering that in Scheme 2, the same MAP is activated for (t_1, t_2)

and for time-slot 1 and 2, the optimal ML detector for Scheme 2 of the proposed MBSTBC-CSM and MBSTBC-SM may be defined as:

$$\left[\hat{\ell}, \hat{z}_k, \hat{p}, \hat{q}\right] = \underset{\substack{\hat{\ell}\in[1:c],\, \hat{z}_k\in\left[1:M_{rf}\right] \\ \hat{x}_p\in\Omega_1,\, \hat{x}_q\in\Omega_2}}{\operatorname{argmin}} \left(\left\| \boldsymbol{y}_1 - \sqrt{\frac{\rho}{2}} \left(\boldsymbol{h}^{1,\ell}_{t_1,z_k} s_{p_1} + \boldsymbol{h}^{1,\ell}_{t_2,z_k} s_{q_1} \right) \right\|_F^2 + \left\| \boldsymbol{y}_2 - \sqrt{\frac{\rho}{2}} \left(\boldsymbol{h}^{2,\ell}_{t_1,z_k} s_{q_2} + \boldsymbol{h}^{2,\ell}_{t_2,z_k} s_{p_2} \right) \right\|_F^2 \right) \quad \text{(C.6.1)}$$

while, for Scheme 1 and Scheme 3, it may be defined as:

$$\left[\hat{\ell}, \hat{z}_k, \hat{z}_l, \hat{p}, \hat{q}\right] = \underset{\substack{\hat{\ell}\in[1:c],\, \hat{z}_k\in\left[1:M_{rf}\right] \\ \hat{x}_p\in\Omega_1\, \hat{x}_q\in\Omega_2 \\ \hat{z}_l\in\left[1:M_{rf}\right]}}{\operatorname{argmin}} \left(\left\| \boldsymbol{y}_1 - \sqrt{\frac{\rho}{2}} \left(\boldsymbol{h}^{1,\ell}_{t_1,z_k} s_{p_1} + \boldsymbol{h}^{1,\ell}_{t_2,z_l} s_{q_1} \right) \right\|_F^2 + \left\| \boldsymbol{y}_2 - \sqrt{\frac{\rho}{2}} \left(\boldsymbol{h}^{2,\ell}_{t_1,z_m} s_{q_2} + \boldsymbol{h}^{2,\ell}_{t_2,z_n} s_{p_2} \right) \right\|_F^2 \right) \quad \text{(C.6.2)}$$

where $\hat{\ell}$, $\hat{z}_k$, $\hat{z}_l$, $\hat{p}$ and $\hat{q}$ are estimates of ℓ, z_k, z_l, p and q, respectively.

The expressions in (C.6.1) and (C.6.2) may be further simplified as [23]:

$$\begin{aligned}\left[\hat{\ell}, \hat{z}_k, \hat{p}, \hat{q}\right] &= \sqrt{\frac{\rho}{2}} \left\| \boldsymbol{g}^k_{p_1} \right\|_F^2 + \sqrt{\frac{\rho}{2}} \left\| \boldsymbol{g}^k_{q_1} \right\|_F^2 - 2\Re\left(\boldsymbol{y}_1^H \boldsymbol{g}^k_{p_1} \right) \\ &\quad - 2\Re\left(\boldsymbol{y}_1^H \boldsymbol{g}^k_{q_1} \right) + \sqrt{2\rho}\Re\left(\left(\boldsymbol{g}^k_{p_1} \right)^H \boldsymbol{g}^k_{q_1} \right) + \sqrt{\frac{\rho}{2}} \left\| \boldsymbol{g}^k_{q_2} \right\|_F^2 + \sqrt{\frac{\rho}{2}} \left\| \boldsymbol{g}^k_{p_2} \right\|_F^2 - 2\Re\left(\boldsymbol{y}_2^H \boldsymbol{g}^k_{q_2} \right) \\ &\quad - 2\Re\left(\boldsymbol{y}_2^H \boldsymbol{g}^k_{p_2} \right) + \sqrt{2\rho}\Re\left(\left(\boldsymbol{g}^k_{q_2} \right)^H \boldsymbol{g}^k_{p_2} \right) \quad \text{(C.7.1)}\end{aligned}$$

where $\boldsymbol{g}^k_{p_1} = \boldsymbol{h}^{1,\ell}_{t_1,z_k} s_{p_1}$, $\boldsymbol{g}^k_{q_1} = \boldsymbol{h}^{1,\ell}_{t_2,z_k} s_{q_1}$, $\boldsymbol{g}^k_{q_2} = \boldsymbol{h}^{2,\ell}_{t_1,z_k} s_{q_2}$, $\boldsymbol{g}^k_{p_2} = \boldsymbol{h}^{2,\ell}_{t_2,z_k} s_{p_2}$, and

$$\begin{aligned}\left[\hat{\ell}, \hat{z}_k, \hat{z}_l, \hat{p}, \hat{q}\right] &= \sqrt{\frac{\rho}{2}} \left\| \boldsymbol{g}^k_{p_1} \right\|_F^2 + \sqrt{\frac{\rho}{2}} \left\| \boldsymbol{g}^l_{q_1} \right\|_F^2 - 2\Re\left(\boldsymbol{y}_1^H \boldsymbol{g}^k_{p_1} \right) \\ &\quad - 2\Re\left(\boldsymbol{y}_1^H \boldsymbol{g}^l_{q_1} \right) + \sqrt{2\rho}\Re\left(\left(\boldsymbol{g}^k_{p_1} \right)^H \boldsymbol{g}^l_{q_1} \right) + \sqrt{\frac{\rho}{2}} \left\| \boldsymbol{g}^m_{q_2} \right\|_F^2 + \sqrt{\frac{\rho}{2}} \left\| \boldsymbol{g}^n_{p_2} \right\|_F^2 - 2\Re\left(\boldsymbol{y}_2^H \boldsymbol{g}^k_{q_2} \right) \\ &\quad - 2\Re\left(\boldsymbol{y}_2^H \boldsymbol{g}^l_{p_2} \right) + \sqrt{2\rho}\Re\left(\left(\boldsymbol{g}^m_{q_2} \right)^H \boldsymbol{g}^n_{p_2} \right) \quad \text{(C.7.2)}\end{aligned}$$

where $\boldsymbol{g}^k_{p_1} = \boldsymbol{h}^{1,\ell}_{t_1,z_k} s_{p_1}$, $\boldsymbol{g}^l_{q_1} = \boldsymbol{h}^{1,\ell}_{t_2,z_l} s_{q_1}$, $\boldsymbol{g}^m_{q_2} = \boldsymbol{h}^{2,\ell}_{t_1,z_m} s_{q_2}$ and $\boldsymbol{g}^n_{p_2} = \boldsymbol{h}^{2,\ell}_{t_2,z_n} s_{p_2}$.

3 Theoretical ABEP of MBSTBC-CSM and MBSTBC-SM

In this section, the theoretical ABEP of MBSTBC-CSM/MBSTBC-SM over a fast frequency-flat Rayleigh fading channel employing ML detection is formulated.

Considering that the MBSTBC-CSM/MBSTBC-SM can be viewed as an $N_t M_{rf} \times N_r$ STBC-CSM/STBC-SM system [27], having the transmitted codeword $\boldsymbol{X} = \left[(s_{p_1}\boldsymbol{e}_{z_k} + s_{q_1}\boldsymbol{e}_{z_l}) \quad (s_{q_2}\boldsymbol{e}_{z_m} + s_{p_2}\boldsymbol{e}_{z_n})\right]$ being erroneously detected as $\hat{\boldsymbol{X}} = \left[(s_{\hat{p}_1}\boldsymbol{e}_{\hat{z}_k} + s_{\hat{q}_1}\boldsymbol{e}_{\hat{z}_l}) \quad (s_{\hat{q}_2}\boldsymbol{e}_{\hat{z}_m} + s_{\hat{p}_2}\boldsymbol{e}_{\hat{z}_n})\right]$, where $p, q \in [1:M]$, $t_1, t_2 \in [1:N_t]$, $t_1 \neq t_2$, $z_k, z_l, z_m, z_n \in [1:Mrf]$, $\boldsymbol{e}_{z_b}$ and $\boldsymbol{e}_{\hat{z}_b}$, $z_b, \hat{z}_b \in [1:M_{rf}]$ are $N_t M_{rf} \times 1$ vectors, which have the r-th element as unity, where $r = M_{rf}(t_a - 1) + z_b$, $a \in [1:2]$ and z_b is the MAP index associated with the t_a-th transmit antenna, while other elements are zeros.

The ABEP of MBSTBC-CSM/MBSTBC-SM may be defined as:

$$ABEP \leq \frac{1}{cM_{rf}^{\gamma}M^2} \sum_{\boldsymbol{X}} \sum_{\hat{\boldsymbol{X}}} \frac{N_{\boldsymbol{X}\hat{\boldsymbol{X}}} P\left(\boldsymbol{X} \rightarrow \hat{\boldsymbol{X}}\right)}{(\log_2 c + 2\log_2 M + \gamma \log_2 M_{rf})} \tag{C.8}$$

where $P(\boldsymbol{X} \rightarrow \hat{\boldsymbol{X}})$ is the pairwise error probability (PEP), when $\boldsymbol{X}$ is transmitted and detected erroneously as $\hat{\boldsymbol{X}}$. $N_{\boldsymbol{X}\hat{\boldsymbol{X}}}$ is the number of bits detected in error given the PEP event $P(\boldsymbol{X} \rightarrow \hat{\boldsymbol{X}})$.

Given that $\boldsymbol{H}_1 = [\boldsymbol{H}^1_{\ell,t_1} \ \boldsymbol{H}^1_{\ell,t_2}]$ and $\boldsymbol{H}_2 = [\boldsymbol{H}^2_{\ell,t_1} \ \boldsymbol{H}^2_{\ell,t_2}]$ are the channel matrix for time-slot 1 and 2, respectively, the conditional PEP $P(\boldsymbol{X} \rightarrow \hat{\boldsymbol{X}} \mid \boldsymbol{H}_1, \boldsymbol{H}_2)$ may be formulated as [23]:

$$\begin{aligned} P\left(\boldsymbol{X} \rightarrow \hat{\boldsymbol{X}} \mid \boldsymbol{H}_1, \boldsymbol{H}_2\right) = P\Bigg(&\left\|\boldsymbol{y}_1 - \sqrt{\frac{\rho}{2}}\left(\boldsymbol{H}^1_{\hat{\ell},t_1} s_{\hat{p}_1}\boldsymbol{e}_{\hat{z}_k} + \boldsymbol{H}^1_{\hat{\ell},t_2} s_{\hat{q}_1}\boldsymbol{e}_{\hat{z}_l}\right)\right\|_F^2 \\ &+ \left\|\boldsymbol{y}_2 - \sqrt{\frac{\rho}{2}}\left(\boldsymbol{H}^2_{\hat{\ell},t_1} s_{\hat{q}_2}\boldsymbol{e}_{\hat{z}_m} + \boldsymbol{H}^2_{\hat{\ell},t_2} s_{\hat{p}_2}\boldsymbol{e}_{\hat{z}_n}\right)\right\|_F^2 < \|\boldsymbol{\eta}_1\|_F^2 + \|\boldsymbol{\eta}_2\|_F^2\Bigg) \end{aligned} \tag{C.9}$$

In a similar method as [28], (C.9) may be simplified as:

$$P\left(\boldsymbol{X} \rightarrow \hat{\boldsymbol{X}} \mid \boldsymbol{H}_1, \boldsymbol{H}_2\right) = Q\left(\sqrt{\frac{\rho}{8}\left(\|\boldsymbol{H}_1\|_F^2 \|\boldsymbol{X}_1\|_F^2 + \|\boldsymbol{H}_2\|_F^2 \|\boldsymbol{X}_2\|_F^2\right)}\right) \tag{C.10}$$

where $\boldsymbol{X}_1 = \hat{\boldsymbol{X}}_{c_1} - \boldsymbol{X}_{c_1}$ and $\boldsymbol{X}_2 = \hat{\boldsymbol{X}}_{c_2} - \boldsymbol{X}_{c_2}$, $\hat{\boldsymbol{X}}_{c_i}$ and $\boldsymbol{X}_{c_i}$, $i \in [1:2]$ denotes the i-th column of $\hat{\boldsymbol{X}}$ and $\boldsymbol{X}$, respectively.

Applying a similar method to [28], which employs the approach of the moment generating function (MGF), the unconditional PEP $P(\boldsymbol{X} \rightarrow \hat{\boldsymbol{X}})$ may be formulated as [20]:

$$P\left(\boldsymbol{X}\rightarrow\hat{\boldsymbol{X}}\right)=\frac{1}{2g}\left[\frac{1}{2}M_1\left(\frac{1}{2}\right)M_2\left(\frac{1}{2}\right)+\sum_{\upsilon=1}^{g-1}M_1\left(\frac{1}{2\sin^2\theta_\upsilon}\right)M_2\left(\frac{1}{2\sin^2\theta_\upsilon}\right)\right] \tag{C.11}$$

where $M_i(w)=\left(\frac{1}{1+2w\sigma_{\alpha_i}^2}\right)^{N_r}$, $\sigma_{\alpha_i}^2=\frac{\rho}{8}\left\|\boldsymbol{X}_i\right\|_F^2$, $i\in[1:2]$, and $\theta_\upsilon=\frac{\upsilon\pi}{2g}$, g denotes the number of iterations needed for convergence of the trapezoidal approximation of the Q-function.

4 Low-complexity detector for MBSTBC-CSM/MBSTBC-SM

In this section, a low-complexity detector for MBSTBC-CSM/MBSTBC-SM over a fast frequency-flat Rayleigh fading channel, is proposed. This is because the optimal ML detector for MBSTBC-CSM/MBSTBC-SM has an extremely large computational complexity as it employs $cM^2{M_{rf}}^{\gamma}$ search iterations. Considering an $N_t\times N_r$ MBSTBC-CSM/MBSTBC-SM transceiver system having m_{rf} RF mirrors associated with each transmit antenna. The proposed low-complexity near-ML detector of MBSTBC-CSM/MBSTBC-SM which employs orthogonal projection [24, 26], firstly determines ζ_1 and ζ_2 most likely estimates $\boldsymbol{z}_p^{\ell}=\begin{bmatrix}\hat{z}_{z_k,1}^{\ell,p} & \hat{z}_{z_k,2}^{\ell,p} & \cdots & \hat{z}_{z_k,\zeta_1}^{\ell,p}\end{bmatrix}$, $\boldsymbol{z}_p^{\ell}\subseteq\Omega_1 e^{\theta_k}$ and $\boldsymbol{z}_q^{\ell}=\begin{bmatrix}\hat{z}_{z_l,1}^{\ell,q} & \hat{z}_{z_l,2}^{\ell,q} & \cdots & \hat{z}_{z_l,\zeta_1}^{\ell,q}\end{bmatrix}$, $\boldsymbol{z}_q^{\ell}\subseteq\Omega_2 e^{\theta_k}$ of the transmitted symbols s_{p_1} and s_{q_1}, for every transmit antenna pair (t_1,t_2) and every MAP combination (z_k,z_l), respectively, where $z_k,z_l\in[1:M_{rf}]$, $M_{rf}=2^{m_{rf}}$, $p,q\in[1:M]$, $t_1,t_2\in[1:N_t]$, $t_1\neq t_2$ and $\zeta_1\zeta_2\ll M^2$.

To determine the most likely candidate of the transmitted symbol, the orthogonal projection matrix $\boldsymbol{P}_{t_a,z_b}^{i,\ell}$, $i,a\in[1:2]$ and $z_b\in[1:M_{rf}]$ corresponding to the channel subspace $\boldsymbol{h}_{t_a,z_b}^{i,\ell}$ is computed, such that $\boldsymbol{P}_{t_a,z_b}^{i,\ell}\boldsymbol{h}_{t_a,z_b}^{i,\ell}=0$. $\boldsymbol{P}_{t_a,z_b}^{i,\ell}$ may be expressed as [26]:

$$\boldsymbol{P}_{t_a,z_b}^{i,\ell}=\boldsymbol{I}_{N_r}-\boldsymbol{h}_{t_a,z_b}^{i,\ell}\left(\left(\boldsymbol{h}_{t_a,z_b}^{i,\ell}\right)^H\boldsymbol{h}_{t_a,z_b}^{i,\ell}\right)^{-1}\left(\boldsymbol{h}_{t_a,z_b}^{i,\ell}\right)^H \tag{C.12}$$

where $\boldsymbol{P}_{t_a,z_b}^{i,\ell}$ is the projection matrix of the t_a-th transmit antenna during the i-th time-slot, given that the ℓ-th transmit antenna pair is selected and the z_b-th MAP is activated. If $\hat{z}_{z_k,u_1}^{\ell,p}=s_{p_1}$, $u_1\in[1:\zeta_1]$ and $\hat{z}_{z_l,u_2}^{\ell,q}=s_{q_1}$, $u_2\in[1:\zeta_2]$, then the sum of the projections can be formulated as [26]:

$$\boldsymbol{P}_{t_2,z_l}^{1,\ell}\left(\boldsymbol{y}_1-\sqrt{\frac{\rho}{2}}\boldsymbol{h}_{t_1,z_k}^{1,\ell}\hat{z}_{z_k,u_1}^{\ell,p}\right)+\boldsymbol{P}_{t_1,z_m}^{2,\ell}\left(\boldsymbol{y}_2-\sqrt{\frac{\rho}{2}}\boldsymbol{h}_{t_2,z_n}^{2,\ell}(\hat{z}_{z_k,u_1}^{\ell,p})^*\right)=\boldsymbol{P}_{t_2,z_l}^{1,\ell}\boldsymbol{\eta}_1+\boldsymbol{P}_{t_1,z_m}^{2,\ell}\boldsymbol{\eta}_2 \tag{C.13.1}$$

$$\boldsymbol{P}_{t_1,z_k}^{1,\ell}\left(\boldsymbol{y}_1-\sqrt{\frac{\rho}{2}}\boldsymbol{h}_{t_2,z_l}^{1,\ell}\hat{z}_{z_l,u_2}^{\ell,q}\right)+\boldsymbol{P}_{t_2,z_n}^{2,\ell}\left(\boldsymbol{y}_2+\sqrt{\frac{\rho}{2}}\boldsymbol{h}_{t_1,z_m}^{2,\ell}(\hat{z}_{z_l,u_2}^{\ell,q})^*\right)=\boldsymbol{P}_{t_1,z_k}^{1,\ell}\boldsymbol{\eta}_1+\boldsymbol{P}_{t_2,z_n}^{2,\ell}\boldsymbol{\eta}_2 \tag{C.13.2}$$

however, if $\hat{z}_{z_k,u_1}^{\ell,p}\neq s_{p_1}$ and $\hat{z}_{z_l,u_2}^{\ell,q}\neq s_{q_1}$, (C.13.1) and (C.13.2), respectively, yield [26]:

$$\sqrt{\frac{\rho}{2}}\boldsymbol{P}_{t_2,z_l}^{1,\ell}\boldsymbol{h}_{t_1,z_k}^{1,\ell}\left(s_{p_1}-\hat{z}_{z_k,u_1}^{\ell,p}\right)+\sqrt{\frac{\rho}{2}}\boldsymbol{P}_{t_1,z_m}^{2,\ell}\boldsymbol{h}_{t_2,z_n}^{2,\ell}\left(s_{p_2}-(\hat{z}_{z_k,u_1}^{\ell,p})^*\right)+\boldsymbol{P}_{t_2,z_l}^{1,\ell}\boldsymbol{\eta}_1+\boldsymbol{P}_{t_1,z_m}^{2,\ell}\boldsymbol{\eta}_2 \tag{C.14.1}$$

$$\sqrt{\frac{\rho}{2}}\boldsymbol{P}_{t_1,z_k}^{1,\ell}\boldsymbol{h}_{t_2,z_l}^{1,\ell}\left(s_{q_1}-\hat{z}_{z_l,u_2}^{\ell,q}\right)+\sqrt{\frac{\rho}{2}}\boldsymbol{P}_{t_2,z_n}^{2,\ell}\boldsymbol{h}_{t_1,z_m}^{2,\ell}\left(s_q^2+(\hat{z}_{z_l,u_2}^{\ell,q})^*\right)+\boldsymbol{P}_{t_1,z_k}^{1,\ell}\boldsymbol{\eta}_1+\boldsymbol{P}_{t_2,z_n}^{2,\ell}\boldsymbol{\eta}_2 \tag{C.14.2}$$

Since the Frobenius norms of (C.14.1) and (C.14.2) are greater than (C.13.1) and (C.13.2), respectively, then, ζ_1 and ζ_2 symbols, which yields the smallest Frobenius norms are selected as the most likely candidates of the transmitted symbols. Secondly, an exhaustive search across the most likely candidate sets $\boldsymbol{z}_p^\ell$ and $\boldsymbol{z}_q^\ell$ is performed by employing the ML rule. The algorithm for the proposed low-complexity detector of MBSTBC-CSM/MBSTBC-SM is as follows.

Step 1: Determine the projection spaces $\boldsymbol{r}_{t_a,p,z_b}^{i,\ell}$ and $\boldsymbol{r}_{t_a,q,z_b}^{i,\ell}$, and the projection matrix $\boldsymbol{P}_{t_a,z_b}^{i,\ell}$, such that $\boldsymbol{P}_{t_a,z_b}^{i,\ell}\boldsymbol{h}_{t_a,z_b}^{i,\ell}=0$ where $i,a\in[1:2]$, $\ell\in[1:c]$, $p,q\in[1:M]$, $z_b\in[1:M_{rf}]$. The projection spaces for the ℓ-th pair of transmit antennas for the proposed system are expressed as [24, 26]:

$$\boldsymbol{r}_{t_1,p,z_k}^{1,\ell}=\boldsymbol{y}_1-\sqrt{\frac{\rho}{2}}\boldsymbol{h}_{t_1,z_k}^{1,\ell}s_{p_1},\quad p_1\in[1:M] \tag{C.15.1}$$

$$\boldsymbol{r}_{t_2,q,z_l}^{1,\ell}=\boldsymbol{y}_1-\sqrt{\frac{\rho}{2}}\boldsymbol{h}_{t_2,z_l}^{1,\ell}s_{q_1},\quad q_1\in[1:M] \tag{C.15.2}$$

$$\boldsymbol{r}_{t_1,q,z_m}^{2,\ell}=\boldsymbol{y}_2-\sqrt{\frac{\rho}{2}}\boldsymbol{h}_{t_1,z_m}^{2,\ell}s_{q_2},\quad q_2\in[1:M] \tag{C.16.1}$$

$$\boldsymbol{r}_{t_2,p,z_n}^{2,\ell}=\boldsymbol{y}_2-\sqrt{\frac{\rho}{2}}\boldsymbol{h}_{t_2,z_n}^{2,\ell}s_{p_2},\quad p_2\in[1:M] \tag{C.16.2}$$

where $\boldsymbol{h}_{t_1,z_k}^{1,\ell}$, $\boldsymbol{h}_{t_2,z_l}^{1,\ell}$, $\boldsymbol{h}_{t_1,z_m}^{2,\ell}$ and $\boldsymbol{h}_{t_2,z_n}^{2,\ell}$ corresponds to the z_k-th, z_l-th, z_m-th and z_n-th columns of $\boldsymbol{H}_{\ell,t_1}^{1}$, $\boldsymbol{H}_{\ell,t_2}^{1}$, $\boldsymbol{H}_{\ell,t_1}^{2}$ and $\boldsymbol{H}_{\ell,t_2}^{2}$, respectively, for the ℓ-th antenna pair. The projection matrices $\boldsymbol{P}_{t_1,z_k}^{1,\ell}$, $\boldsymbol{P}_{t_2,z_l}^{1,\ell}$, $\boldsymbol{P}_{t_1,z_m}^{2,\ell}$ and $\boldsymbol{P}_{t_2,z_n}^{2,\ell}$ are given in (C.17.1)-(C.18.2) as [24, 26]:

$$\boldsymbol{P}_{t_1,z_k}^{1,\ell} = \boldsymbol{I}_{N_r} - \boldsymbol{h}_{t_1,z_k}^{1,\ell} \left(\left(\boldsymbol{h}_{t_1,z_k}^{1,\ell} \right)^H \boldsymbol{h}_{t_1,z_k}^{1,\ell} \right)^{-1} \left(\boldsymbol{h}_{t_1,z_k}^{1,\ell} \right)^H \tag{C.17.1}$$

$$\boldsymbol{P}_{t_2,z_l}^{1,\ell} = \boldsymbol{I}_{N_r} - \boldsymbol{h}_{t_2,z_l}^{1,\ell} \left(\left(\boldsymbol{h}_{t_2,z_l}^{1,\ell} \right)^H \boldsymbol{h}_{t_2,z_l}^{1,\ell} \right)^{-1} \left(\boldsymbol{h}_{t_2,z_l}^{1,\ell} \right)^H \tag{C.17.2}$$

$$\boldsymbol{P}_{t_1,z_m}^{2,\ell} = \boldsymbol{I}_{N_r} - \boldsymbol{h}_{t_1,z_m}^{2,\ell} \left(\left(\boldsymbol{h}_{t_1,z_m}^{2,\ell} \right)^H \boldsymbol{h}_{t_1,z_m}^{2,\ell} \right)^{-1} \left(\boldsymbol{h}_{t_1,z_m}^{2,\ell} \right)^H \tag{C.18.1}$$

$$\boldsymbol{P}_{t_2,z_n}^{2,\ell} = \boldsymbol{I}_{N_r} - \boldsymbol{h}_{t_2,z_n}^{2,\ell} \left(\left(\boldsymbol{h}_{t_2,z_n}^{2,\ell} \right)^H \boldsymbol{h}_{t_2,z_n}^{2,\ell} \right)^{-1} \left(\boldsymbol{h}_{t_2,z_n}^{2,\ell} \right)^H \tag{C.18.2}$$

Step 2: Determine the ζ_1 and ζ_2 most likely estimates of s_{p_1} and s_{q_1}, $\boldsymbol{z}_p^{\ell} = \begin{bmatrix} \hat{z}_{z_k,1}^{\ell,p} & \hat{z}_{z_k,2}^{\ell,p} & \cdots & \hat{z}_{z_k,\zeta_1}^{\ell,p} \end{bmatrix}$ and $\boldsymbol{z}_q^{\ell} = \begin{bmatrix} \hat{z}_{z_l,1}^{\ell,q} & \hat{z}_{z_l,2}^{\ell,q} & \cdots & \hat{z}_{z_l,\zeta_1}^{\ell,q} \end{bmatrix}$ for the ℓ-th, $\ell = [1:c]$ transmit antenna pair and all $(M_{rf})^{\gamma}$ MAP combinations formulated as [26]:

$$\hat{z}_{z_k,u_1}^{\ell,p} = \underset{\substack{\boldsymbol{r}_{t_1,p,z_k}^{1,\ell}, \\ \boldsymbol{r}_{t_2,p,z_n}^{2,\ell}}}{\operatorname{argmin}} \left\| \boldsymbol{P}_{t_2,z_l}^{1,\ell} \boldsymbol{r}_{t_1,p,z_k}^{1,\ell} + \boldsymbol{P}_{t_1,z_m}^{2,\ell} \boldsymbol{r}_{t_2,p,z_n}^{2,\ell} \right\|_F^2 \tag{C.19.1}$$

$$\hat{z}_{z_l,u_2}^{\ell,q} = \underset{\substack{\boldsymbol{r}_{t_2,q,z_l}^{1,\ell}, \\ \boldsymbol{r}_{t_1,q,z_m}^{2,\ell}}}{\operatorname{argmin}} \left\| \boldsymbol{P}_{t_1,z_k}^{1,\ell} \boldsymbol{r}_{t_2,q,z_l}^{1,\ell} + \boldsymbol{P}_{t_2,z_n}^{2,\ell} \boldsymbol{r}_{t_2,q,z_m}^{2,\ell} \right\|_F^2 \tag{C.19.2}$$

where $\ell \in [1:c]$, $z_k, z_l, z_m, z_n \in [1:M_{rf}]$, $p, q \in [1:M]$.

Step 3: Perform an exhaustive search of all elements in $\boldsymbol{z}_p^{\ell}$ and $\boldsymbol{z}_q^{\ell}$ employing the ML rule over all c transmit antenna pairs and for all $(M_{rf})^{\gamma}$ MAP combinations. The ML expression for Scheme 2 is formulated as [26]:

$$\begin{aligned} [\hat{\ell}, \hat{p}, \hat{q}, \hat{z}_k] = \underset{\boldsymbol{z}_p^{\ell}, \boldsymbol{z}_q^{\ell}}{\operatorname{argmin}} \Bigg\{ & \left\| \boldsymbol{y}_1 - \sqrt{\frac{\rho}{2}} \left(\boldsymbol{h}_{t_1,z_k}^{1,\ell} \hat{z}_{z_k,u_1}^{\ell,p} + \boldsymbol{h}_{t_2,z_k}^{1,\ell} \hat{z}_{z_l,u_2}^{\ell,q} \right) \right\|_F^2 \\ & + \left\| \boldsymbol{y}_2 - \sqrt{\frac{\rho}{2}} \left(\boldsymbol{h}_{t_2,z_k}^{2,\ell} (\hat{z}_{z_k,u_1}^{\ell,p})^* - \boldsymbol{h}_{t_1,z_k}^{2,\ell} (\hat{z}_{z_l,u_2}^{\ell,q})^* \right) \right\|_F^2 \Bigg\} \end{aligned} \tag{C.20.1}$$

while, for Scheme 1 and Scheme 3, (C.20.1) may be formulated as [26]:

$$[\hat{\ell},\hat{p},\hat{q},\hat{z}_k,\hat{z}_l] = \underset{\boldsymbol{z}_p^{\ell},\boldsymbol{z}_q^{\ell}}{\operatorname{argmin}} \left\{ \left\| \boldsymbol{y}_1 - \sqrt{\frac{\rho}{2}} \left(\boldsymbol{h}_{t_1,z_k}^{1,\ell} \hat{z}_{z_k,u_1}^{\ell,p} + \boldsymbol{h}_{t_2,z_l}^{1,\ell} \hat{z}_{z_l,u_2}^{\ell,q} \right) \right\|_F^2 \right.$$
$$\left. + \left\| \boldsymbol{y}_2 - \sqrt{\frac{\rho}{2}} \left(\boldsymbol{h}_{t_2,z_m}^{2,\ell} (\hat{z}_{z_k,u_1}^{\ell,p})^* - \boldsymbol{h}_{t_1,z_n}^{2,\ell} (\hat{z}_{z_l,u_2}^{\ell,q})^* \right) \right\|_F^2 \right\} \quad \text{(C.20.2)}$$

where $\hat{z}_{z_k,u_1}^{\ell,p} \in \boldsymbol{z}_p^{\ell}$, $\hat{z}_{z_l,u_2}^{\ell,q} \in \boldsymbol{z}_q^{\ell}$, $\ell \in [1:c]$, $u_1 \in [1:\zeta_1]$ and $u_2 \in [1:\zeta_2]$.

5 Computational complexity analysis of MBSTBC-CSM/MBSTBC-SM

In this section, the computational complexities of the proposed ML and low-complexity near-ML detectors are compared for MBSTBC-CSM/MBSTBC-SM in terms of the number of complex operations [26, 27].

5.1 Computational complexity of the ML detector for MBSTBC-CSM/MBSTBC-SM

Each term in (C.7.1) and (C.7.2) employs N_r complex multiplications. This is because the vectors in the Frobenius norm terms have been calculated, hence, it does not have to be calculated again, when it is needed. Furthermore, the additions of the six terms in (C.7.1) and (C.7.2), which require the real part of the complex numbers, is ignored. This is because the addition of the real components entail real operations only [23]. Since an exhaustive search involving $cM_{rf}^{\gamma}M^2$ iterations of the complex operations already mentioned are employed, the total computational complexity in terms of complex operations of the proposed ML detector becomes:

$$cM_{rf}^{\gamma}M^2\left(10N_r\right) \quad \text{(C.21)}$$

5.2 Computational complexity of the low-complexity near-ML detector for MBSTBC-CSM/MBSTBC-SM

The computational complexity involved in computing the projection matrices $\boldsymbol{P}_{t_1,z_k}^{1,\ell}$, $\boldsymbol{P}_{t_2,z_l}^{1,\ell}$, $\boldsymbol{P}_{t_1,z_m}^{2,\ell}$ and $\boldsymbol{P}_{t_2,z_n}^{2,\ell}$ in (C.17.1)-(C.18.2) is given in [26] as $8N_r^2 + 12N_r - 4$. Since this operation involves cM_{rf}^{γ} iterations, the total computational complexity for computing the projection matrices in terms of complex operations may be formulated as:

$$\delta_{pm} = cM_{rf}^{\gamma}\left(8N_r^2 + 12N_r - 4\right) \tag{C.22}$$

In order to determine the ζ_1 and ζ_2 most likely estimates of s_{p_1} and s_{q_1}, given in (C.19.1) and (C.19.2), respectively, $8MN_r^2 + 16MN_r + 4N_r - 4M$ complex operations are performed [26]. Since these operations involves cM_{rf}^{γ} iterations, the total number of complex operations employed in determining the ζ_1 and ζ_2 most likely candidate sets for all transmit antenna pairs and all MAP settings may be formulated as:

$$\delta_{lc} = cM_{rf}^{\gamma}\left(8MN_r^2 + 16MN_r + 4N_r - 4M\right) \tag{C.23}$$

The computational complexity of the exhaustive ML search in (C.20.1) and (C.20.2) across the most likely candidate sets $\boldsymbol{z}_p^{\ell}$ and $\boldsymbol{z}_q^{\ell}$ is similar to the ML search in (C.7.1) and (C.7.2), however, the computational complexity is reduced because the search is across $\zeta_1\zeta_2$ symbols, and $\zeta_1\zeta_2 << M^2$. Since these computations undergo cM_{rf}^{γ} iterations, then, the total computational complexity for this stage is given as:

$$\delta_{ML} = cM_{rf}^{\gamma}\zeta_1\zeta_2(10N_r) \tag{C.24}$$

The total computational complexity in terms of complex operations for the proposed low-complexity near-ML detector may be defined as:

$$\begin{aligned}\delta_{MBSTBC-SM} \neq \delta_{MBSTBC-CSM}& \\ = \delta_{pm} + \delta_{lc} + \delta_{ML} &= 2cM_{rf}^{\gamma}\left[4N_r^2(M+1)\right. \\ &\left. +N_r(8M + 5\zeta_1\zeta_2 + 8) - 2(M+1)\right]\end{aligned} \tag{C.25}$$

where $c = \lfloor N_t\left(N_t - 1\right)\rfloor_{2p}$ for MBSTBC-CSM, whereas, $c = \lfloor\frac{N_t(N_t-1)}{2}\rfloor_{2p}$ for MBSTBC-SM, as noted earlier.

The numerical values of the computational complexities in terms of complex operations, for the ML and the low-complexity detectors are presented in Table C.4 for a spectral efficiency of 7 bpcu. It should be noted that although the computational complexities of MBSTBC-CSM and MBSTBC-SM are the same for a given spectral efficiency δ_{SE}, the number of transmit antennas employed by MBSTBC-SM is more than that of MBSTBC-CSM.

Table C.4: Computational complexity of ML with low-complexity detector

CONFIGURATION	δ_{SE}	ML	LC	DIFFERENCE	REDUCTION
MBSTBC-CSM $c = 4$, $\zeta_1 = 1$, $\zeta_2 = 1$, 16-QAM $N_t = 3$, $N_r = 2$, $m_{rf} = 2$	7	327,680	66,560	261,120	79.7%
MBSTBC-CSM $c = 4$, $\zeta_1 = 10$, $\zeta_2 = 10$, 16-QAM $N_t = 3$, $N_r = 2$, $m_{rf} = 2$	7	327,680	193,280	134,400	41.0%
MBSTBC-SM $c = 4$, $\zeta_1 = 1$, $\zeta_2 = 1$, 16-QAM $N_t = 4$, $N_r = 2$, $m_{rf} = 2$	7	327,680	66,560	261,120	79.7%
MBSTBC-SM $c = 4$, $\zeta_1 = 10$, $\zeta_2 = 10$, 16-QAM $N_t = 4$, $N_r = 2$, $m_{rf} = 2$	7	327,680	193,280	134,400	41.0%

6 Numerical results and discussion

This section presents the BER performances of the proposed MBSTBC-CSM and MBSTBC-SM employing ML and low-complexity detectors. The theoretical union bound on the ABEP of the ML detectors for MBSTBC-CSM and MBSTBC-SM is evaluated and employed to validate the Monte Carlo simulation results. Furthermore, error performance comparisons between the ML detector, low-complexity detector and theoretical ABEP of the proposed MBSTBC-CSM and MBSTBC-SM are presented. It is assumed that the channel state information is fully known by the receiver and have constant gains during each time-slot and independent values for different time-slots. Also, it is assumed that the transmit antennas are separated wide enough to prevent correlation of the signals. In Figs. C.2-C.5, the notations (M, N_t, N_r) are employed for STBC-CSM and STBC-SM, while (Scheme, M, N_t, N_r, m_{rf}) is employed for MBSTBC-CSM and MBSTBC-SM.

6.1 MBSTBC-CSM and MBSTBC-SM

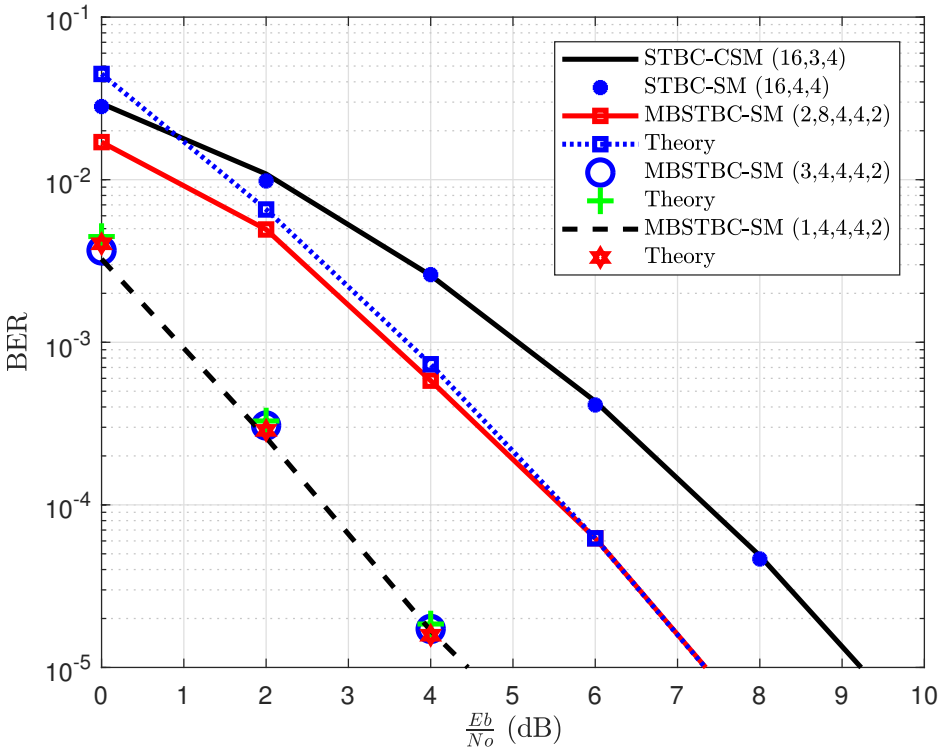

Fig. C.2: BER performance of STBC-CSM, STBC-SM and MBSTBC-SM for 5 bpcu.

Fig. C.2 and Fig. C.3 displays the theoretical and simulated average BER performances of MBSTBC-SM for 5 and 6 bpcu, respectively, employing Schemes 1, 2 and 3. These results are compared with the traditional STBC-CSM and STBC-SM.

Considering Fig. C.2, which displays numerical plots for BER versus the normalized SNR per bit $\frac{Eb}{No}$ of MBSTBC-SM for a spectral efficiency of 5 bpcu. The numerical results of the theoretical union bound average BER shows a close match with the simulated results for Scheme 1, 2 and 3. Scheme 1 and 3 demonstrate a very tight match in terms of error performance, while Scheme 1 and 3 outperforms Scheme 2 by $\approx$ 3 dB. A major improvement in SNR of 5 dB gain is demonstrated by Scheme 1 and Scheme 3 over STBC-CSM and STBC-SM when the BER is 10^{-5}, while Scheme 2 outperforms STBC-CSM and STBC-SM by a 2 dB gain in SNR.

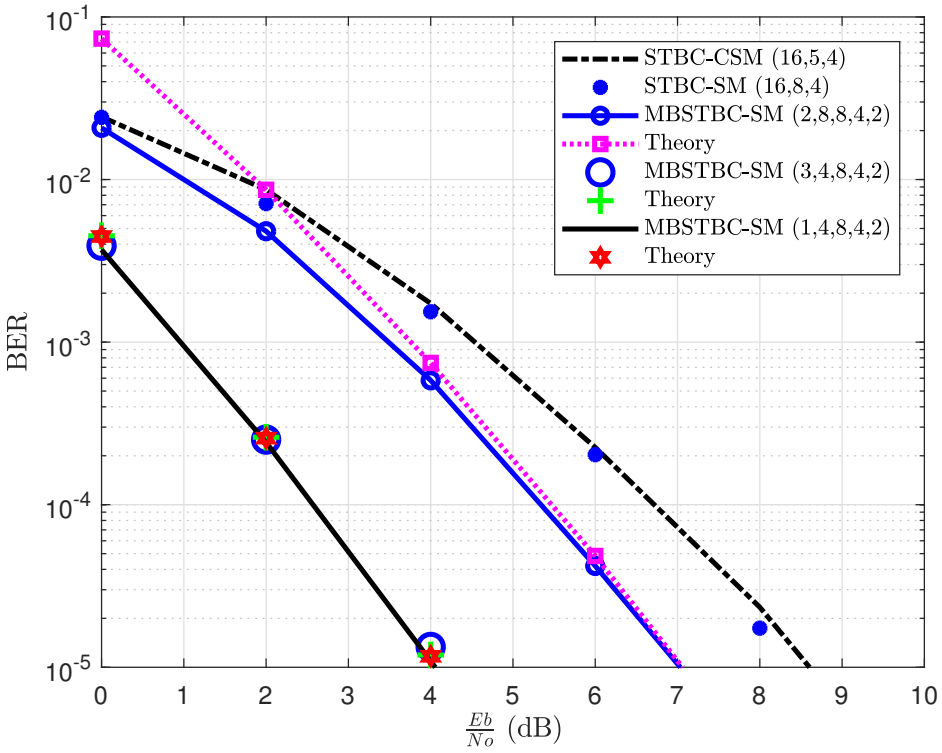

Fig. C.3: BER performance of STBC-CSM, STBC-SM and MBSTBC-SM for 6 bpcu.

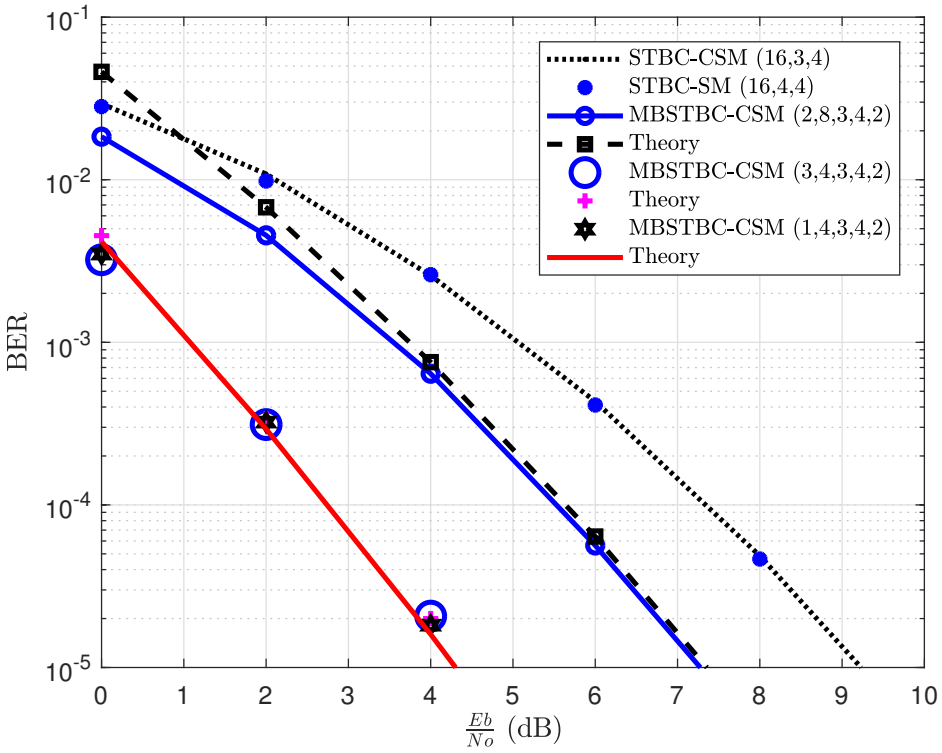

Fig. C.4: BER performance of STBC-CSM, STBC-SM and MBSTBC-CSM for 5 bpcu.

In Fig. C.3, numerical results of MBSTBC-SM for Schemes 1, 2 and 3 with STBC-CSM and STBC-SM are compared for 6 bpcu. The theoretical framework for these schemes agrees well with corresponding simulated values. Scheme 1 demonstrates a close match with Scheme 3, while Scheme 1 and 3 outperforms Scheme 2 by 3 dB and $\approx$ 4.5 dB gain in SNR over STBC-CSM and STBC-SM, when the BER is 10^{-5}. STBC-SM yields a marginal improvement of 0.05 dB gain in SNR over STBC-CSM, which was not visible in the plots for 5 bpcu shown in Fig. C.2.

Fig. C.4 and Fig. C.5 presents the BER versus $\frac{Eb}{No}$ for Scheme 1, 2 and 3 of MBSTBC-CSM, which employs 4-QAM and 8-QAM with $m_{rf} = 2$ for spectral efficiencies of 5 and 6 bpcu, respectively.

The MBSTBC-CSM in Fig. C.4 and Fig. C.5 presents similar results as its MBSTBC-SM counterpart. For example, in Fig. C.4 there is a tight match between the theoretical BER and the Monte Carlo simulated results of MBSTBC-CSM for Scheme 1, 2 and 3. Furthermore, Scheme 1 and 3 demonstrate a tight match in SNR as depicted in Fig. C.4 and Fig. C.5, while Scheme 1 and Scheme 3 outperforms Scheme 2 in terms of error performance by $\approx$ 3 dB, when the BER $= 10^{-5}$ and a 5 dB gain is observed over STBC-CSM and STBC-SM, when the BER is 10^{-5}. Scheme 2 outperforms STBC-CSM and STBC-SM by a $\approx$ 2 dB gain in SNR.

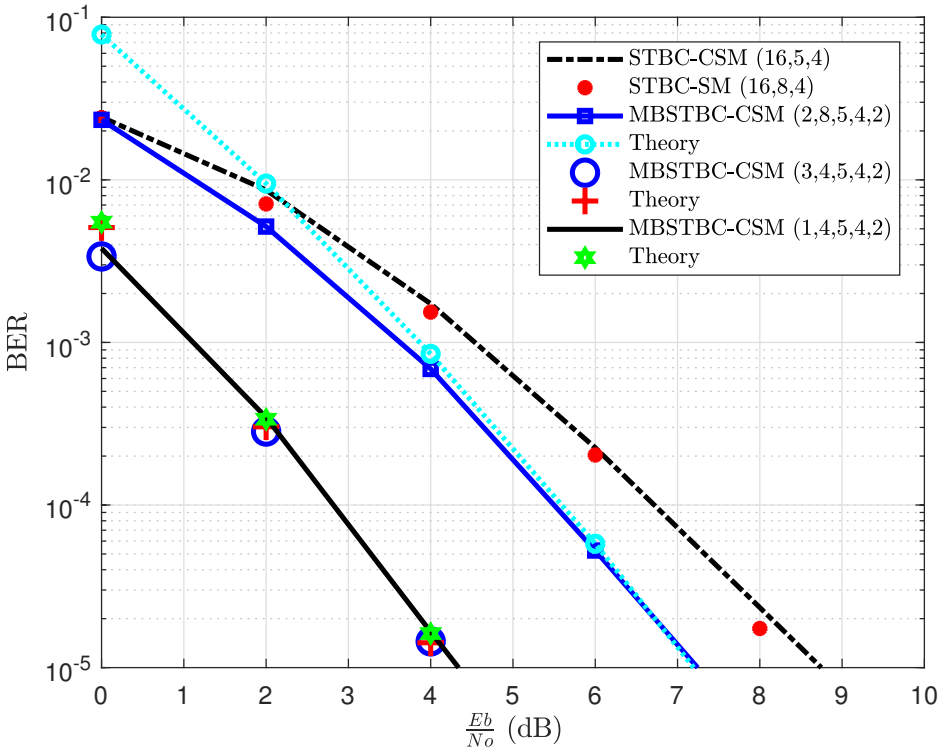

Fig. C.5: BER performance of STBC-CSM, STBC-SM and MBSTBC-CSM for 6 bpcu.

6.2 Low-complexity detector

Fig. C.6 and C.7, displays the plots showing the effect of varying the resolution ζ_1 and ζ_2 of the low-complexity detector. Keeping $N_t = 3$, $N_r = 2$, $\gamma = 2$, $c = 4$ and 16-QAM constant, and varying the resolution, it can be observed that an increase in the resolution of the low-complexity detector leads to an improved error performance until the ML error performance is reached and further increase in resolution can no longer yield better error performance, however this comes at a trade-off, as an increase in resolution ultimately yields an increase in the computational complexity of the low-complexity detector. For example, when $\zeta_1 = 1$ and $\zeta_2 = 1$, there is $\approx$ 15 dB loss in SNR by MBSTBC-CSM and MBSTBC-SM from the ML error performance as demonstrated by both Fig. C.7 and C.6, while the computational complexity is reduced by $\approx 80\%$. whereas, if the resolution is chosen such that it achieves ML error performance, i.e. $\zeta_1 = 10$ and $\zeta_2 = 10$, the computational complexity reduction is 41%.

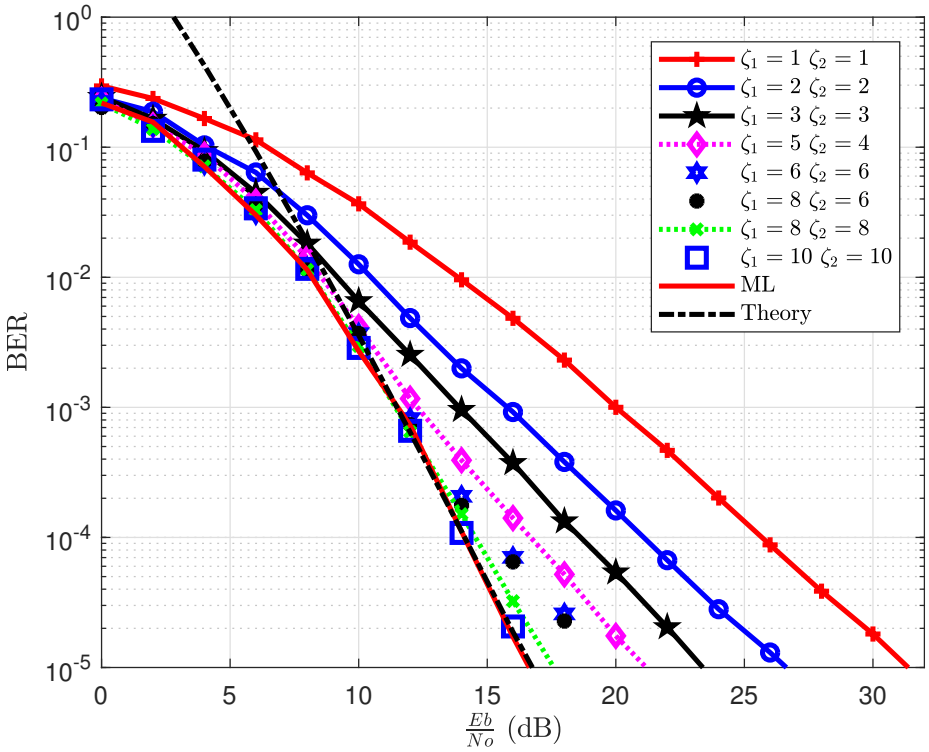

Fig. C.6: BER performance of different low-complexity detector resolutions, ML detector including theoretical ABEP of MBSTBC-CSM, $N_t = 3,\ N_r = 2,\ M = 16,\ m_{rf} = 2$.

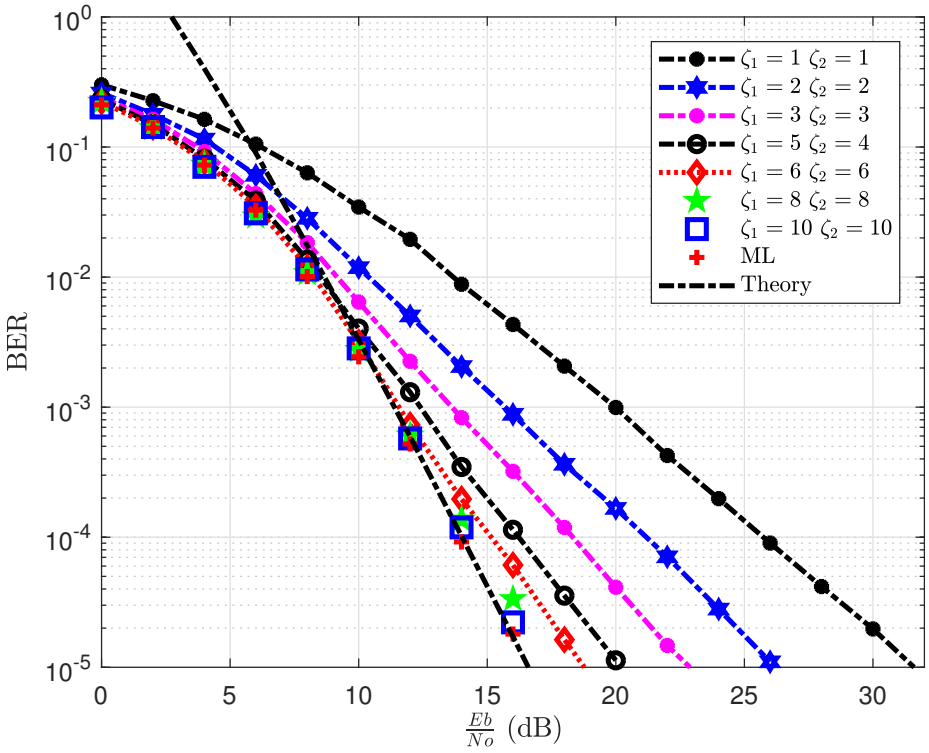

Fig. C.7: BER performance of different low-complexity detector resolutions, ML detector including theoretical ABEP of MBSTBC-SM, $N_t = 4,\ N_r = 2,\ M = 16,\ m_{rf} = 2$.

7 Conclusion

This paper investigated MBSTBC-CSM and MBSTBC-SM employing different MAP positioning schemes. Significant improvements in SNR was achieved over the traditional STBC-CSM and STBC-SM. However, as expected, Scheme 1 and 3 demonstrated superior error performance over Scheme 2. The theoretical expression for the union bound on the ABEP of MBSTBC-CSM and MBSTBC-SM was presented and shown to validate the Monte Carlo simulation results. Furthermore, a low-complexity near-ML detector, which employs orthogonal projection of signals was proposed for MBSTBC-CSM and MBSTBC-SM. As expected, the proposed low-complexity detector achieves a 41% reduction in the computational complexity of the ML detector, while retaining a close match in the error performance. The nearness in terms of error performance of the low-complexity detector to the ML detector is directly proportional to the increment in the resolution of the low-complexity detector. However, the overall computational complexity needed to achieve the error performance of the ML detector is not as large as the computational complexity of the ML detector.

References

[1] E. Telatar, "Capacity of multi-antenna Gaussian channels," *European Transactions on Telecommunications*, vol. 10, no. 6, pp. 585–595, Nov. 1999.

[2] R. Mesleh, H. Haas, S. Sinanovic, C. W. Ahn, and S. Yun, "Spatial modulation," *IEEE Transactions on Vehicular Technology*, vol. 57, no. 4, pp. 2228–2241, Jul. 2008.

[3] R. Mesleh, H. Haas, C. W. Ahn, and S. Yun, "Spatial modulation - a new low complexity spectral efficiency enhancing technique," in *Proceedings of First International Conference on Communications and Networking in China*, Oct. 2006, pp. 1–5.

[4] E. Basar, U. Aygolu, E. Panayirci, and H. V. Poor, "Space-time block coded spatial modulation," *IEEE Transactions on Communications*, vol. 59, no. 3, pp. 823–832, Mar. 2011.

[5] P. Yang, M. D. Renzo, Y. Xiao, S. Li, and L. Hanzo, "Design guidelines for spatial modulation," *IEEE Communications Surveys Tutorials*, vol. 17, no. 1, pp. 6–26, Jan.-Mar. 2015.

[6] N. Pillay and H. Xu, "Low-complexity transmit antenna selection schemes for spatial modulation," *IET Communications*, vol. 9, no. 2, pp. 239–248, 2015.

[7] M. Maleki and K. Mohamed-Pour, "Transmit precoding aided spatial modulation for multi-user correlated large-scale MIMO channels," in *Proceedings of 8th International Symposium on Telecommunications*, Sep. 2016, pp. 337–342.

[8] H. Xu and N. Pillay, "Simple near-maximum-likelihood low-complexity detection scheme for Alamouti space-time block coded spatial modulation," *IET Communications*, vol. 8, no. 15, pp. 2611–2618, 2014.

[9] L. Wang, Z. Chen, and X. Wang, "A space-time block coded spatial modulation from (n,k) error correcting code," *IEEE Wireless Communications Letters*, vol. 3, no. 1, pp. 54–57, Feb. 2014.

[10] M. Le, V. Ngo, H. Mai, and X. Tran, "High-rate space-time block coded spatial modulation," in *Proceedings of International Conference on Advanced Technologies for Communications*, Oct. 2012, pp. 278–282.

[11] B. T. Vo, H. H. Nguyen, and N. Quoc-Tuan, "High-rate space-time block coded spatial modulation," in *Proceedings of International Conference on Advanced Technologies for Communications (ATC)*, Sep. 2015, pp. 1–5.

[12] A. G. Helmy, M. D. Renzo, and N. Al-Dhahir, "Enhanced-reliability cyclic generalized spatial-and-temporal modulation," *IEEE Communications Letters*, vol. 20, no. 12, pp. 2374–2377, Dec. 2016.

[13] X. Li and L. Wang, "High rate space-time block coded spatial modulation with cyclic structure," *IEEE Communications Letters*, vol. 18, no. 4, pp. 532–535, Apr. 2014.

[14] A. K. Khandani, "Media-based modulation: A new approach to wireless transmission," in *Proceedings of IEEE International Symposium on Information Theory*, Jul. 2013, pp. 3050–3054.

[15] ——, "Media-based modulation: Converting static Rayleigh fading to AWGN," in *Proceedings of IEEE International Symposium on Information Theory*, Jun. 2014, pp. 1549–1553.

[16] E. Seifi, M. Atamanesh, and A. K. Khandani, "Media-based modulation: A new frontier in wireless communications," Oct. 2015.

[17] Z. Bouida, H. El-Sallabi, A. Ghrayeb, and K. A. Qaraqe, "Reconfigurable antenna-based space-shift keying (SSK) for MIMO Rician channels," *IEEE Transactions on Wireless Communications*, vol. 15, no. 1, pp. 446–457, Jan. 2016.

[18] J. Jeganathan, A. Ghrayeb, L. Szczecinski, and A. Ceron, "Space shift keying modulation for MIMO channels," *IEEE Transactions on Wireless Communications*, vol. 8, no. 7, pp. 3692–3703, Jul. 2009.

[19] Y. Naresh and A. Chockalingam, "On media-based modulation using RF mirrors," in *Proceedings of Information Theory and Applications Workshop (ITA)*, Jan. 2016, pp. 1–10.

[20] N. Pillay and H. Xu, "Quadrature spatial media-based modulation with RF mirrors," *IET Communications*, vol. 11, no. 16, pp. 2440–2448, 2017.

[21] I. Yildirim, E. Basar, and I. Altunbas, "Quadrature channel modulation," *IEEE Wireless Communications Letters*, vol. 6, no. 6, pp. 790–793, Dec. 2017.

[22] E. Basar and I. Altunbas, "Space-time channel modulation," *IEEE Transactions on Vehicular Technology*, vol. 66, no. 8, pp. 7609–7614, Aug. 2017.

[23] N. Pillay and H. Xu, "Uncoded space-time labeling diversity: Application of media-based modulation with RF mirrors," *IEEE Communications Letters*, vol. 22, no. 2, pp. 272–275, Feb. 2018.

[24] S. Bahng, S. Shin, and Y. O. Park, "ML approaching MIMO detection based on orthogonal projection," *IEEE Communications Letters*, vol. 11, no. 6, pp. 474–476, Jun. 2007.

[25] X. Zhang and C. Xu, "A new OSIC detection algorithm for V-BLAST systems," in *International Conference on Wireless Communications, Networking and Mobile Computing*, Sept 2007, pp. 1352–1355.

[26] K. Govindasamy, H. Xu, and N. Pillay, "Space-time block coded spatial modulation with labeling diversity," *International Journal of Communication Systems*, vol. 31, no. 1, 2017.

[27] B. S. Adejumobi, N. Pillay, and S. H. Mneney, "A study of spatial media-based modulation using RF mirrors," in *Proceedings of IEEE AFRICON*, Sep. 2017, pp. 336–341.

[28] H. Xu, K. Govindasamy, and N. Pillay, "Uncoded space-time labeling diversity," *IEEE Communications Letters*, vol. 20, no. 8, pp. 1511–1514, Aug. 2016.

Paper D

A Study Of Spatial Media-Based Modulation Using RF Mirrors

Babatunde S. Adejumobi, Narushan Pillay, and Stanley H. Mneney

Published

Proceedings of IEEE AFRICON 18-20 September, 2017.

Abstract

Media-based modulation (MBM) with radio frequency (RF) mirrors is a recently proposed concept in wireless communication, which uses RF mirrors located around transmit antennas to create distinct channel paths to the receiver, primarily allowing an improvement in spectral efficiency. Existing literature has proposed spatial media-based modulation (SMBM); however, results were not presented or benchmarked. Hence, this paper, firstly presents Monte Carlo simulation results for SMBM. In addition, an easy to evaluate theoretical average bit error probability bound for SMBM has been formulated and agrees well with simulation results. Finally, low-complexity mirror activation pattern selection for SMBM is investigated. Two low-complexity suboptimal selection schemes are proposed and improve the error performance of SMBM significantly.

1 Introduction

The next generation of wireless communication systems, require substantial improvements in throughput and link reliability, in order to support the demand for multimedia applications and services [1].

Multiple-input multiple-output (MIMO) systems are well known and have the potential to meet these demands; however, several challenges to its realization still exist, viz. high system complexity/cost, inter-channel interference (ICI), inter-antenna synchronization and low energy efficiency [1]. On this note, index modulation MIMO-based schemes have shown much promise [2, 3].

Spatial modulation (SM) is one of the key index modulation schemes that counteract the challenges of classical MIMO, while maintaining its advantages [2, 3]. SM employs a MIMO-based architecture; however, the key idea is to employ a single-active transmit antenna per time-slot to transmit a symbol. SM allows the mapping of additional bits to an antenna index. thus allowing a spectral efficiency of $\eta_{SM} = \log_2 M N_t$ bits/s/Hz, where N_t is the number of transmit antennas and M is the amplitude and/or phase modulation (APM) constellation order. In terms of error performance, SM has been demonstrated as superior to vertical Bell Laboratories layered space-time architecture (VBLAST) [4]. A drawback of SM is the logarithmic relationship between the spectral efficiency and the number of transmit antennas. Therefore, very large numbers of transmit antennas are required for highly efficient communication.

Recently, a new technique termed media-based modulation (MBM) has been proposed in literature [5,

6]. MBM involves the embedding of information in the channel states by changing the radio frequency (RF) properties, such as permittivity, permeability or resistivity in the vicinity of the transmitter, such as to create distinct channel perturbations [5]. The embedding of information in the channel is utilized to achieve the following advantages [5]:

a. A single antenna can increase the number of possible constellation points without an increase in energy, as each channel state makes up a single constellation point. Hence, a large increase in spectral efficiency can be realized.

b. A subset of the overall channel realizations may be selected; this attribute can improve the error performance as channel paths which yield superior error performance may be chosen.

c. Multipath fading channels are evectively converted into Gaussian noise with an increase in constellation due to constellations diversity, since the constellation is made up of good and bad channel realizations.

Several methods for MBM are reported in literature. For example, a basic form of MBM is space shift keying (SSK) modulation [7], where the transmitted alphabet is the channel realization of the transmitted tone [5, 7, 8]. However, multiple transmit antennas are needed to create complex fade symbols of the alphabets in SSK. In [9], the use of RF switches for SSK was considered as another form of MBM, however, a major drawback of employing RF switches is that high-speed switching, low insertion loss, and good isolation becomes a crucial consideration for the design.

Of particular interest is the use of RF mirrors to create the distinct channel perturbations in the form of mirror activation patterns (MAPs), i.e. a combination of the ON/OFF status of the mirrors [8], which results in different channel realizations. Each channel realization corresponds to a MAP of the MBM system. These MAPs, which are regarded as the constellation, increase the spectral efficiency of MBM, linearly compared to SM, where the number of transmit antennas are logarithmically related.

In [8, 10], a single-input multiple-output model for MBM (SIMO-MBM) using RF mirrors as scatterers was investigated. The spectral efficiency is improved over the traditional SIMO system. However, there is a limit to the number of mirrors that can be employed by a single antenna, since training requires transmitting test signals, and the use of a large number of mirrors for the system becomes resource intensive and endangered due to channel time variations [10].

In [8], MBM was further investigated for generalized SM (GSM). Although there were improvements in terms of spectral efficiency and error performance, ICI is a major limitation as it requires more than one RF chain as is the case for MIMO-based MBM [8].

Different MAP selection techniques for MBM have been considered in literature, for example, in [8, 10], the Euclidean distance (ED) and mutual information-based selection techniques were considered. A major limitation of the ED-MAP optimization is that it involves many iterations over all possible map enumerations for its search algorithm.

Although there are numerical results for the average bit-error probability (ABEP) of SIMO-MBM, MIMO-MBM, and GSM-MBM [8], there are no evaluated numerical or theoretical results for the ABEP of SMBM reported in literature. Furthermore, there are no simulation results that have been reported in the literature, which demonstrate the effect of MAP selection techniques on the ABEP performance of SMBM.

Based on the motivations mentioned, our contributions in this paper are as follows:

a. An easy to evaluate theoretical ABEP bound for the SMBM system is formulated.

b. The numerical results for the ABEP using Monte Carlo simulations considering an independent and identically distributed (i.i.d.) Rayleigh frequency-flat fading channel are presented to validate the theoretical ABEP bound for SMBM.

c. Two low-complexity suboptimal MAP optimization techniques are investigated, viz. the norm-based (NORM-MAP) selection, and the correlation and norm-based (CNB-MAP) selection techniques. The effects of the MAP optimization techniques on the ABEP and the proposed computational complexity for SMBM system are discussed.

The remainder of the paper is organized as follows: Section 2 presents the system model of the SMBM system for an i.i.d. frequency-flat Rayleigh fading channel. The formulated theoretical ABEP framework for the SMBM system is presented in Section 3. Section 4 investigates low-complexity suboptimal MAP selection techniques for a closed-loop SMBM system. Section 5 presents the numerical results and related discussions. Finally, Section 6 draws the conclusion of this paper.

Notation: The following notations are employed throughout this paper; bold and capital letters represent matrices, while bold small letters denote column vectors of matrices. Other notations include $(\cdot)^T$, $(\cdot)^H$, $|\cdot|$, $\|\cdot\|_F$, which represents transpose, Hermitian, Euclidean norm and Frobenius norm, respectively. Also, $\Re(\cdot)$ represents the real part of a complex variable, $\mathrm{argmax}_w(\cdot)/\,\mathrm{argmin}_w(\cdot)$ represents the maximum/minimum of an argument with respect to w, $\max_w(\cdot)$ denotes the maximum value with respect to w and $\binom{\cdot}{\cdot}$ represents the binomial coefficient.

2 System model of SMBM

The model of the SMBM system, having m_{rf} RF mirrors at each transmit antenna is depicted in Fig. D.1, where m_{rf} is the number of RF mirrors employed by an antenna. The feedback region represented with dashed outline represents a closed-loop version of SMBM, and will be discussed in Section IV.

A typical $N_r \times N_t$ M-ary quadrature amplitude modulation (M-QAM) configuration is investigated, where N_t and N_r denote the number of transmit antennas and receive antennas, respectively.

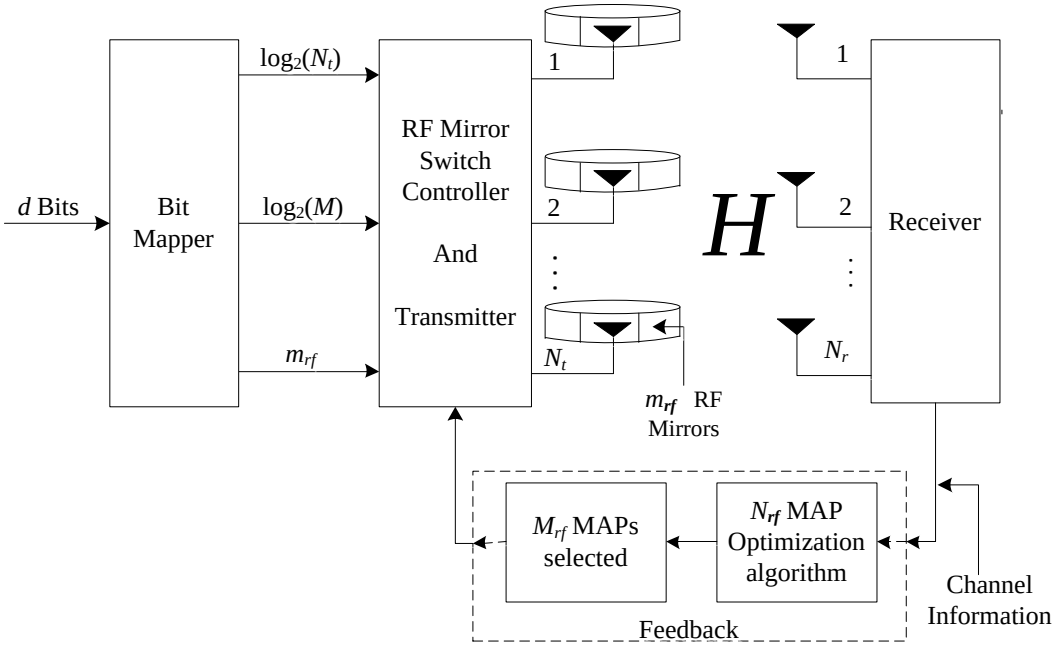

Fig. D.1: System model of SMBM

The SMBM system takes advantage of the m_{rf} RF mirrors to increase the spectral efficiency of the traditional SM system by m_{rf} bits/s/Hz. In Fig. D.1, an input bit stream consisting of $d = \log_2 MN_t + m_{rf}$ input bits are fed into the SMBM system. These d bits are partitioned into three sub-streams, such that; $\log_2 M$ bits are mapped to select a symbol x_k from an M-QAM constellation, where $k \in [1 : M]$, $\log_2 N_t$ bits are employed to select a transmit antenna with index l, $l \in [1 : N_t]$, and the remaining m_{rf} bits are employed to select the m-th MAP, $m \in [1 : M_{rf}]$, where $M_{rf} = 2^{m_{rf}}$. A tabular illustration of the output, from the SMBM bit mapper is presented in Table D.1. The SMBM system in Table D.1 assumes a 4×4, 4-QAM SMBM system, having $m_{rf} = 2$ RF mirrors at each antenna.

Table D.1: Illustration of bit mapping for SMBM system

x_k	l	m
11	11	11
00	00	01
10	11	00
10	01	11

Table D.2 shows the modulated outputs x_k, l and m from the RF mirror switch controller and transmitter.

The frequency flat Rayleigh fading channel $\boldsymbol{H}$ for the SMBM system is an i.i.d. random variable according to $CN(0,1)$ and is given as $\boldsymbol{H} = [\boldsymbol{H}_1\ \boldsymbol{H}_2\ \cdots\ \boldsymbol{H}_{N_t}]$, where $\boldsymbol{H}_l = [\boldsymbol{h}_{l,1}\ \boldsymbol{h}_{l,2}\ \cdots\ \boldsymbol{h}_{l,M_{rf}}]$, $l \in [1 : N_t]$ and $\boldsymbol{h}_{l,m} = [h^m_{1,l}\ h^m_{2,l}\ \ldots\ h^m_{N_r,l}]^T$, $m \in [1 : M_{rf}]$.

Table D.2: Output of the SMBM switch controller

Bits	Symbol	Antenna	MAP
d	x_k	l	m
111111	$+1+i$	4	4
000001	$-1-i$	1	2
101100	$+1-i$	4	1
100111	$+1-i$	2	4

The $N_r \times 1$ receive signal vector $\boldsymbol{y} = [y_1\ y_2\ \cdots\ y_{N_r}]^T$ is given as [8]:

$$\boldsymbol{y} = \sqrt{\rho}\boldsymbol{H}_l x^l_k \boldsymbol{e}_m + \boldsymbol{n} \tag{D.1}$$

where ρ is the average signal-to-noise ratio (SNR) at the receiver, x^l_k is the k-th symbol of a M-QAM constellation, $k \in [1 : M]$, which is to be transmitted by the l-th activated antenna, $l \in [1 : N_t]$. $\boldsymbol{H}_l$ is the channel matrix for the l-th transmit antenna, $\boldsymbol{e}_m$ is an $M_{rf} \times 1$ vector having the m-th element as the only single unit entry, $m \in [1 : M_{rf}]$. The vector $\boldsymbol{n}$ is an $N_r \times 1$ AWGN vector, whose entries are an i.i.d. random variable with distribution $CN(0,1)$.

The received signal vector $\boldsymbol{y}$ in (D.1) can be also written as:

$$\boldsymbol{y} = \sqrt{\rho}\boldsymbol{H}_l \boldsymbol{s}_{k,m}^l + \boldsymbol{n} \tag{D.2}$$

where $\boldsymbol{s}_{k,m}^l = x_k^l \boldsymbol{e}_m$, such that the m-th entry of $\boldsymbol{s}_{k,m}^l$ is x_k^l.

The SMBM system under study employs the maximum-likelihood (ML) rule for detection and is defined as [8]:

$$[\hat{k}, \hat{l}, \hat{m}] = \underset{k\in[1:M], l\in[1:N_t], m\in[1:M_{rf}]}{\operatorname{argmin}} \left(\left\| \boldsymbol{y} - \sqrt{\rho}\boldsymbol{H}_l \boldsymbol{s}_{k,m}^l \right\|_F^2 \right) \tag{D.3}$$

where $\hat{k}$, $\hat{l}$ and $\hat{m}$ are estimates of the transmitted symbol, transmit antenna and MAP employed, respectively.

The detector in (D.3) can be further simplified as [4]:

$$[\hat{k}, \hat{l}, \hat{m}] = \underset{k\in[1:M], l\in[1:N_t], m\in[1:M_{rf}]}{\operatorname{argmin}} \left(\|\boldsymbol{g}\|_F^2 - 2\Re\left(\boldsymbol{y}^H \boldsymbol{g}\right) \right) \tag{D.4}$$

where $\boldsymbol{g} = \sqrt{\rho}\boldsymbol{H}_l \boldsymbol{s}_{k,m}^l$.

3 Theoretical ABEP of SMBM

In this section, the theoretical framework for calculating the ABEP of SMBM is presented. Referring to (D.2), the SMBM system can be viewed as an $N_t M_{rf} \times N_r$ SM system. Hence, the theoretical result of SM [11] may be extended to SMBM. Assume that P_a denotes the bit error probability for the antenna index given that the symbol is correctly estimated, and P_d represents the bit error probability of the symbol given that the transmit antenna index is correctly estimated. It therefore means that the total probability of detecting the transmitted bits incorrectly (P_e) is bounded by [11]:

$$P_e \geq P_a + P_d - P_a P_d \tag{D.5}$$

Hence, from [11] and [12], P_d can be expressed as:

$$P_d \cong \frac{1}{n}\left\{\frac{a}{c}\left[\frac{1}{2}\left(\frac{2}{b\rho+2}\right)^{N_r} - \frac{a}{2}\left(\frac{1}{b\rho+1}\right)^{N_r} + (1-a)\sum_{i=1}^{c-1}\left(\frac{\eta_i}{b\rho+\eta_i}\right)^{N_r} + \sum_{i=c}^{2c-1}\left(\frac{\eta_i}{b\rho+\eta_i}\right)^{N_r}\right]\right\} \quad \text{(D.6)}$$

where $a = \frac{1}{1-\sqrt{M}}$, $b = \frac{3}{M-1}$, $n = \log_2 M$, $\eta_i = 2\sin^2\theta_i$, $\theta_i = \frac{i\pi}{4c}$, N_r is the number of receive antennas and c is the number of summations required for convergence of the trapezoidal approximation of the Q-function. Also, adopting the expression in [11] for P_a, P_a can be modified as:

$$P_a \leq \sum_{l=1}^{N_t M_{rf}} \sum_{\hat{l}=1}^{N_t M_{rf}} \sum_{k=1}^{M} \frac{N\left(l,\hat{l}\right)\mu_\alpha^{N_r}\sum_{w=0}^{N_r-1}\binom{N_r-1+w}{w}[1-\mu_\alpha]^w}{N_t M_{rf} M \log_2\left(N_t M_{rf}\right)} \quad \text{(D.7)}$$

where $N(l,\hat{l})$ is the number of bit errors between the transmit antenna with index l, and the estimated transmit antenna with index $\hat{l}$, $\mu_\alpha = \frac{1}{2}\left(1-\sqrt{\frac{\sigma_\alpha^2}{1+\sigma_\alpha^2}}\right)$ and $\sigma_\alpha^2 = \frac{\rho}{2}|x_k|^2$.

4 Low-complexity suboptimal MAP selection for closed-loop SMBM

An alternative design to improve the error performance of the SMBM system is a closed-loop SMBM system presented in Fig. D.1 (inclusive of the feedback represented with a dashed outline). Assume that the system has n_{rf} mirrors of which m_{rf} mirrors are employed for the transmission. The system is designed such that, based on perfect channel knowledge, the receiver employs a MAP optimization algorithm. The algorithm optimizes $N_{rf} = 2^{n_{rf}}$ MAPs, such that $M_{rf} = 2^{m_{rf}}$ MAPs are selected, where $n_{rf} > m_{rf}$. A requirement for this system is a perfect feedback communication link, so that the selected M_{rf} MAPs for the next transmission are relayed to the transmitter without errors. The MAP criteria for RF mirrors is like that of the antenna selection [3, 13, 14] criteria for MIMO systems. Considerable work has been performed on antenna selection, in the context of SM MIMO. Such as [13, 14], where maximization of the minimum ED was proposed, however, the computational complexity is extremely high. Low-complexity suboptimal antenna selection was considered in [3], where minimization of antenna correlation was investigated. Some of these antenna selection schemes can be employed as a criterion for optimizing MAPs in SMBM systems.

4.1 NORM-MAP selection for SMBM

The NORM-MAP selection [3] is employed by sorting in descending order the N_{rf} channel vector norms in (D.8) for each transmit antenna:

$$\|\boldsymbol{h}_{l,1}\|_F^2, \quad \|\boldsymbol{h}_{l,2}\|_F^2, \quad \cdots \quad \left\|\boldsymbol{h}_{l,M_{rf}}\right\|_F^2, \quad \cdots \quad \left\|\boldsymbol{h}_{l,N_{rf}}\right\|_F^2 \tag{D.8}$$

where $l \in [1 : N_t]$, $N_{rf} = 2^{n_{rf}}$ and n_{rf} is the number of RF mirrors for the l-th antenna. The M_{rf} MAPs selected corresponds to the channel vectors in (D.8) having the largest amplitudes and is given as:

$$\|\boldsymbol{h}_{z,1}\|_F^2 \quad \geq \quad \|\boldsymbol{h}_{z,2}\|_F^2 \quad \geq \quad \cdots \quad \geq \quad \left\|\boldsymbol{h}_{z,M_{rf}}\right\|_F^2 \tag{D.9}$$

where $z \in [1 : N_t]$, $M_{rf} = 2^{m_{rf}}$ and m_{rf} is the number of optimized mirrors for the l-th antenna.

The computational complexity of the NORM-MAP selection scheme in terms of floating point operations is as follows: computing the Frobenius norms in (D.8) requires N_r multiplications and $N_r - 1$ additions. Since the computation is performed for N_{rf} MAPs and N_t antennas, the total computational complexity imposed by this method is only $\delta_{\mathrm{NORM-MAP}} = N_{rf} N_t \left(2N_r - 1\right)$.

4.2 CNB-MAP selection for SMBM

Consider the channel matrix $\boldsymbol{H}_l^{N_{rf}} = [\boldsymbol{h}_{l,1}\ \boldsymbol{h}_{l,2}\ \cdots\ \boldsymbol{h}_{l,N_{rf}}]$ having $I_{N_{rf}} = \binom{N_{rf}}{M_{rf}}$ sets having M_{rf} combinations. The correlation MAP optimization criterion [3] for MAP selection employs the correlation of all $\binom{M_{rf}}{2}$ combinations of the channel matrix $\boldsymbol{H}_l^{M_{rf}} = [\boldsymbol{h}_{l,1}\ \boldsymbol{h}_{l,2}\ \cdots\ \boldsymbol{h}_{l,M_{rf}}]$, which is a subset of $\boldsymbol{H}_l^{N_{rf}}$ for all $I_{N_{rf}}$ sets. The channels for the selected MAP set $\overline{\boldsymbol{H}}_l$ is selected according to [3]:

$$\overline{\boldsymbol{H}}_l = \underset{\boldsymbol{I}_{N_{rf}}}{\operatorname{argmin}} \left(\max_{p,q,\ p \neq q} \left(\frac{\left|\boldsymbol{h}_{l,p}{}^H \boldsymbol{h}_{l,q}\right|}{\|\boldsymbol{h}_{l,p}\|_F \|\boldsymbol{h}_{l,q}\|_F} \right) \right) \tag{D.10}$$

where $(\boldsymbol{h}_{l,p},\ \boldsymbol{h}_{l,q})$ is a member in the set of the $\binom{M_{rf}}{2}$ combinations of the channel matrix $\boldsymbol{H}_l^{M_{rf}}$, $p, q \in [1 : M_{rf}]$, $l \in [1 : N_t]$. However, this method becomes impracticable for real-world application. Some of the reasons are: a) high computational complexity in calculating the channel Frobenius norms of (D.10), for a large number of iterations; e.g. when $M_{rf} = 16$ and $N_{rf} = 32$, a minimum of 7.21×10^{10} iterations are employed; b) redundancy in the computation of repeated channel combinations, e.g.

redundancy in the computation of (D.10), and c) memory requirement needed in storing the outputs of (D.10). To reduce the computational complexity, based on [3] a hybrid MAP selection may be considered. Hence, the NORM-MAP optimization in (D.9) is firstly employed, such that $M_{rf}+1$ MAPs are chosen. Then the correlation metric in (D.10) is employed to obtain the M_{rf} suboptimal MAPs from the $M_{rf}+1$ MAPs. To eliminate multiple redundant computations, the optimized M_{rf} MAPs $\boldsymbol{I}_{M_{rf}}$ are chosen according to:

$$\boldsymbol{I}_{M_{rf}} = \underset{I \in I_{M_{rf}+1}}{\operatorname{argmin}} \left(\max_{p,q \; p \neq q} \boldsymbol{I}_{\varphi}(I) \right) \tag{D.11}$$

where $I_{M_{rf}+1}$ is the enumeration size $\binom{M_{rf}+1}{M_{rf}}$, $\boldsymbol{I}_{\varphi}(I)$ is an $M_{rf} \times M_{rf}$ matrix obtained by deleting the rows and columns absent in the I-th enumeration of $\boldsymbol{I}_{\varphi}$, $I \in [1 : I_{M_{rf}+1}]$. $\boldsymbol{I}_{\varphi}$ is an $(M_{rf}+1) \times (M_{rf}+1)$ upper-triangular matrix with $\binom{M_{rf}+1}{2}$ non-zero entries represented as:

$$I_{\varphi} = \begin{bmatrix} 0 & j_{1,2} & \cdots & j_{1,M_{rf}+1} \\ 0 & 0 & \cdots & j_{2,M_{rf}+1} \\ \vdots & \vdots & \ddots & \vdots \\ 0 & 0 & \cdots & j_{M_{rf},M_{rf}+1} \\ 0 & 0 & \cdots & 0 \end{bmatrix} \tag{D.12}$$

Each non-zero element $j_{p,q}$ in (D.12) corresponds to the correlation outputs of the $(\boldsymbol{h}_{z,p},\ \boldsymbol{h}_{z,q})$ combinations of the $M_{rf}+1$ MAP channels selected using the NORM-MAP in (D.9), where $p, q \in [1 : M_{rf}]$ and $p > q$.

The non-zero elements $j_{p,q}$ in $\boldsymbol{I}_{\varphi}$ are defined according to:

$$j_{p,q} = \frac{\left| (\boldsymbol{h}_{z,p})^H \boldsymbol{h}_{z,q} \right|}{\|\boldsymbol{h}_{z,p}\|_F \|\boldsymbol{h}_{z,q}\|_F} \tag{D.13}$$

The algorithm for the CNB-MAP selection is summarized as follows:

Algorithm 1 : CNB-MAP selection

1. Arrange the norm of the channel vectors in descending order as in (D.9).
2. Select $M_{rf}+1$ suboptimal MAPs from N_{rf} MAPs according to (D.9).
3. Obtain $M_{rf}+1$ MAP sets having M_{rf} MAPs given by $\binom{M_{rf}+1}{M_{rf}}$.
4. For I = 1 to $I_{M_{rf}+1}$
   i. Select the MAP set for I-th enumeration.
   ii. Find all $\binom{M_{rf}}{2}$ combinations in $\boldsymbol{H}_z^{M_{rf}}$ for the I-th enumeration.
   iii. Compute all elements of $\boldsymbol{I}_\varphi$ according to (D.13).
   iv. Obtain the maximum and store in $I_{M_{rf}+1}(I)$.

   End
5. The suboptimal MAP set is the MAP set that gives the minimum value in $I_{M_{rf}+1}(I)$.

The computational complexity imposed by the CNB-MAP selection algorithm in terms of floating point operations is computed as follows: since Step 1 uses the NORM-MAP algorithm in (D.9), the computational complexity imposed by Step 1 is $\delta_{\text{step 1}} = N_{rf}N_t(2N_r - 1)$. The computational complexity imposed by calculating a single entry $j_{p,q}$ of $\boldsymbol{I}_\varphi$ as expressed in (D.13) is $2N_r + 2$. This is computed for $\binom{M_{rf}}{2}$ entries of $\boldsymbol{I}_\varphi$. Since Step 4 undergoes $M_{rf}+1$ iterations across N_t antennas, the computational complexity imposed by Step 4 is $\delta_{\text{step 4}} = \binom{M_{rf}}{2}N_t(M_{rf}+1)(2N_r+2)$. Hence, the overall computational complexity of the CNB-MAP can be represented as $\delta_{\text{CNB-MAP}} = \delta_{\text{step 1}} + \delta_{\text{step 4}} = N_{rf}N_t\left(2N_r-1\right) + \binom{M_{rf}}{2}N_t\left(M_{rf}+1\right)\left(2N_r+2\right)$.

A summary of the computational complexities of the different MAP optimization techniques in terms of complex operations is given in Table D.3.

Table D.3: Computational complexities of NORM-MAP and CNB-MAP

CONFIGURATION	NORM-MAP	CNB-MAP
$N_t = 4$, $N_r = 4$, $M_{rf} = 16$, $N_{rf} = 32$	896	82,496
$N_t = 4$, $N_r = 4$, $M_{rf} = 16$, $N_{rf} = 64$	1,792	83,392
$N_t = 4$, $N_r = 4$, $M_{rf} = 16$, $N_{rf} = 128$	3,584	85,184

From Table D.3, it can be deduced that the NORM-MAP has a very reduced computational complexity when compared with the CNB-MAP. There is a 100% increment in the computational complexity when the MAPs to be optimized are increased by the addition of an RF mirror for the NORM-MAP and 1.09% for CNB-MAP, however, the NORM-MAP still maintains a lower computational complexity when compared to the CNB-MAP optimization. For example, given $n_{rf} = 5$ and $M_{rf} = 16$, it

means that 16 MAPs are chosen of the 32 MAPs available. The computational complexity involved in optimizing these MAPs are 896 and 82,496, for NORM-MAP and CNB-MAP, respectively. If n_{rf} is increased to 6, while $M_{rf} = 16$, the computational complexity of NORM-MAP is doubled while a 1.09% increase is achieved for CNB-MAP. However, the computational complexity for NORM-MAP is far less than the computational complexity needed by CNB-MAP optimization algorithm as can be seen from Table D.3.

5 Numerical results and discussion

This section validates the theoretical frameworks presented in Section 3 using the Monte Carlo simulations. All simulations in this section, are performed over an i.i.d. frequency-flat Rayleigh fading channel in the presence of AWGN. The average SNR is plotted against the average bit-error rate (BER).

Fig. D.2 employs the notation (N_t, N_r, m_{rf}, M, d) for SMBM, while the notation for SM is represented as (N_t, N_r, M, d). Fig. D.2a) compares the theoretical ABEP of SMBM with the ABEP of the simulated SMBM system for several spectral efficiencies, viz. 9, 10 and 11 bits/s/Hz. As expected, there is a close match between the simulated and theoretical ABEP at high SNR (SNR $\geq$ 14 dB) because of the bound being employed.

In Fig. D.2b), the ABEP of SMBM is compared with the ABEP of SM employing different configurations but at the same spectral efficiency, viz. 9 and 13 bits/s/Hz. The results show that for SM to have the same error performance as the SMBM system, the number of transmit antennas for SM should be $N_t M_{rf}$. For example, the BER of SM is the same as SMBM with $N_t = 2$ and $M_{rf} = 2$ when SM employs $N_t = 8$ transmit antennas.

Considering Fig. D.3, the notation (M_{rf}, N_{rf}, d, M) is employed for NORM-MAP and CNB-MAP. The BER for NORM-MAP optimization and the CNB-MAP optimization from $N_{rf} = 32$ and 64 MAPs to $M_{rf} = 16$ MAPs are compared. In Fig. D.3a), the 8 bits/s/Hz is considered employing 4-QAM modulation. It is noteworthy that both MAP optimization schemes match closely at lower SNR, specifically when the SNR is $\leq$ 12 dB for both $N_{rf} = 32$ and 64 MAPs. However, at SNR $>$ 12dB the error performance of the CNB-MAP displays an improved error performance over the NORM-MAP. Also, the error performance is improved as the number of N_{rf} MAPs being optimized increases. For example, a 4 dB gain is observed when the MAPs are optimized from 64 MAPs to 16 MAPs and approximately 3 dB when the MAPs are optimized from 32 MAPs to 16 MAPs at a BER of 10^{-5}.

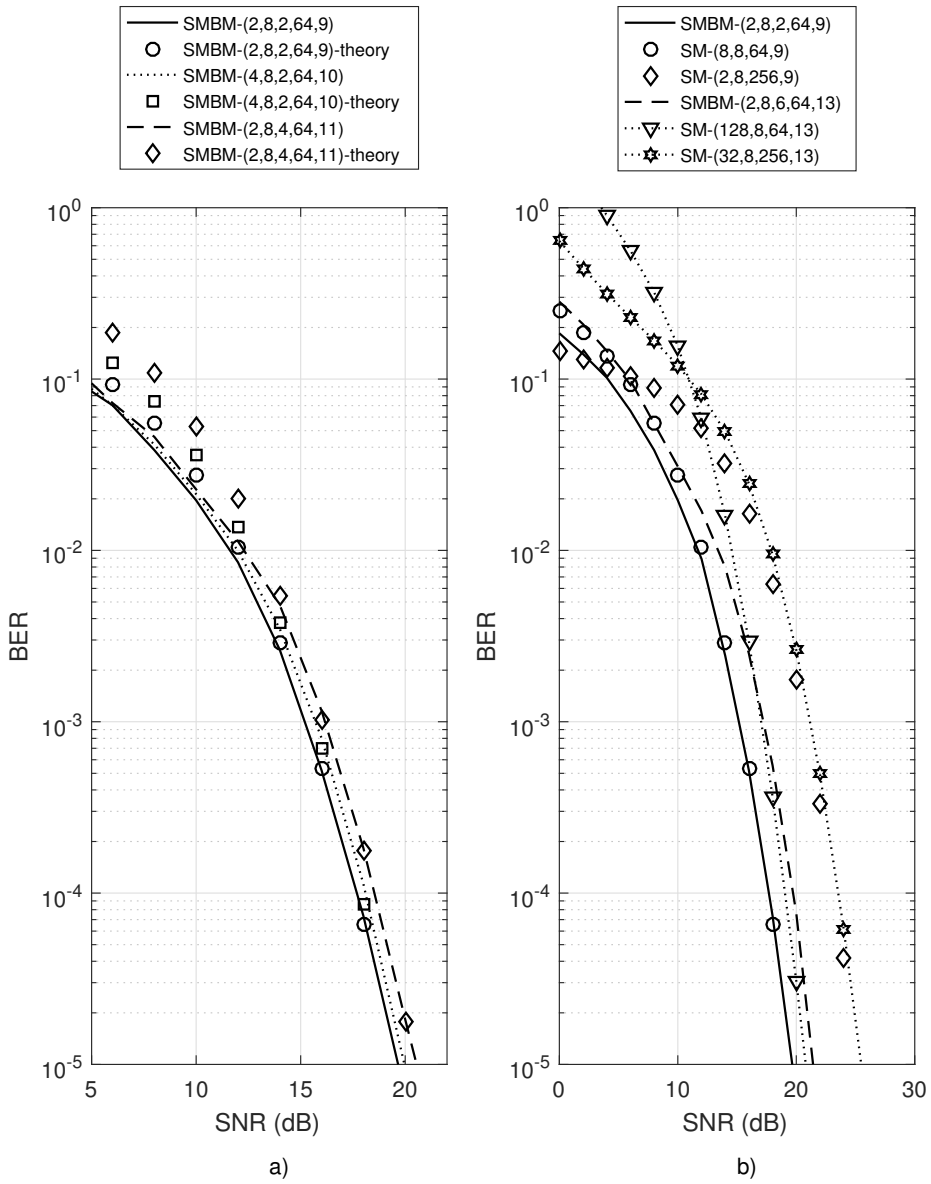

Fig. D.2: Comparison between: a) theoretical and simulated BER performances of SMBM for $d = 9$, 10 and 11 bits/s/Hz. b) BER of SMBM and SM for $d = 9$ and 13. bits/s/Hz.

In Fig. D.3b), the 10 bits/s/Hz employing 16-QAM modulation is considered. The optimization schemes show a tight match in error performances when the SNR is $\leq$ 20 dB for both $N_{rf} = 32$ and 64 MAPs, above this SNR, a marginal improvement of the CNB-MAP over the NORM-MAP is seen. The CNB-MAP and NORM-MAP show an enhanced error performance of approximately 3 dB and 2 dB, for 64 and 32 MAPs, respectively, over the open-loop SMBM system at a BER of 10^{-5}.

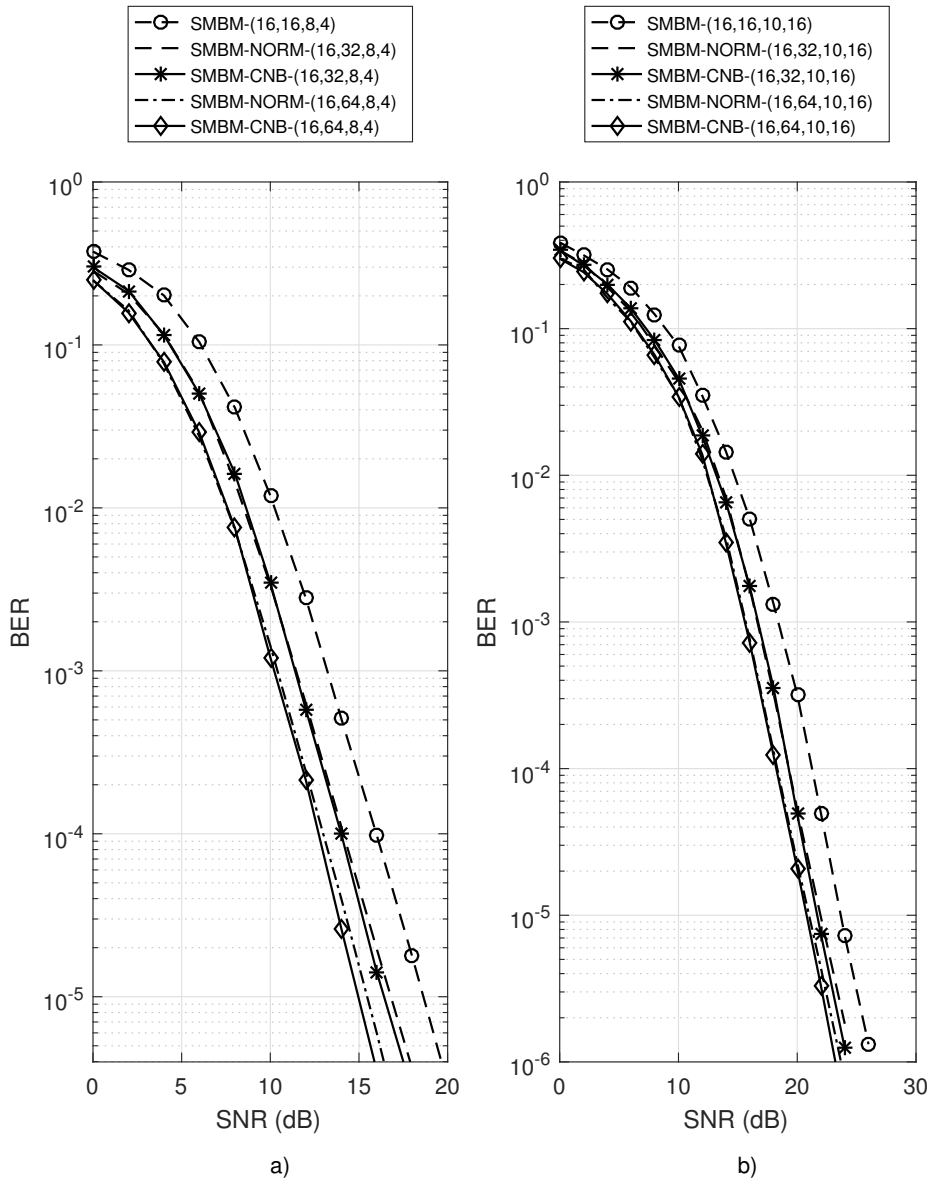

Fig. D.3: Comparison of error performances for traditional SMBM system with SMBM employing the NORM-MAP and CNB-MAP optimization technique, for a) 4×4, 4-QAM, $M_{rf} = 16$, $N_{rf} = 32$ and 64. b) 4×4, 16-QAM, $M_{rf} = 16$, $N_{rf} = 32$ and 64.

6 Conclusion

In this paper, the SMBM system for an i.i.d. Rayleigh frequency-flat fading channel has been investigated. The formulated theoretical ABEP of SMBM closely matches the Monte Carlo simulation for the SMBM system in an i.i.d. frequency-flat Rayleigh fading channel, hence,

validating the proposed theoretical ABEP framework. Low-complexity suboptimal MAP selection is investigated; numerical results showed that MAP selection techniques improves the BER of SMBM. The study also confirms that the NORM-MAP selection scheme and the CNB-MAP selection algorithm show close performance at lower SNR, while the CNB-MAP selection method outperforms the NORM-MAP selection scheme at higher SNR. However, this comes as a trade-off in terms of the computational complexity, as the computational complexity of NORM-MAP is 98.9% less than the computational complexity of CNB-MAP.

References

[1] S. Bahng, S. Shin, and Y. O. Park, "ML approaching MIMO detection based on orthogonal projection," *IEEE Communications Letters,*, vol. 11, no. 6, pp. 474–476, Jun. 2007.

[2] R. Y. Mesleh, H. Haas, S. Sinanovic, C. W. Ahn, and S. Yun, "Spatial modulation," *IEEE Transactions on Vehicular Technology*, vol. 57, no. 4, pp. 2228–2241, Jul. 2008.

[3] N. Pillay and H. Xu, "Low-complexity transmit antenna selection schemes for spatial modulation," *IET Communications*, vol. 9, no. 2, pp. 239–248, Jan. 2015.

[4] J. Jeganathan, A. Ghrayeb, and L. Szczecinski, "Spatial modulation: optimal detection and performance analysis," *IEEE Communications Letters*, vol. 12, no. 8, pp. 545–547, Aug. 2008.

[5] A. K. Khandani, "Media-based modulation: A new approach to wireless transmission," in *Proceedings of IEEE International Symposium on Information Theory*, Jul. 2013, pp. 3050–3054.

[6] ——, "Media-based modulation: Converting static Rayleigh fading to AWGN," in *Proceedings of IEEE International Symposium on Information Theory*, Jun. 2014, pp. 1549–1553.

[7] J. Jeganathan, A. Ghrayeb, L. Szczecinski, and A. Ceron, "Space shift keying modulation for MIMO channels," *IEEE Transactions on Wireless Communications*, vol. 8, no. 7, pp. 3692–3703, Jul. 2009.

[8] Y. Naresh and A. Chockalingam, "On media-based modulation using RF mirrors," in *Proceedings of Information Theory and Applications Workshop (ITA)*, Jan. 2016, pp. 1–10.

[9] Z. Bouida, H. El-Sallabi, A. Ghrayeb, and K. A. Qaraqe, "Reconfigurable antenna-based space-shift keying (SSK) for MIMO Rician channels," *IEEE Transactions on Wireless Communications*, vol. 15, no. 1, pp. 446–457, Jan. 2016.

[10] E. Seifi, M. Atamanesh, and A. K. Khandani, "Media-based modulation: A new frontier in wireless communications," 2015.

[11] N. R. Naidoo, H.-J. Xu, and T. A.-M. Quazi, "Spatial modulation: optimal detector asymptotic performance and multiple-stage detection," *IET communications*, vol. 5, no. 10, pp. 1368–1376, 2011.

[12] H. Xu, "Symbol error probability for generalized selection combining reception of M-QAM," *SAIEE Africa Research Journal*, vol. 100, no. 3, pp. 68–71, Sep. 2009.

[13] R. Rajashekar, K. Hari, and L. Hanzo, "Quantifying the transmit diversity order of Euclidean distance based antenna selection in spatial modulation," *IEEE Signal Processing Letters*, vol. 22, no. 9, pp. 1434–1437, Sep. 2015.

[14] P. Yang, Y. Xiao, L. Li, Q. Tang, Y. Yu, and S. Li, "Link adaptation for spatial modulation with limited feedback," *IEEE Transactions on Vehicular Technology*, vol. 61, no. 8, pp. 3808–3813, Oct. 2012.

Part III

Conclusion

Conclusion

1 Conclusion

This thesis has focused mainly on exploiting the advantages of index modulation in the form of media-based modulation or antenna indexing based modulation. The wireless systems considered have demonstrated significant improvement in terms of error performance and spectral efficiency over the respective traditional schemes. For example, QSM-OFDM demonstrated significant improvement over SM-OFDM, MIMO-OFDM and MRC-OFDM by 4 dB, 6 dB and 5 dB gain in SNR, respectively, as depicted in Paper A. Furthermore, MBSTBC-CSM and MBSTBC-SM yielded a major improvement, which is greater than 5 dB in SNR over the traditional STBC-CSM and STBC-SM, respectively.

Also, low-complexity detection schemes, which employ the method of orthogonal projection of signal is employed to reduce the computational complexity of STBC-CSM, MBSTBC-CSM and MBSTBC-SM have been presented. The low-complexity scheme is able to achieve near-ML error performance with a 41% reduction in computational complexity for MBSTBC-CSM and MBSTBC-SM. This reduction in computational complexity occurs at a trade-off with respect to the resolution of the detector.

MAP optimization techniques to further improve the BER of SMBM have been presented in this thesis, as expected, an improved error performance was demonstrated for the SMBM system. Hence, it can be concluded that, index modulation is the way forward for next generation wireless systems.

2 Possible Future Work

The objective of future research of index modulated systems will involve the following:

1. Channel estimation: Although this thesis demonstrates that index modulation of different forms can improve the spectral efficiency/error performance of next generation systems, a perfect

channel knowledge at the receiver has been assumed. In real life scenarios, this is not the often case. Hence, it is necessary to investigate the effect of different channel estimation techniques and channel estimation errors on index modulation systems.

2. Link reliability: The application of precoders/channel coding techniques can further improve the error performance of index modulated systems. An in-depth investigation to further improve the BER of index modulated systems will be beneficial.

3. Computational complexity: The schemes which have been presented in this thesis, have improved the spectral efficiency/error performance of traditional MIMO schemes. However, it may become impracticable to implement, if the computational complexity is very large. Hence, it is important to investigate more techniques which reduce the computational complexities of the different index modulation systems, and are implementable in real-life.

4. MAP optimization techniques: Investigation of optimal/suboptimal MAP optimization techniques, which improve error performance of media-based systems are necessary for the enhancement of next generation media-based index modulation systems.